

ELECTROMAGNETIC MODELING OF LABORATORY-SCALE 2D SOIL-BED SETUP

by

Lilian J. Certuche-Alzate

A thesis submitted in partial fulfillment of the requirements for the degree of

MASTER OF SCIENCE
in
ELECTRICAL ENGINEERING

UNIVERSITY OF PUERTO RICO
MAYAGÜEZ CAMPUS
2009

Approved by:

Rafael A. Rodríguez Solís, PhD
President, Graduate Committee

Date

Ingrid Padilla, PhD
Member, Graduate Committee

Date

José Colom Ustariz, PhD
Member, Graduate Committee

Date

Pedro Vasquez, PhD
Representative of Graduate Studies

Date

Isidoro Couvertier, PhD
Chairperson of the Department

Date

ABSTRACT

This work presents the development of electromagnetic model for the laboratory 2-D Soil-Bed setup, which was developed at the Civil Engineering Department of the University of Puerto Rico, Mayaguez, to verify the possibility to detect a contaminant (DNAPL) in the subsurface, using Cross Well Radar (CWR) technologies.

The electromagnetic model developed using two electromagnetic simulators, Ansoft's HFSS and Remcom's XFDTD. The simulations are done for dry and saturated sand, with and without the contaminant, with different shapes and positions of the contaminant pools within the tank, transmitting through all the different ports independently, where we observed for each case the E-field propagation and S-parameters at the three analysis frequencies of 285 MHz, 515 MHz and 1.5 GHz.

The results of the XFDTD simulator are used to verify the results in the HFSS simulator. The analysis of the S-parameters, taking into account the position of the ports, shows it is possible to detect the contaminant in dry sand and saturated sand at the analysis frequencies.

RESUMEN

Este trabajo presenta el desarrollo del modelo electromagnético computacional de un tanque de flujo en dos dimensiones, el cual fue desarrollado en Ingeniería Civil de la Universidad de Puerto Rico, para verificar la posible detección en el subsuelo de un contaminante (DNAPL), usando tecnología CWR.

El modelo fue desarrollado usando dos simuladores electromagnéticos Ansoft's HFSS y Remcom's XFDTD. Las simulaciones son hechas para arena seca y húmeda, con y sin contaminante, con diferentes formas y posiciones del contaminante dentro del tanque, transmitiendo a través de todos los puertos independientemente, donde nosotros observamos para cada caso la propagación del campo eléctrico y los parámetros S a las tres frecuencias de análisis 285 MHz, 515 MHz y 1.5 GHz.

Los resultados del simulador XFDTD son usados para verificar los resultados del simulador HFSS. El análisis de los parámetros S, tomando en cuenta la posición de los puertos muestra detección del contaminante en arena seca y saturada a las frecuencias de analisis.

To God, my family and my friends . . .

ACKNOWLEDGEMENTS

During the development of my graduate studies at the University of Puerto Rico several persons and institutions collaborated with my research. Without their support I would have not finish this work.

I want to begin by expressing my most sincere gratitude and acknowledgement to my advisor, Dr. Rafael A. Rodriguez Solis because he gave me the opportunity to conduct this research under his guidance and supervision. I would also like to thank Professor Dr. Ingrid Padilla by her motivation; encouragement and support during all my research. I want to thank to Dr. José Colom Ustáriz for teaching me excellent courses that contributed to my professional formation. Also I want to thank to CenSSIS team for providing a friendly work environment.

This work was supported in part by CenSSIS, the Center for Subsurface Sensing and Imaging Systems, under the Engineering Research Centers Program of the National Science Foundation (Award Number ECE-9986821).

Last, but most importantly I would like to thank God, my family, especially to my sister Julia P. Certuche, all my friends, and my boyfriend, for their unconditional support, inspiration and love.

Table of Contents

ABSTRACT.....	II
RESUMEN	III
ACKNOWLEDGEMENTS.....	V
TABLE OF CONTENTS	VI
TABLE LIST.....	VIII
FIGURE LIST	X
1 INTRODUCTION.....	2
1.1 JUSTIFICATION	4
1.2 OBJECTIVES	5
1.3 THESIS STRUCTURE.....	6
2 BACKGROUND THEORY AND LITERATURE REVIEW.....	7
2.1 OVERVIEW	7
2.2 BACKGROUND THEORY	8
2.2.1 <i>Electromagnetic Fields Propagation</i>	8
2.2.2 <i>Scattering Parameters Analysis</i>	14
2.3 LITERATURE REVIEW ON NUMERICAL METHODS	16
2.3.1 <i>Finite Difference method (FD)</i>	17
2.3.1.1 <i>Finite Difference Time Domain FDTD</i>	14
2.3.1.2 <i>Finite Difference Frequency Domain (FDTD)</i>	18
2.3.2 <i>Finite Element method (FE)</i>	24
3 MODELING OF THE ELECTROMAGNETIC FIELD OF THE SOIL-BED.....	30
3.1 OVERVIEW	30
3.2 DESCRIPTION OF THE LABORATORY SCALE 2D SOIL-BED	30
3.3 ELECTROMAGNETIC MODEL DESCRIPTION	31
3.3.1 <i>Mesh</i>	32
3.3.2 <i>Boundary Conditions</i>	33
3.3.3 <i>Frequencies of Operation</i>	35
3.3.4 <i>Excitations Ports</i>	37
3.3.4.1 <i>Excitation ports in HFSS</i>	38
3.3.4.2 <i>Excitation ports in XFDTD</i>	39
3.3.5 <i>Medium</i>	40
4 RESULTS AND ANALYSIS.....	42
4.1 OVERVIEW	42
4.2 EXPERIMENTAL SIMULATION.....	42
4.3 FINAL ELECTROMAGNETIC MODEL.....	48
4.3.1 <i>Simulations without DNAPL</i>	50
4.3.1.1 <i>Dry sand</i>	50
4.3.1.2 <i>Saturated sand</i>	53
4.3.1.3 <i>EM response for varying degrees of soil saturation level</i>	57
4.3.1.3.1 <i>First Level (L1)</i>	57

4.3.1.3.2	Second Level (L2).....	60
4.3.1.3.3	Third Level (L3).....	63
4.3.1.3.4	Fourth Level (L4).....	66
4.3.1.4	Analysis of S-parameters for varying degrees of soil saturation level.....	68
4.3.1.4.1	Dry Sand vs Saturated level L1.....	69
4.3.1.4.2	Dry Sand vs Saturated level L2.....	71
4.3.1.4.3	Dry Sand vs Saturated level L3.....	72
4.3.1.4.4	Dry Sand vs Saturated level L4.....	73
4.3.2	Simulations with DNAPL.....	73
4.3.2.1	Dry sand with DNAPL.....	74
4.3.2.1.1	DNAPL1.....	74
4.3.2.1.2	DNAPL2.....	76
4.3.2.1.3	DNAPL3.....	79
4.3.2.1.4	DNAPL4.....	81
4.3.2.2	Analysis of S-parameters in dry sand without and with DNAPL.....	84
4.3.2.3	Saturated Sand with DNAPL.....	87
4.3.2.3.1	DNAPL1.....	87
4.3.2.3.2	DNAPL2.....	90
4.3.2.3.3	DNAPL3.....	92
4.3.2.3.4	DNAPL4.....	95
4.3.2.4	Analysis of S-parameters in saturated sand.....	97
4.4	ELECTROMAGNETIC MODEL USING XFDTD	101
4.4.1	Dry Sand.....	101
4.4.1.1	Dry Sand with DNAPL1.....	103
4.4.1.2	Dry Sand with DNAPL2.....	104
4.4.1.3	Analysis of S-parameters in dry sand.....	106
4.4.2	Saturated Sand.....	109
4.4.2.1	Saturated sand with DNAPL1.....	111
4.4.2.2	Saturated sand with DNAPL2.....	112
4.4.2.3	Analysis of S-parameters.....	113
5	SUMMARY, CONCLUSIONS AND RECOMMENDATIONS.....	117
5.1	SUMMARY AND CONCLUSIONS	117
5.2	RECOMMENDATIONS.....	119

Table List

Tables	Page
Table 3.1: Electrical properties for dry and wet sand [32]	41
Table 3.2: Electrical properties for DNAPL (PCE) [7]	41
Table 4.1: S-parameters values for different sizes the ports size.....	46
Table 4.2: S-parameters for dry sand at frequency 285 MHz.....	52
Table 4.3: S-parameters for dry sand at frequency 515 MHz.....	52
Table 4.4: S-parameters for dry sand at frequency 1.5 GHz.....	52
Table 4.5: S-parameters for saturated sand at frequency 285 MHz.....	55
Table 4.6: S-parameters for saturated sand at frequency 515 MHz.....	55
Table 4.7: S-parameters for saturated sand at frequency 1.5 GHz	55
Table 4.8: S-parameters when saturated level L_1 inserted at 285 MHz	59
Table 4.9: S-parameters when saturated level L_1 inserted at 515 MHz	59
Table 4.10: S-parameters when saturated level L_1 inserted at 1.5 GHz.....	60
Table 4.11: S-parameters when saturated level L_2 inserted at 285 MHz	62
Table 4.12: S-parameters when saturated level L_2 inserted at 515 MHz	62
Table 4.13: S-parameters when saturated level L_2 inserted at 1.5 GHz.....	62
Table 4.14: S-parameters when saturated level L_3 inserted at 285 MHz	65
Table 4.15: S-parameters when saturated level L_3 inserted at 515 MHz	65
Table 4.16: S-parameters when saturated level L_3 inserted at 1.5 GHz.....	65
Table 4.17: S-parameters when saturated level L_4 inserted at 285 MHz	67
Table 4.18: S-parameters when saturated level L_4 inserted at 515 MHz	67
Table 4.19: S-parameters when saturated level L_4 inserted at 1.5 GHz.....	68
Table 4.20: S-parameters for dry sand at 285 MHz with DNAPL1	75
Table 4.21: S-parameters for dry sand at 515 MHz with DNAPL1	75
Table 4.22: S-parameters for dry sand at 1.5 GHz with DNAPL1	76
Table 4.23: S-parameters for dry sand at 285 MHz with DNAPL2	78
Table 4.24: S-parameters for dry sand at 515 MHz with DNAPL2	78
Table 4.25: S-parameters for dry sand at 1.5 GHz with DNAPL2	78
Table 4.26: S-parameters for dry sand at 285 MHz with DNAPL3	80
Table 4.27: S-parameters for dry sand at 515 MHz with DNAPL3	80
Table 4.28: S-parameters for dry sand at 1.5 GHz with DNAPL3	81
Table 4.29: S-parameters for dry sand at 285 MHz with DNAPL4	83
Table 4.30: S-parameters for dry sand at 515 MHz with DNAPL4	83
Table 4.31: S-parameters for dry sand at 285 MHz with DNAPL4	83
Table 4.32: S-parameters for saturated sand at 285 MHz with DNAPL1	89
Table 4.33: S-parameters for saturated sand at 515 MHz with DNAPL1	89
Table 4.34: S-parameters for saturated sand at 1.5 GHz with DNAPL1	89

Table 4.35: S-parameters for saturated sand at 285 MHz with DNAPL2	91
Table 4.36: S-parameters for saturated sand at 515 MHz with DNAPL2	91
Table 4.37: S-parameters for saturated sand at 1.5 GHz with DNAPL2	92
Table 4.38: S-parameters for saturated sand at 285 MHz with DNAPL3	94
Table 4.39: S-parameters for saturated sand at 515 MHz with DNAPL3	94
Table 4.40: S-parameters for saturated sand at 1.5 GHz with DNAPL3	94
Table 4.41: S-parameters for saturated sand at 285 MHz with DNAPL4	96
Table 4.42: S-parameters for saturated sand at 515 MHz with DNAPL4	96
Table 4.43: S-parameters for saturated sand at 1.5 GHz with DNAPL4	97
Table 4.44: S-parameters of dry sand at 285 <i>MHz</i> with XFDTD	102
Table 4.45: S-parameters of dry sand at 515 <i>MHz</i> with XFDTD	102
Table 4.46: S-parameters of dry sand at 1.5 <i>GHz</i> with XFDTD.....	102
Table 4.47: S-parameters of dry sand with DNAPL1 at 285 <i>MHz</i>	103
Table 4.48: S-parameters in dry sand with DNAPL1 at 515 <i>MHz</i>	104
Table 4.49 : S-parameters in dry sand with DNAPL1 at 1.5 <i>GHz</i>	104
Table 4.50: S-parameters in dry sand with DNAPL2 at 285 <i>MHz</i>	105
Table 4.51: S-parameters in dry sand with DNAPL2 at 515 <i>MHz</i>	105
Table 4.52: S-parameters in dry sand with DNAPL2 at 1.5 <i>GHz</i>	105
Table 4.53: S-parameters in saturated sand at 285 <i>MHz</i> with XFDTD	110
Table 4.54: S-parameters in saturated sand at 515 <i>MHz</i> with XFDTD	110
Table 4.55: S-parameters in saturated sand at 1.5 <i>GHz</i> with XFDTD.....	110
Table 4.56: S-parameters in saturated sand with DNAPL1 at 285 <i>MHz</i>	111
Table 4.57: S-parameters in saturated sand with DNAPL1 at 515 <i>MHz</i>	111
Table 4.58: S-parameters in saturated sand with DNAPL1 at 1.5 <i>GHz</i>	112
Table 4.59: S-parameters in saturated sand with DNAPL2 at 285 <i>MHz</i>	112
Table 4.60: S-parameters in saturated sand with DNAPL2 at 515 <i>MHz</i>	113
Table 4.61: S-parameters in saturated sand with DNAPL2 at 1.5 <i>GHz</i>	113

Figure List

Figures	Page
Figure 2.1: Electromagnetic waves propagations [11]	8
Figure 2.2: An arbitrary N-port network [10]	14
Figure 2.3: Unit cell with labeled field components [23]	19
Figure 2.4: Schematic representation of the borehole dipole antenna geometry [21]	22
Figure 2.5: Grid for a 3D structure for discretization of Maxwell's equations [15]	24
Figure 2.6: Typical triangular element [28]	25
Figure 3.1: Two-Dimensional flow setup [4]	31
Figure 3.2: Boundary conditions in HFSS Simulator	34
Figure 3.3 Boundary conditions in XFDTD Simulator	35
Figure 3.4. Standing wave patterns.....	37
Figure 3.5: Excitations ports in HFSS	38
Figure 3.6: Excitation ports in XFDTD	39
Figure 4.1: E-field propagation with three experimental frequencies: a) 300 MHz, b) 600 MHz, and c) 1 GHz.....	44
Figure 4.2: E-field propagation, with 5 receiver ports at 515 MHz in dry sand at	47
Figure 4.3: Design for the final electromagnetic model at 285 MHz	48
Figure 4.4: E-field propagation without DNAPL with P3 as transmitter port for dry sand, a) 285 MHz, b) 515 MHz and, c) 1.5 GHz	51
Figure 4.5: E-field propagation without DNAPL with P3 as transmitter port for wet sand:..	54
Figure 4.6: Reciprocity analysis of S-parameters for saturated sand at the frequency 1.5 GHz: a) Reciprocity P ₁ -P ₅ , b) Reciprocity P ₂ -P ₆ , c) Reciprocity P ₃ -P ₇ ,.....	57
Figure 4.7: E-field distribution from P ₃ with 10% saturated level (L ₁) inserted: a) 285 MHz, b) 515 MHz and c) 1.5 GHz.....	58
Figure 4.8: E-field distribution from P3 with 33.3% saturated level (L ₂) inserted:.....	61
Figure 4.9: E-field distribution from P3 with 50% saturated level (L ₃) inserted: a) 285 MHz, b) 515 MHz and c) 1.5 GHz.....	64
Figure 4.10: E-field distribution from P3 with 66.6% saturated level (L ₄) inserted:.....	66
Figure 4.11: Comparison of S-parameters at 285 MHz for the four soils saturated:	69
Figure 4.12: Comparison of S-parameters at 515 MHz for the four soils saturated:	70
Figure 4.13: Comparison of S-parameters at 1.5 GHz for the four soils saturated:.....	71
Figure 4.14: E-field distribution in dry sand with DNAPL1 from P ₃ : a) 285 MHz,	74
Figure 4.15: E-field distribution in dry sand with DNAPL2 from P ₃ : a) 285 MHz,	77
Figure 4.16: E-field distribution in dry sand with DNAPL3 from P ₃ : a) 285 MHz,	79
Figure 4.17: E-field distribution in dry sand with DNAPL4 from P ₃ : a) 285 MHz,	82
Figure 4.18: Comparison of S-parameters obtain in dry sand with average DNAPL	85
Figure 4.19: Comparison of S-parameters obtain in dry sand with average DNAPL	86

Figure 4.20: Comparison of S-parameters obtain in dry sand with average DNAPL	87
Figure 4.21: E-field distribution in saturated sand with DNAPL1 from P ₃ : a) 285 MHz,	88
Figure 4.22: E-field distribution in saturated sand with DNAPL2 from P ₃ : a) 285 MHz,	90
Figure 4.23: E-field distribution in saturated sand with DNAPL3 from P ₃ : a) 285 MHz,	93
Figure 4.24: E-field distribution in saturated sand with DNAPL4 from P ₃ : a) 285 MHz,	95
Figure 4.25: Comparison of S-parameters obtain in saturated sand with average DNAPL ...	98
Figure 4.26: Comparison of S-parameters obtain in saturated sand with average DNAPL ...	99
Figure 4.27: Comparison of S-parameters obtain in saturated sand with average DNAPL .	100
Figure 4.28: Comparison of S-parameters in dry sand with average DNAPL at 285MHz for a) Transmitter P ₁ , b) Transmitter P ₂ , c) Transmitter P ₃ ,	107
Figure 4.29: Comparison of S-parameter in dry sand with average DNAPL at 515MHz	108
Figure 4.30: Comparison of S-parameters in dry sand with average DNAPL at 1.5 GHz ...	109
Figure 4.31: Comparison of S-parameters in saturated sand with average DNAPL at 285 MHz, for a) Transmitter P ₁ , b) Transmitter P ₂ , c) Transmitter P ₃ ,	114
Figure 4.32: Comparison of S-parameters in saturated sand with average DNAPL at 515MHz for a) Transmitter P ₁ , b) Transmitter P ₂ , c) Transmitter P ₃ ,	115
Figure 4.33: Comparison of S-parameters in saturated sand with average DNAPL at 1.5 GHz for a) Transmitter P ₁ , b) Transmitter P ₂ , c) Transmitter P ₃ ,	116

1 INTRODUCTION

In the past years, the study of contaminated sites had covered much interest in soil and environmental engineering, due to amount of harm caused on environment and human health. Most of these contaminants found in soil and groundwater are Dense Non-Aqueous Phase Liquids (DNAPL), which are liquids denser than water that don't dissolve or mix easily in water. Many of these DNAPL are chlorinated solvents, wood preservatives, coal tar wastes and pesticides [1]. Furthermore, these contaminants pose long-term perseverance and heterogeneous distribution that limits its detection and characterization [2].

Currently, there are studies on various techniques to detect DNAPLs in the subsurface such as monitoring wells, multi-level samplers, organic chemical analyses of soil samples at different depths, and soils borings or cone penetrometers to determine site stratigraphy; these techniques of detection are divided into invasive and non-invasive methods [3]. The invasive techniques of detecting underground contaminants can require drilling, testing, and sampling, such as Direct Push Probe Technologies (DPT) and In-Situ Tracers (IST), increasing the risk of establishing a new path for the spreading of the DNAPL. The non-invasive techniques such as Geophysical Methods (GM), offer rapid and relatively inexpensive characterization avoiding the risk of additional vertical migration of pooled DNAPL [4], [5].

Geophysical methods of locating subsurface DNAPL include Ground Penetrating Radar (GPR), Cross-Well Radar (CWR), Electrical Resistance Tomography (ERT), Vertical Induction Profiling, and Seismic Reflection [6]. These technologies do not involve penetrability in the DNAPL zone. They have a conceptual advantage over conventional methods of characterizing DNAPL zones, in that they do not risk alter the geosystem and increase the DNAPL distribution. However, since they rely on properties of the system rather than direct measurements of the contaminated medium, they are subject to numerous interferences and interpretive errors [6].

The Center for Subsurface Sensing and Imaging Systems (CenSSIS) is a National Science Foundation (NSF) Engineering Research Center (ERC), which combines multi-disciplinary resources to revolutionize the existing technology for the detection of source of contaminants and the characterization of the soil in the subsurface [7]. CenSSIS developed Cross Well Radar (CWR) technologies to detect and monitor DNAPL contaminants in underground environments. As part of this effort, a laboratory-scale 2-D Soil-BED setup has been developed to establish controlled flow and electromagnetic conditions, and minimize the generation of DNAPL contaminated soil [4].

1.1 Justification

To prevent the effects in human health and environment caused by the contamination of the subsurface and groundwater, it is necessary to detect and to characterize the contaminated sites in order to obtain a possible remediation. Detection of Dense non-aqueous Phase Liquids (DNAPL) contaminants is limited because of their heterogeneous distribution in subsurface environments. Additionally, invasive techniques in polluted areas can cause spreading of contaminants in contrast with the non-invasive detection methods that to avoid the movement of pooled DNAPL [2].

Non-invasive electromagnetic methods have been developed based in knowledge of electrical properties of soils and groundwater, such as Ground Penetrating Radar (GPR) and Cross-Well Radar (CWR). Ground Penetrating Radar uses antennas located on the surface of the ground for transmitting and receiving high frequency electromagnetic waves in the tens of megahertz to gigahertz range. This method is used to delineate near surface, map the extent of buried waste, locate the water table, and find buried utilities [8]. GPR detection technologies depend on the contrast between the dielectric permittivities of the soil medium, water and DNAPLs to determine water contents, and detect contamination of organic immiscible fluids [2]. The GPR method is applied at the soil surface and detection in underground systems is limited to shallow depths. Furthermore, the results are highly dependent on soil moisture conditions and soil type, because the radar signal is attenuated by the soil [1].

Cross-Well Radar is similar to Ground Penetrating Radar except that antennas are located in wells. This method overcomes the GPR depth limitations but the distance between the wells strongly influences the effectiveness of the method [6]. As the distance between transmitting and receiving wells increases, radar wave amplitudes attenuate, which creates greater difficulty in distinguishing the wave from background noise [1].

Computational methods get around problem of to detect and to characterize by approximating the waves over small regions of space and combining them with simple relations. Given a computer with enough memory and power, arbitrarily large wave problems can be accurately solved [9].

The purpose of this research is to analyze electromagnetic simulations for the laboratory-scale 2-D Soil-BED developed by CenSSIS, using some computational methods with the objective of create a benchmark for characterization of soil studying the electromagnetic wave propagation.

1.2 Objectives

The objective of this thesis is to determine the possibility to detect a contaminant in the subsurface with CWR technology, by means of a computational model of the laboratory-scale 2-D Soil-BED. This model is based on electromagnetic simulations that serve as a

benchmark for laboratory experiments and to verify the possibility of detection of the contaminant in the soil. Specific objectives for this work are:

- Describe the laboratory-scale 2-D Soil-BED setup at the Civil Engineering building at the University of Puerto Rico (Mayaguez campus).
- Determine the electromagnetic field distribution under different subsurface conditions and different excitation frequencies.
- Analyze the wave propagation characteristics to determine if it is possible to detect any pollution in soil
- Analyze the network parameters to determine if it is possible to detect any pollution in soil.

1.3 Thesis Structure

This thesis document consists of five additional chapters. Chapter 2 contains the background theory of different methods of electromagnetic analysis. Chapter 3 provides a complete description of the electromagnetic model for laboratory of the Soil-Bed with different soil conditions using commercial electromagnetic design software. Chapter 4 presents the results obtained and its analysis. Finally, Chapter 5 presents the conclusions and recommendations for future work.

2 BACKGROUND THEORY AND LITERATURE REVIEW

2.1 Overview

The Center for Subsurface Sensing and Imaging Systems (CenSSIS) combines multi-disciplinary resources to revolutionize the existing technology for the detection of source of contaminants and the characterization of the soil in the subsurface [7]. CenSSIS developed several laboratory-scales Soil-BED setup to detect and monitor DNAPL contaminants site in underground environments using Cross Well Radar (CWR) technologies [4], [5].

Cross Well Radar technology uses antennas that are placed into sampling wells. The waves emitted from an antenna are received in another in order to observe possible change in the radar waves caused by contrasting of the electromagnetic (EM) properties between the medium and DNAPL [3]. Therefore, is necessary to study some characteristics of the EM wave propagation to analyze these changes.

The next section gives a basic electromagnetic wave propagation theory and network parameters theory.

2.2 Background Theory

2.2.1 *Electromagnetic Fields Propagation*

Electromagnetic (EM) field theory is a discipline concerned with the study of charges, at rest and in motion, that produce currents and electric-magnetic fields. The electromagnetic fields are a combination of strengths field electric and magnetic, which oscillate in phase perpendicular to each other and to the direction of energy propagation [10]. See Figure 2-1.

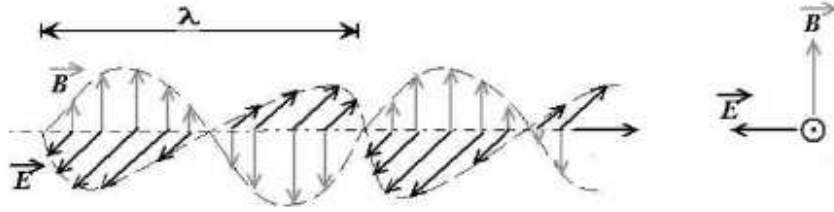


Figure 2.1: Electromagnetic waves propagations [11]

Electric and magnetic phenomena at the macroscopic level are described by Maxwell's equations, which can be written either in differential or in integral form [10]. According to [12], the differential form of Maxwell's equations is the most widely used representation to solve boundary-value electromagnetic problems used to describe the field vectors in space and in time. Maxwell's equations in differential form are shown in (2.1) - (2.4).

$$\nabla \times \vec{E} = -\frac{\partial \vec{B}}{\partial t} - \vec{M} \quad 2.1$$

$$\nabla \times \vec{H} = \frac{\partial \vec{D}}{\partial t} + \vec{J} \quad 2.2$$

$$\nabla \cdot \vec{D} = \rho_{ev} \quad 2.3$$

$$\nabla \cdot \vec{B} = \rho_{mv} \quad 2.4$$

Maxwell's equations in the integral form (2.5) - (2.8), describe the relations of the field vectors, charge densities, and current densities over an extended region of space. The integral form can be derived from its differential form by utilizing the Stokes' and divergence theorems [12].

$$\oint_c \vec{E} \cdot d\vec{l} = -\iint_s \vec{M} \cdot d\vec{s} - \frac{\partial}{\partial t} \iint_s \vec{B} \cdot d\vec{s} \quad 2.5$$

$$\oint_c \vec{H} \cdot d\vec{l} = \iint_s \vec{J} \cdot d\vec{s} + \frac{\partial}{\partial t} \iint_s \vec{D} \cdot d\vec{s} \quad 2.6$$

$$\oiint_s \vec{D} \cdot d\vec{s} = Q_e \quad 2.7$$

$$\oiint_s \vec{B} \cdot d\vec{s} = Q_m \quad 2.8$$

These quantities E, H, D, B, J, M and Q represent time-varying vector fields and are real functions of spatial coordinates x, y, z , and the time variable t . These quantities are defined as follows [12]:

\vec{E} is the electric field intensity, in V/m.

\vec{H} is the magnetic field intensity, in A/m.

\vec{D} is the electric flux density, in Coul/m².

\vec{B} is the magnetic flux density, in Wb/m².

\vec{M} is the magnetic current density, V/m².

\vec{J} is the conduction current density, in A/m².

ρ_{ev} is the electric charge density, in Coul/m³.

ρ_{mv} is the magnetic charge density, in Wb/m³.

Q_e is the electric charge, in Coul.

Q_m is the magnetic charge, in Coul.

All of materials contain charged particles, and are subjected to electromagnetic fields. Their charged particles interact with the electromagnetic vectors, producing currents and modifying the electromagnetic wave propagation in the media compared to that in free space. These currents and modified electromagnetic field depend on the constitutive parameters (ϵ , μ and σ) where μ is the magnetic permeability, ϵ is the dielectric permittivity and σ is the electrical conductivity of the medium respectively. The constitutive parameters are used to characterize the electrical properties of a material [12].

The following equations, shown the relation among the electric and magnetic field intensities, flux densities and the constitutive parameters in the free space:

$$\vec{B} = \mu \vec{H} \quad 2.9$$

$$\vec{D} = \epsilon \vec{E} \quad 2.10$$

$$\vec{J} = \sigma \vec{E} \quad 2.11$$

$$\vec{M} = \chi_m \mu \vec{H} \quad 2.12$$

where, χ_m is the magnetic susceptibility, for magnetic materials. The expressions (2.9-2.12) are referred to as the constitutive relations; μ , ϵ and σ are referred to as the *constitutive parameters*, which are functions of the applied field strength, the position within the medium, the direction of the applied field, and the frequency of operation. In general, materials are characterized as dielectric, magnetic, and conductors depending on the predominant phenomenon as polarization, magnetization, or conduction [12].

Media can be considered lossless or lossy. Inside a lossless medium the electromagnetic wave is not attenuated, then $\sigma \cong 0$ or $\sigma \ll \omega \epsilon$; and in lossy media, the electromagnetic wave is attenuated then $\sigma \neq 0$ or $\sigma \gg \omega \epsilon$.

In other words, the wave propagation in the medium depends not only of the constitutive parameters but also of the operation frequency. Therefore, solving the equation (2.2) for a lossy medium, the permittivity is treated as a complex function like as is in the equation (2.12) [13],

$$\varepsilon = \varepsilon' - j\varepsilon'' \quad 2.13$$

Where ε' is the real part of the permittivity, which is related to the stored energy within the medium, and ε'' is the imaginary part of the permittivity, which is related to the dissipation (or loss) of energy within the medium.

Generally, the dielectric permittivity is compared to free space, as the *relative dielectric permittivity*:

$$\varepsilon_r' = \frac{\varepsilon'}{\varepsilon_0} \quad 2.14$$

$$\varepsilon_r'' = \frac{\varepsilon''}{\varepsilon_0} + \frac{\sigma}{\omega\varepsilon_0} \quad 2.15$$

where, σ is the electrical conductivity of the medium, ω is the angular frequency.

Rewriting the equation (2.2) in terms of equation (2.12), it is obtained the equation (2.16).

$$\begin{aligned} \nabla \times H &= J + j\omega\varepsilon E = \sigma E + j\omega(\varepsilon' - j\varepsilon'')E \\ &= (\sigma + \omega\varepsilon'') + j\omega\varepsilon' E \end{aligned} \quad 2.16$$

The term $(\sigma + \omega\varepsilon'')$ is the equivalent electrical conductivity, which is the sum of the AC and DC terms, (2.15) [14].

$$\sigma_{equiv} = \sigma_{DC} + \sigma_{AC} \quad 2.17$$

Where, σ_{DC} and σ_{AC} are the static conductivity and alternating conductivity of the media. The alternating conductivity is calculated by (2.17) [14]:

$$\sigma_{DC} = -q_{ve}\mu_e \quad 2.18$$

$$\sigma_{AC} = \omega\epsilon_r'' \quad 2.19$$

where, q_{ve} is the electron charge density and μ_e is defined to be the electron mobility of the material. The conductivity varies as a function of frequency [12].

In real world problems, the fields undergo reflection and transmission due to boundaries, scatterers and other objects encountered in the medium. In order to obtain the portion of wave reflected or transmitted into the medium, it is necessary to derive the reflection and transmission coefficients. The reflection and transmission coefficients are functions of the constitutive parameters (μ , ϵ and σ) of the two mediums, the direction of wave travel (angle of incidence), and the direction of the electric and magnetic fields (wave polarization) [12].

The basic analysis of the reflection and transmission coefficients when an electromagnetic wave changes from one medium to other one is presented in the next section.

2.2.2 Scattering Parameters Analysis

The scattering parameters or S-parameters are used to analyze microwave circuits (high frequencies) \. These parameters relate the input and output variables of the circuits.

When the analysis of the S-parameters is made in a multi-port network analyzer, the parameters are stored in a matrix named a *scattering matrix* [10].

According to the N-port network shown in Figure 2-2, the scattering matrix, or S-matrix, is defined in relation to these incident and reflected voltage wave as (equations 2.18-219):

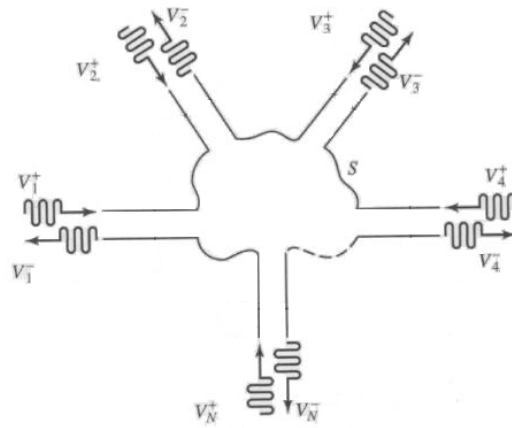


Figure 2.2: An arbitrary N-port network [10]

$$\begin{bmatrix} V_1^- \\ V_2^- \\ \vdots \\ V_N^- \end{bmatrix} = \begin{bmatrix} S_{11} & S_{12} & \cdots & S_{1N} \\ S_{21} & & & \vdots \\ \vdots & & & \\ S_{N1} & \cdots & & S_{NN} \end{bmatrix} \begin{bmatrix} V_1^+ \\ V_2^+ \\ \vdots \\ V_N^+ \end{bmatrix} \quad 2.20$$

or

$$[V^-] = [S][V^+] \quad 2.21$$

where, V_n^+ is the amplitude of the voltage wave incident on port n , and V_n^- is the amplitude of the voltage wave reflected from port n [10].

A specific element of the $[S]$ matrix can be determined as:

$$S_{ij} = \left. \frac{V_i^-}{V_j^+} \right|_{V_k^+ = 0 \quad k \neq j} \quad 2.22$$

In equation (2.18), the terms S_{ij} represent transmission coefficients, and the terms S_{ii} represent reflection coefficients.

Different numerical methods have been applied to provide electromagnetic models computational based on Maxwell's equations. The literature reviews on some of these are mentioned in the next section.

2.3 Literature Review on Numerical Methods

The electromagnetic analysis of real world problems can present difficulties because closed-form solutions to the differential equations often do not exist due to its geometry. Numerical methods get around this problem by approximating the waves over small regions of space and combining them with simple relations [9]. Most of the numerical methods are restricted to special geometries [15].

Some applicable techniques are:

Spectral-domain approach (SDA), is an analytical and numerical technique that applies integral transforms, such as the Fourier and Hankel transforms, to the solution of boundary-value and initial-value problems [16], this method can only be applied to planar structures and losses are introduced by a perturbational calculation [17].

Method of Moments (MOM), requires the knowledge of special functions as the Green's function [17] and are therefore mainly restricted to planar or symmetrical structures [15].

Finite Element method (FE), investigates the propagation characteristics of any arbitrarily shaped structure using a triangular mesh in the frequency domain [18].

Finite Difference method (FD), discretizes the differential Maxwell's equations in space and time [19].

The Finite Difference method (FD) and Method of Moments (MOM) are conceptually simpler and easier to program than the Finite Elements method (FE) [20]. However, FE method is a more powerful and versatile numerical technique for handling problems involving complex geometries and inhomogeneous media [20]. The electromagnetic (EM) simulators more commonly used are based on the Finite Element method and the Finite Difference method.

The objective of this research is to verify if it is possible the contaminant detection through electromagnetic model based on simulations, using various EM softwares. The next sections give fundamentals of the numerical methods FE and FD.

2.3.1 Finite Difference method (FD)

The FD methods provide a simple way to study wave scattering in the time and frequency domains. These methods approximate Maxwell's Partial Differential Equations (PDE) by multi-dimensional centered difference equations in space. Since it finely discretizes space, FD methods effectively capture rapid field changes, as well as intricate geometry variations, and are well suited for problems involving inhomogeneous volumes and rough boundaries [9]. The more common computational approaches in FD for studying dielectric structures are the Finite Difference Time Domain (FDTD) and Finite Difference in the Frequency Domain (FDFD).

2.3.1.1 *Finite Difference Time Domain (FDTD)*

The FDTD method is rapidly becoming one of the most widely used computational methods in electromagnetic analysis [21], since it can cover a wide frequency range with a single simulation run, and the interest in electromagnetic interactions with complicated geometries, which include penetrable dielectric and magnetic materials [22]. One of the advantages to using the FDTD technique is that all the frequency components of the scattered field may be computed simultaneously [21].

The FDTD method belongs in the general class of grid based on differential Maxwell's equations in time domain and are modified to central-difference equations, discretized, and implemented in software. A FDTD algorithm solves the electric field at a given instant in time, then the magnetic field are solved at the next instant in time, and the process is repeated over and over again [23].

A unit cell with its electric and magnetic fields is shown in Figure 2-3.

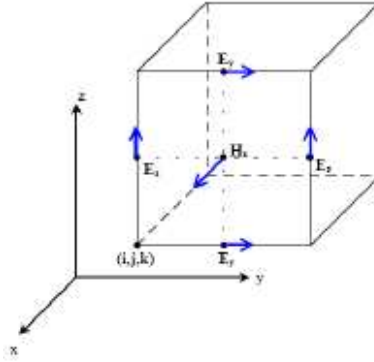


Figure 2.3: Unit cell with labeled field components [23]

FDTD algorithms have been applied to model wave propagation in lossy, dispersive, inhomogeneous soils. This type of modeling is extremely useful for predicting the performance of Ground Penetrating Radar (GPR) systems in specified inhomogeneous environments. The computer modeling the electromagnetic fields scattered by various types of scattering objects such as buried waste drums, metallic or dielectric pipes, and pollution plumes. Also are useful for testing GPR detection and imaging algorithms with synthetic data [21].

Three-dimensional FDTD methods (3D FDTD) have been applied to accommodate dispersive medium using a wave propagation model in heterogeneous soils. A 3D FDTD code was used to model electromagnetic waves for Cross Well Radar (CWR) and Ground Penetrating Radar (GPR) systems [24]. The code was developed at Northeastern University's (NU) Center for Subsurface Sensing and Imaging Systems (CenSSIS) to study effectiveness in detecting mines buried in the soil [25]. The code was modified to model non-homogenous

soil (different regions or layers), water and also was modified for simulation of monopole and dipole antennas in soil boreholes [24].

The 3D FDTD code is derived from the differential form of Maxwell's equations, where all field quantities \vec{D} , \vec{E} , \vec{B} , \vec{H} and \vec{J} are a function of the space coordinates and time. Here D is the electric flux density, E is the electric field, B is the magnetic flux density, H is the magnetic field, J electric current density, and μ ; ϵ y σ are the constitutive parameters [12]. In rectangular coordinates, the Maxwell's equations may be combined as shown in (2.15).

$$\epsilon \frac{\partial E_z}{\partial t} = \frac{\partial H_y}{\partial t} - \frac{\partial H_x}{\partial t} - \sigma E_z \quad 2.23$$

These partial differential equations are discretized in a 3D rectangular grid $(x, y, z) = (i\Delta_x, j\Delta_y, k\Delta_z)$ using the central-difference approximation of two consecutive values for the field components in both space and time [19], where, Δ_x, Δ_y , and Δ_z are the space increments; and i, j , and k represent the cell location. In space discretization, the electric and magnetic field components are assigned to edges of complementary interlocking cubical mesh. The electric fields are computed at integer time steps, while the magnetic fields are iteratively computed on half integer time steps. Thus, the finite difference equations are second order in both space and time [24].

The grid size in 3D FDTD limits the stability and the accuracy of the method, and the time step size. Therefore, for better results, the largest side of a grid cell should be much smaller than the smallest wavelength, and the time increment should satisfy the Courant condition [22] given in (2.22),

$$V_{p,\max} \Delta t \leq \left[\frac{1}{\Delta x^2} + \frac{1}{\Delta y^2} + \frac{1}{\Delta z^2} \right]^{-1/2} \quad 2.24$$

where, $V_{p,\max}$, is the maximum wave phase velocity within the model and Δt is the time increment. A third restriction for the grid size is the geometric size of the modeled problem, and the time-step size must be proportional to the spatial grid size for numerical stability. Consequently, if the spatial resolution is doubled, the number of time steps must be doubled. The principal advantage of this technique is that requires only one simulation run to analyze geometry under a broad range of frequencies. [24].

The 3D FDTD was used in [25] to model soil medium along with different antenna types (half-wave dipole antenna and monopole antenna) to evaluate feasibility of Cross Well Radar (CWR) for DNAPL detection. The authors initially analyzed this problem without DNAPL, where they observed that the components of the electromagnetic field were symmetric and propagated outward. They assumed a DNAPL zone like a rectangular pool (see Figure 2-4). The results showed that propagation of the E-field is scattered by the presence of the DNAPL in soil, establishing the magnitude the field perturbation by the contaminant. In addition, they concluded that the results depend on the antenna position and the type of excitation used.

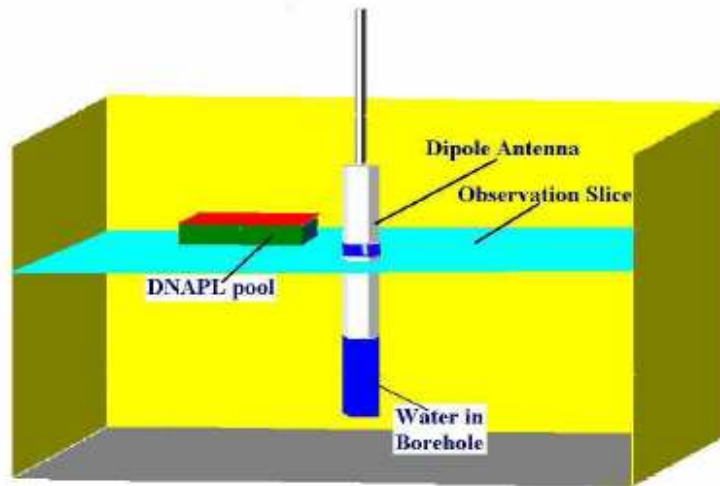


Figure 2.4: Schematic representation of the borehole dipole antenna geometry [21]

The Difference Time Domain (FDTD) is fast, accurate, easy to implement, and intuitive. Also is best for wideband (short pulse) scattering in non-uniform media. Special means must be developed for dispersive media, such as soil and biological tissue [9]. The principal advantage of Finite Difference Time Domain FDTD method is that only is necessary one step for different electromagnetic calculations of a broad range of frequencies.

2.3.1.2 Finite Difference Frequency Domain (FDFD)

The S -parameters are part of electromagnetic studies and represent frequency-domain quantities [26]. The Finite Difference Frequency Domain (FDFD) method gives a straightforward derivation of the scattering matrix (S -parameters). Also, this technique is

used when the materials have a frequency dependence (e.g. lossy medium) causing complex permittivity and permeability [26] in the frequency domain.

A generalized version of FDFD, to model monolithic microwave integrated circuits (MMIC) chip interconnections, was made in [15]. The authors included the discretization and the derivation of the scattering parameters and verified the numerical procedure. They demonstrated the capability of the method and its applicability to practical problems (i.e., monolithic microwave integrated circuits, waveguide transitions, electromagnetic compatibility, and fields in biological media or similar structures). In this paper, the structure under consideration was enclosed in a rectangular box (Figure 2-5), where the whole box was divided into n elementary cells filled with arbitrary materials. Furthermore, the walls of the box were set as perfectly conducting except for the two planes at the front and back sides. Every cell were defined the three field components (x, y, z) for electric and magnetic fields, which were used for discretization of Maxwell's equations. Therefore, there is a relation between the field components of the neighboring cells. For this reason, these equations are solved in the frequency domain by solution of a boundary value problem.

In order to solve the resulting system of equations in [15], it was necessary a supercomputer, which could deal with up to 55,000 elementary cells.

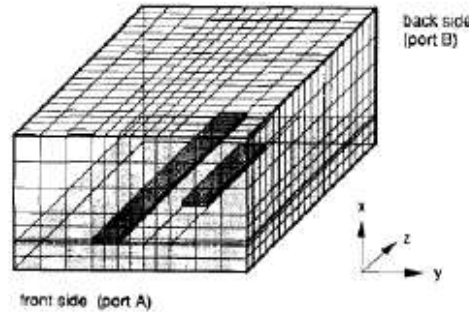


Figure 2.5: Grid for a 3D structure for discretization of Maxwell's equations [15]

FDFD is good for non-uniform media. This method handles frequency dependent media easily and is particularly useful for signal processing forward models. In comparison the FDTD, FDFD is less computationally expensive when only one frequency is analyzed, but for analysis under a broad range of frequencies, it is necessary to do several simulations by incrementing the computational cost [9].

2.3.2 Finite Element method (FE)

The FE method is a good choice for solving the Maxwell's partial differential equations over inhomogeneous or complex domains by representing a geometrically complicated domain as a collection of sub-domains that allow an easy construction of the approximation functions [27].

In this technique, the domain of the problem is viewed as a collection of non-intersecting simple sub-domains called *finite elements*, typically triangular elements (see Figure 2-6). Over each finite element, the solution is approximated by a linear combination of undetermined parameters and preselected algebraic polynomials [27].

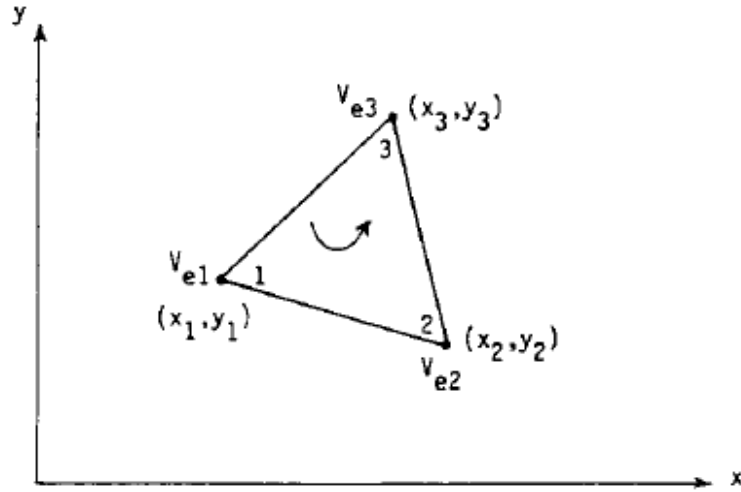


Figure 2.6: Typical triangular element [28]

In Figure 2-6, each vertex number has its coordinate corresponding as $V_{e1} \rightarrow (x_1, y_1)$, $V_{e2} \rightarrow (x_2, y_2)$, and $V_{e3} \rightarrow (x_3, y_3)$. Also, a normal unit vector at each side is assigned: \mathbf{n}_{12} to side (1-2), \mathbf{n}_{23} to side (2-3), and \mathbf{n}_{31} to side (3-1). For each element, the transverse electric and magnetic field components are expressed by using 12 unknown parameters (2.17) [18]:

$$E_t = \sum_{m=1}^6 N_m(x, y) \phi_m \quad 2.25$$

$$H_t = \sum_{m=7}^{12} N_{m-6}(x, y) \phi_m \quad 2.26$$

where, ϕ_m (for $m = 1 \sim 2$) denotes unknown parameters and $N_m(x, y)$ (for $m = 1 \sim 6$) represents linear vectors shape functions [28]. The vector shape functions are determined by the scalar shape functions and the normal unit vectors in the element [18].

The finite element analysis of any problem involves basically four steps: 1) discretizing the solution region into finite number of subregions or elements, 2) deriving governing equations for a typical element, 3) assembling of all elements in the solution region, 4) and solving the system of equations obtained [28].

The Finite Element (FE) method has been employed in diverse areas such as waveguide problems, electric machines, semiconductor devices, microstrips, and absorption of electromagnetic (EM) radiation by biological bodies [20].

Several problems have been identified when the nodal based finite elements are employed to compute vector electromagnetic fields, such as, long computation time, large amount of memory, satisfaction of the appropriate boundary conditions at material and conducting interfaces [29]. An approach for the nodal finite elements has been developed in order to solve these problems. This approximation uses edge finite elements (or vector finite

elements), which are geometrically the same that nodal. The nodal element has one shape function associated with each of the nodes; the edge element has one shape function for each of the edges. Also, edge finite elements satisfy continuity of only tangential or normal field components across interfaces between two adjacent finite elements. For this reason, edge finite element approximations can be used to model electromagnetic field since they do not impose any additional constraints on the approximated field apart from those prescribed by the nature of the field itself [29].

The performance of the software, based on edge finite element method, requires less amount of memory than the software based on nodal finite element method. This fact is important when analyzing complex 3-D electromagnetic field distributions. Some simulation programs have been developed based on Finite Elements method for the analysis of the electromagnetic field that can be used to calculate parameters such as *S* Parameters, resonant frequency, and field. Some of these programs are: ANSYS/Emag (ANSYS Inc.), Maxwell 2D and Maxwell 3D (Ansoft Corporation), COSMOS/EMS (Structural Research & Analysis Corporation), Algor/Electrostatic (Algor Inc.), QuickField (Tera Analysis Ltd.), FlexPDE (PDE Solutions Inc.) and etc. These programs differ in number of solved different electromagnetism problems, computer resource demand, preprocessor and postprocessor possibilities, integration with other finite element and automated design programs [29].

Some comparisons between Finite Difference FD and Finite elements FE methods are [20]:

1. The FD method is an approximation to the Maxwell's partial differential equations; the FE method is an approximation to its solution.
2. FE method is able to handle complex geometries and boundaries, while FD method in its basic form is restricted to handle rectangular shapes and simple alterations.
3. The most attractive feature of FD is that it can be very easy to implement.
4. The disadvantage of the FE method lies in the irregularity of the meshes, which requires additional effort in preparing the input data.

This thesis uses two commercial different software, these are:

HFSS: Ansoft's High Frequency Structure Simulator is based on the Finite Element Method (FE) and can be used to calculate the full 3-D EM field inside a structure. In HFSS, the geometric model is automatically divided into a large number of tetrahedra, where a single tetrahedron is a four-sided pyramid. This collection of tetrahedra is referred to as the finite element mesh. There is a trade-off among the size of the mesh, the desired level of accuracy, and the amount of available computing resources. It is desirable to use a mesh fine enough to obtain an accurate field solution but not so fine that it overwhelms the available computer memory and processing power [29].

XFDTD: Remcom's XFDTD simulator is a three-dimensional full wave electromagnetic solver based on the Finite Difference Time Domain method (FDTD). Applications include microwave, RF, antennas, scattering, biological EM, photonics, packaging, EMC, and specialized materials. An XFDTD simulation is referred to as a project, where each project

has a geometry file with the description of the structure or device to be simulated, and a parameter file that includes the inputs and outputs defined [31].

In order to detect and characterize DNAPL contaminated soils, different models have been developed, using the CWR technique. The model in [32] used transmitter and receiver antennas placed in boreholes equally distributed on a circle with radius 15.3 cm, each borehole is spaced from one another at 45° . These antennas were located below the air-soil interface, at different depths (22.9, 27.9, and 33 cm, respectively). The detection and location of the contaminant in the subsurface was achieved with different positions and depths of the antennas, using a wide frequency range (500 MHz to 2.2 GHz) [32].

The work presented in [32] was analyzed in [33] for three different computational methods, however the analysis of the electromagnetic fields propagation and the analysis for different frequencies were not discussed.

The research in [32] and [33] are of great interest for our work, since those provide an understanding of CWR technology for different structures and computational models by making several detection processes.

3 METHODOLOGY OF THE COMPUTATIONAL MODEL FOR DETECTION OF THE CONTAMINANT

3.1 Overview

This chapter presents the methodology of the electromagnetic model of the Soil-Bed setup. The setup is modeled with two different commercial softwares based on Finite Element (FE) and Finite Difference Time Domain (FDTD) numerical methods, varying the electrical conditions of the soil, geometry of the tank and at operations different frequencies and in this way to know if the detection of the contaminant in the subsurface is possible.

3.2 Description of the laboratory scale 2D Soil-Bed

The laboratory-scale 2D Soil-BED setup developed in [4] consists of a Plexiglass tank with length, height and width of 100 *cm* by 100 *cm* by 7 *cm*, respectively. It has two vertical metal meshes of dimensions 82 *cm* by 82 *cm* of length and height, these mesh panels act as a parallel plate transmission line, forcing a TEM electromagnetic field between the plates. The hole size is selected so that it looks electromagnetically as a solid plate, and it does not interfere with the DNAPL's flow into the system. The metal meshes are centered in the tank

and separated by 2 cm. The Soil-BED system is shown in Figure 3-1. This tank was filled with dry sand, saturated with water, and injected with DNAPL. Also, loop antennas were situated on the lateral sides of the tank, where one of those transmits the electromagnetic signal while the others receive it [4].

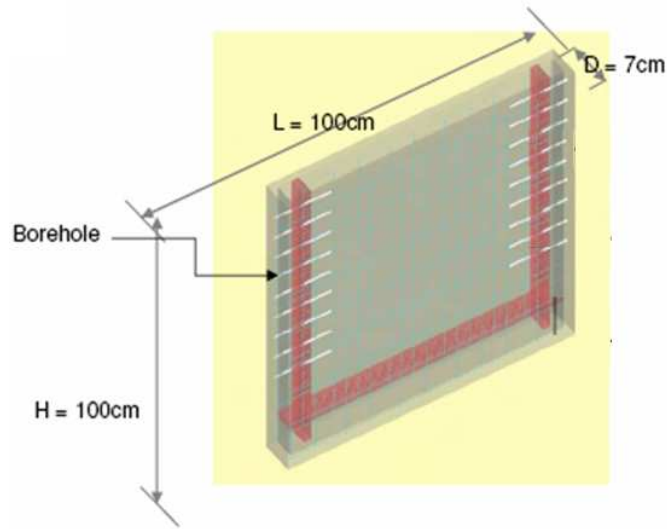


Figure 3.1: Two-Dimensional flow setup [4]

In this thesis, an electromagnetic model is developed for this laboratory scale 2D Soil-BED setup, to describe the electromagnetic field behavior inside it.

3.3 Electromagnetic Model Description

The laboratory-scale 2D Soil-BED contains two parallel flat, conductor meshes separated by a dielectric material (e.g., soil). These meshes are considered as parallel plates conductors for the electromagnetic study of the system. Taking this into consideration, when a signal is

excited between the plates, it propagates into the dielectric and it is totally reflected by the conductors. When the signal travels and finds the edges of the plates, it undergoes multiple reflections and transmissions due to the surroundings of the system.

The electromagnetic model is determined by the region limited by the plate conductors and the dielectric material. This region can be represented into the software simulators as a parallel plate waveguide. The electromagnetic model is a computational model for the waveguide and it considers different characteristics, such as the computational mesh definition in the simulators, boundary conditions, frequency response, excitation ports and medium between the plates. The dimensions of the simulated waveguide are $82\text{cm} \times 82\text{cm} \times 2\text{cm}$, which represent length and height of the plates and the separation between them.

3.3.1 *Mesh*

HFSS constructs an adaptive mesh that is automatically tuned until to the response of interest converges. In XFDTD, a mesh is constructed using a base cell size, this size should be smaller than $\lambda/10$, where λ is wavelength and is calculated as $\lambda = v/f$, where v is the wave velocity (see equation 3.2) in the medium and f is the frequency operation (see section 3.3.3), the cell size depends of the higher permittivity in the simulation. In our case the cell size was selected as $\lambda/24$, considering the higher operation frequency in dry sand (see section 3.3.3) in order to obtain a better resolution. Therefore, the total number of cells is 164 by 164 of length and height and 4 cells of width.

3.3.2 Boundary Conditions

The boundary conditions of the EM tank¹ are implemented as follow:

For the case of HFSS simulator, the EM tank is implemented as a *box*, as shown in Figure 3-2 where the walls parallel to the xz -plane are perfect electric conductors (PEC). These walls simulate the conducting mesh of the laboratory-scale 2D Soil-BED setup. On the other hand, the walls parallel to the yz -plane are considered as absorption boundaries to model the surface as electrically open (i.e., the waves can then radiate out of the structure and toward the absorption boundary). Air boxes are placed above and below of the EM tank to provide a proper termination of the computational space. In order to obtain the better matching between the boxes, the height of the air boxes has to be $\lambda/4$ (*cm*). Moreover, external walls of the air boxes are also absorption boundaries.

¹ EM tank is referred as our region of interest for simulation

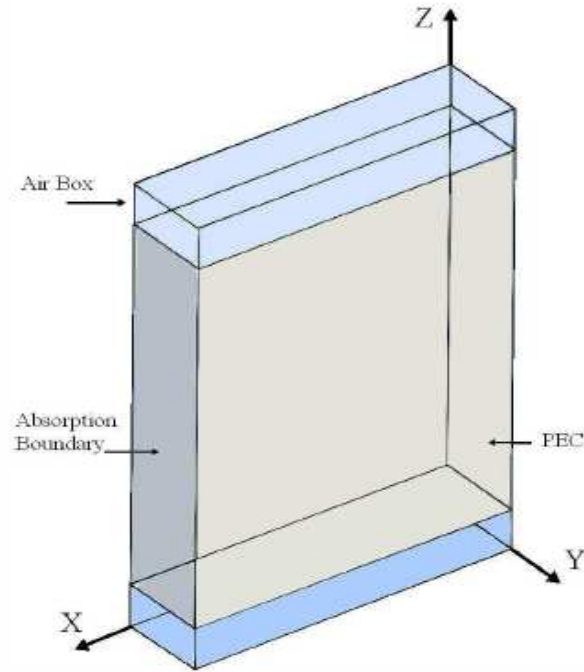


Figure 3.2: Boundary conditions in HFSS Simulator

In the XFDTD simulator, two *plates* (PEC) were placed to simulate the conducting metal mesh panels of the Soil-Bed. The structure is enclosed in a box automatically constructed to obtain a proper termination of the computational space. Then, all walls of this box are considered as PML (perfectly matched layer) absorbing boundaries. The size of this box depends of the *cell* size selected previously to generate the mesh (see section 3.3.1). In the Figure 3.3 shows the boundary conditions of the EM tank in the XFDTD simulator.

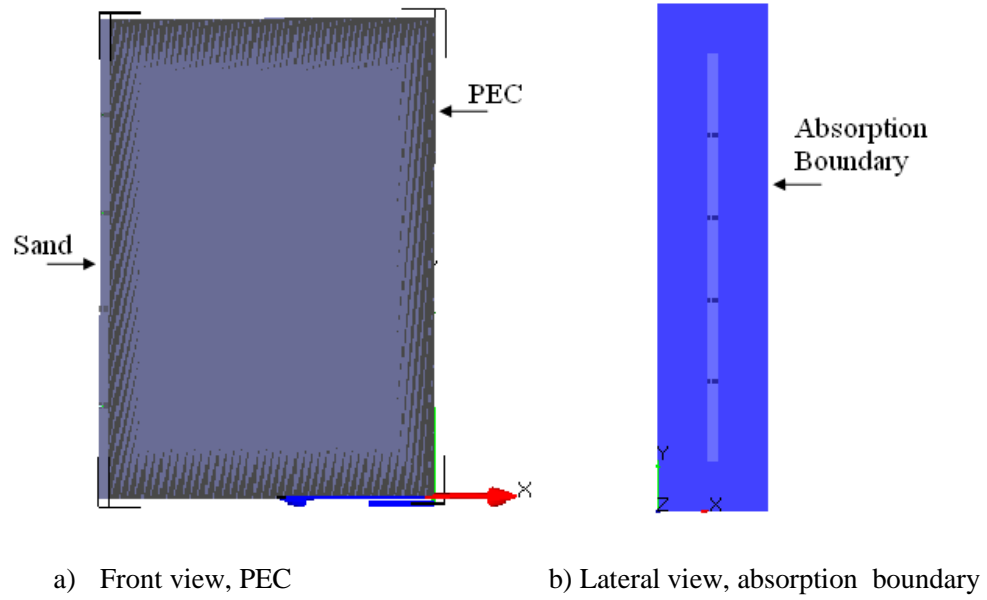


Figure 3.3 Boundary conditions in XFDTD Simulator

3.3.3 Frequencies of Operation

Initially, the frequencies considered were based on preliminary measurements on the laboratory-scale 2D Soil-Bed setup, which included 300 MHz, 600 MHz and 1 GHz [2], and considered only two ports placed at 14.5 cm from the bottom of the EM tank. For this analysis, the transmitter port (P_t) is situated opposite to the receiver port (P_r) (section 4.2). Since, the medium into the model is homogeneous, standing wave patterns inside the EM tank are formed, but at these frequencies the ports did not receive the maximum power of the waves.

Therefore, it is necessary to find other operation frequencies to assure that the maximum power of the waves are received by the ports to do a better analysis of the S-parameters.

The maximum amplitude in a wave is found in the first quarter of cycle ($\lambda/4$). Therefore, the length of the EM tank must be an odd multiple of $\lambda/4$. Hence, the frequencies of operation are calculated by (3.1), considering the propagation velocity of the medium v , the wavelength λ and the quantity of multiples for this n .

$$f = \frac{v}{(n+1/4)\lambda} \quad 3.1$$

The propagation velocity was calculated for dry sand, which depends of the dielectric permittivity ϵ corresponding to this medium (see section 3.3.5) and the light velocity in the vacuum c , (3.2). This equation is for lossless media.

$$v = \frac{c}{\sqrt{\epsilon}} \quad 3.2$$

Using equations (3.1) and (3.2), and selecting $n = 1, 2$ and 5 , the frequencies were calculated are, 285 MHz , 515 MHz and 1.5 GHz .

A comparison between the standing waves for both of these frequencies range is shown in Figure 3.4 where the blue and red rectangles indicate the power received at each port for operation frequencies computed, and for preliminaries operation frequencies.

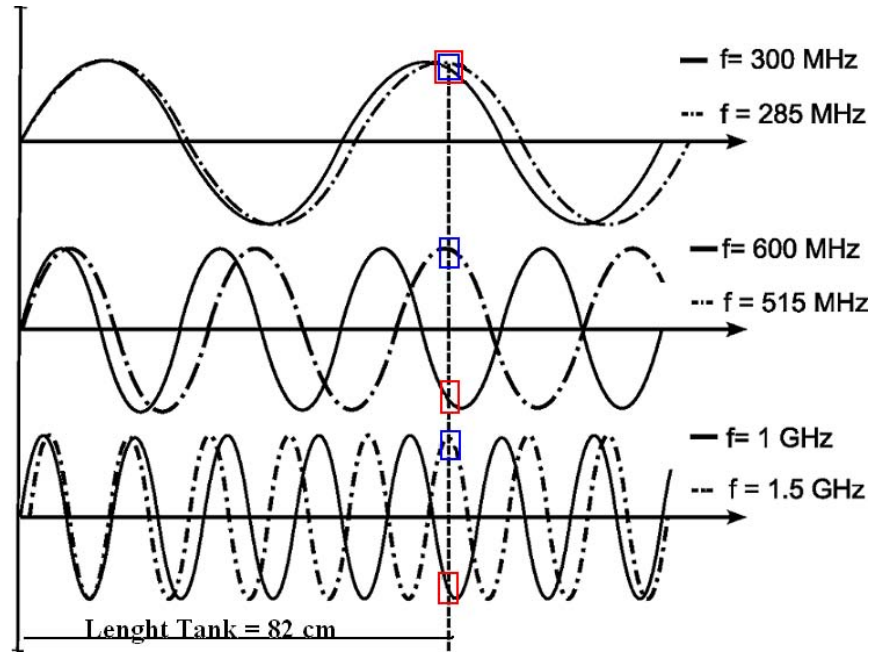


Figure 3.4. Standing wave patterns.

3.3.4 Excitations Ports

After analyzing the frequencies of operation in the section 3.3.3, the quantities, position and sizes of the excitations ports were analyzed to do a better characterization of EM tank. Section 4.2 shows the analysis for the excitations ports in detail.

Eight antennas of the Soil-Bed setup were replaced by excitations ports in the final model of EM tank, which are located at the lateral sides of the tank. Each side has four ports. When a port transmits the others receive. The position of the transmitter port is changed for each simulation. In this way, it acquires the electromagnetic field distribution and S parameters for each case.

The excitations ports are different in the two simulators for changes in the form, location and type of excitation. These are described below.

3.3.4.1 Excitation ports in HFSS

In HFSS, the excitations ports are of type *waveport*. These were placed on the walls parallel to the *yz*-plane. The *waveport* is a square with dimensions 2 cm by 2 cm. The separations between ports are 15.2 cm and are numbered as is shown in Figure 3-5.

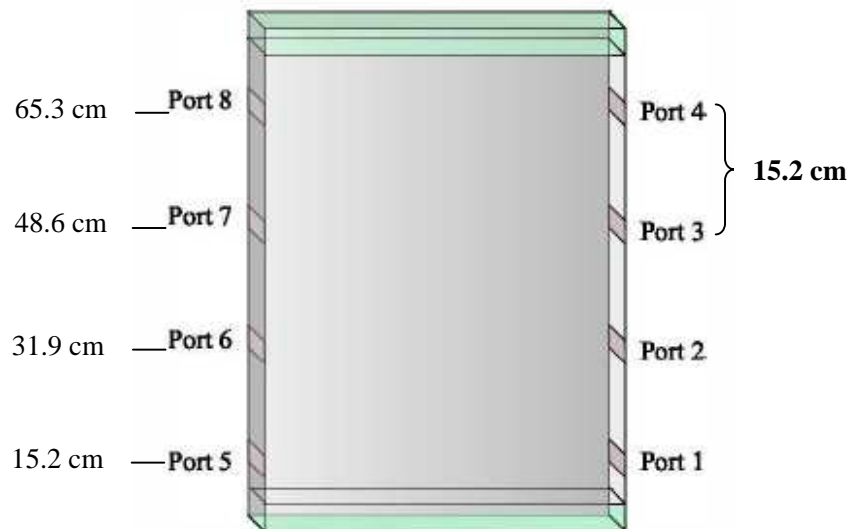


Figure 3.5: Excitations ports in HFSS

HFSS allows exciting individually each *waveport* and the incident wave contains one watt of time-averaged power.

3.3.4.2 Excitation ports in XFDTD

In this case the ports selected are *discrete sources* (feed), composed by a voltage source (1V) in series with a resistance (50 Ω), and since the excitation is related with the desired response (*S*-parameters). This feed is placed on an edge of one cell selected vertically, every 33 cell in the mesh, (see Figure 3-6).

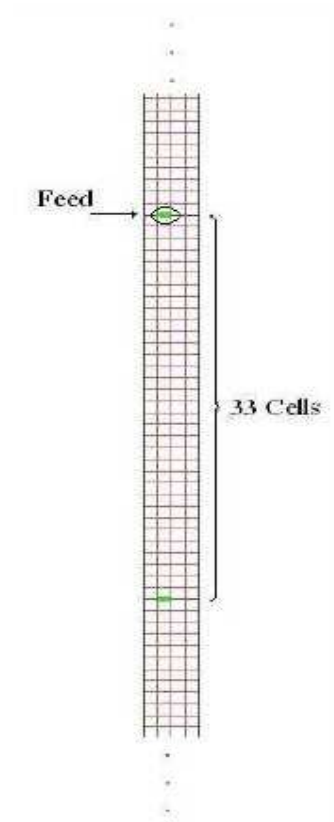


Figure 3.6: Excitation ports in XFDTD

The input wave function is selected as a *Gaussian Derivative* pulse; this provides better results in terms of frequency without DC components. The pulse width of the Gaussian

Derivative depends of the frequencies of operation and the attenuation of the spectrum (dB).

For 1.5 GHz , the pulse width is 200 time steps.

3.3.5 *Medium*

Different soil conditions are simulated (dry sand, wet sand and contaminated sand). It is, then, necessary to know the electromagnetic properties (ϵ , μ and σ) of these media to spatially and temporally analyze the electromagnetic wave propagation at different frequencies of operation. In this work, it is assumed that $\mu \cong \mu_0$, where μ_0 is the permeability of the medium for free space, because usually the soil has no magnetic behavior. This assumption is based on [34].

For lossy media, ϵ and σ generally varies with the frequency; for this reason the permittivity is treated as a complex function (equation 2.12 $\epsilon = \epsilon' - j\epsilon''$ 2.13) [13].

Analyzing the figures for dielectric constant versus frequency given in [34] and [35], it is observed that these constants can be considered with a fixed value for frequencies in the megahertz range. These values of dielectric constants for dry and wet sand are shown in Table 3-1.

The static conductivity in the dry and wet sand is $\sigma_{DC} = 4.4\mu S/m$ and the alternating conductivity were calculated using by (equation 2.19 $\sigma_{AC} = \omega\epsilon''$ 2.19) [34], where the

imaginary part of the permittivity was obtained from [35] for dry and wet sand:

$$\varepsilon''_{Drysand} = 0.19 F/m \text{ and } \varepsilon''_{wetsand} = 1.9 F/m .$$

The equivalent electrical conductivity was calculated using (equation 2.17) at the operation frequencies, the results are shown in Table 3-1.

Table 3.1: Electrical properties for dry and wet sand [34]

Soil Conditions	Dielectric Constant (F/m)	Electrical Conductivity (S/m)		
		f_{285MHz}	f_{515MHz}	$f_{1.5GHz}$
Dry Sand	2.55	0.003	0.0054	0.016
Wet Sand	20	0.03	0.054	0.16

In this study, the DNAPL analyzed is a tetrachloroethene (PCE). The dielectric constant and the electrical conductivity for this contaminant were obtained from [1] and are shown in Table 3-2.

Table 3.2: Electrical properties for DNAPL (PCE) [1]

Dielectric Constant (F/m)	Electrical Conductivity (S/m)		
	f_{285MHz}	f_{515MHz}	$f_{1.5GHz}$
2.28	2.2e-5	4.69e-5	1.52e-4

4 RESULTS AND ANALYSIS

4.1 Overview

Several simulations were made to determine if it is possible to detect DNAPL contamination in the soil. The analysis was made taking into account different conditions of the soil electrical properties and four different shapes of DNAPL within the EM tank. Also, the position of the excitation point was varied and evaluated at the three frequencies, and the *S*-parameters and the distribution of the electromagnetic field in the EM tank were obtained.

HFSS was the principal simulator used to develop the electromagnetic model of the laboratory scale 2D Soil-Bed. The XFDTD simulator was used to validate and to conclude if it is possible to detect contaminants.

4.2 Experimental Simulation

Several experimental simulations were done to optimize the model on the simulator, and to ensure that the data obtained in the final model was representative of the system. The optimization was conducted by varying sizes, position and quantity of ports. These variations are described below.

Initially, the frequencies considered were based on preliminary results of the laboratory scale 2D Soil-BED setup, which included 300 MHz, 600 MHz and 1 GHz [2]. It considered only two ports, which were placed at 14.5 cm from the bottom. The transmitter port (*Pt*) was situated opposite the receiver port (*Pr*). The dimensions of the ports were 0.01 cm by 0.01 cm width and height, respectively.

Initial model runs used electrical properties of dry sand $\epsilon_r = 4$ and $\sigma = 0.01 \text{ S/m}$ at the frequencies 300 MHz, 600 MHz and 1 GHz. According to the literature review, subsequent runs used $\epsilon_r = 2.5$ and, $\sigma = 0.003, 0.0054, 0.016 \text{ S/m}$ [34], at the frequencies 285 MHz, 515 MHz and 1.5 GHz (see Table 3-1).

In Figure 4-1, it is observed that the wave is propagated radially in the direction of negative x into the tank from the *Pt*, at 300 MHz, 600 MHz and 1 GHz, with $\epsilon_r = 4$ and $\sigma = 0.01 \text{ S/m}$. The E-field distribution presents that the port *Pr* (left side) does not receive signals at the location of the port, because of the wave pattern poses a minimum at this point due to the wavelength of the signals emitted (see Equations 4-1, 4-2, 4-3).

$$\lambda_{300\text{MHz}} = 50\text{cm} \quad 4.1$$

$$\lambda_{600\text{MHz}} = 25\text{cm} \quad 4.2$$

$$\lambda_{1\text{GHz}} = 15\text{cm} \quad 4.3$$

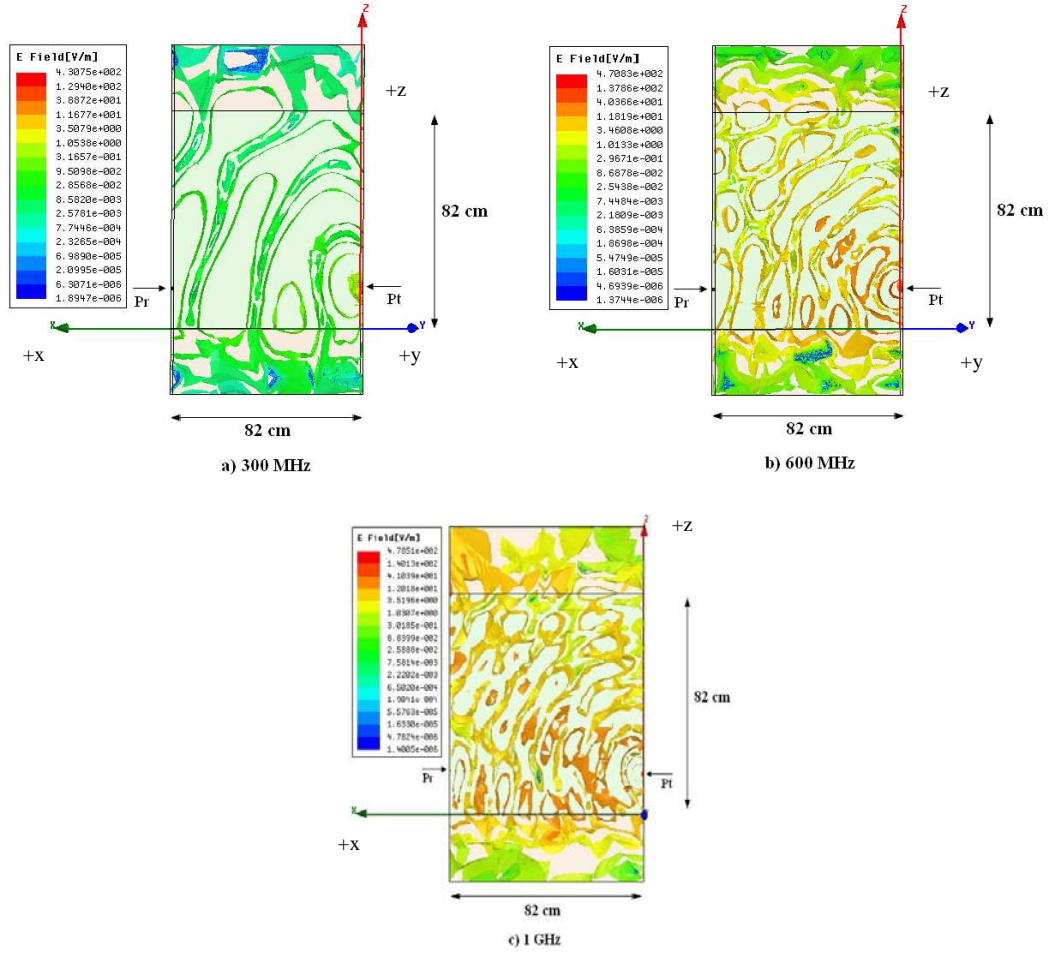


Figure 4.1: E-field propagation with three experimental frequencies: a) 300 MHz, b) 600 MHz, and c) 1 GHz.

Taking into account these electrical constants listed in Table 3-1 and the EM tank geometry, three operation frequencies (285 MHz, 515 MHz and 1.5 GHz) were calculated to ensure that *Pr* receives a maximum of the signal emitted (see section 3.3.3).

In the previous simulations the values for the S -parameters in each port were analyzed for the three frequencies. The Pt shows the reflected energy from soil (S_{11} reflection coefficient), whereas the Pr shows the transmitted energy from Pt (S_{21} transmission coefficient).

The HFSS simulator mentioned in (section 3.3.1), obtains the S -parameters through an iterative process doing a comparison of each adaptive pass between the results of the current mesh and the results of the previous mesh. When the maximum change in the magnitude of the S -parameters between two consecutive iterations (defined as ΔS) is less than 0.02 (2%) the mesh/solution convergence is attained [35].

The values of the S -parameters obtained were very small, lower than -100 dB. Therefore, we attempt to improve the results of the simulations assessing different sizes ports, and a vacuum as a propagation medium ($\epsilon_r = 1$ F/m and $\sigma = 0$ S/m). Table 4-1 presents the value of S -parameters for four different sizes: a) *Size 1*: 0.01 cm by 0.01 cm, b) *Size 2*: 0.02 cm by 0.01 cm, c) *Size 3*: 0.01 cm by 0.02 cm, and d) *Size 4*: 0.02 cm by 0.02 cm width and height, respectively.

The results for the different ports are divided into two parts; S_{11} and S_{21} (see Table 4.1). Note that in *Size 4* the reflected energy in the Pt (S_{11}) is low and the transmitted energy to Pr (S_{21}) is high in comparisons with the other sizes. Therefore a final size of 0.02 cm by 0.02 cm (*Size 4*) was selected for better coupling of the incident energy to the medium.

Table 4.1: S-parameters values for different sizes the ports

Port Size (cm)	S_{11} (dB)	S_{21} (dB)
0.01 by 0.01	-4.2	-62.7
0.02 by 0.01	-6.39	-120
0.01 by 0.02	-0.642	-95
0.02 by 0.02	-11.7	-33.3

With the frequencies of operation, the electrical properties for the medium and the port size defined for the final electromagnetic model, the analysis of the space into the EM tank was performed by increasing the number of receiver ports to 5 (left side), which are separated by 5 cm. The transmitter port is evaluated in two different positions (right side), 14.5 cm and 35 cm from the bottom of the simulated system.

Figure 4-2 shows the E-field distributions at 515 MHz with five receiver ports and the two positions for the transmission port. It was observed that the E-field distribution into the EM tank and the S -parameters in the receiver ports depend on the localization of the transmitter port.

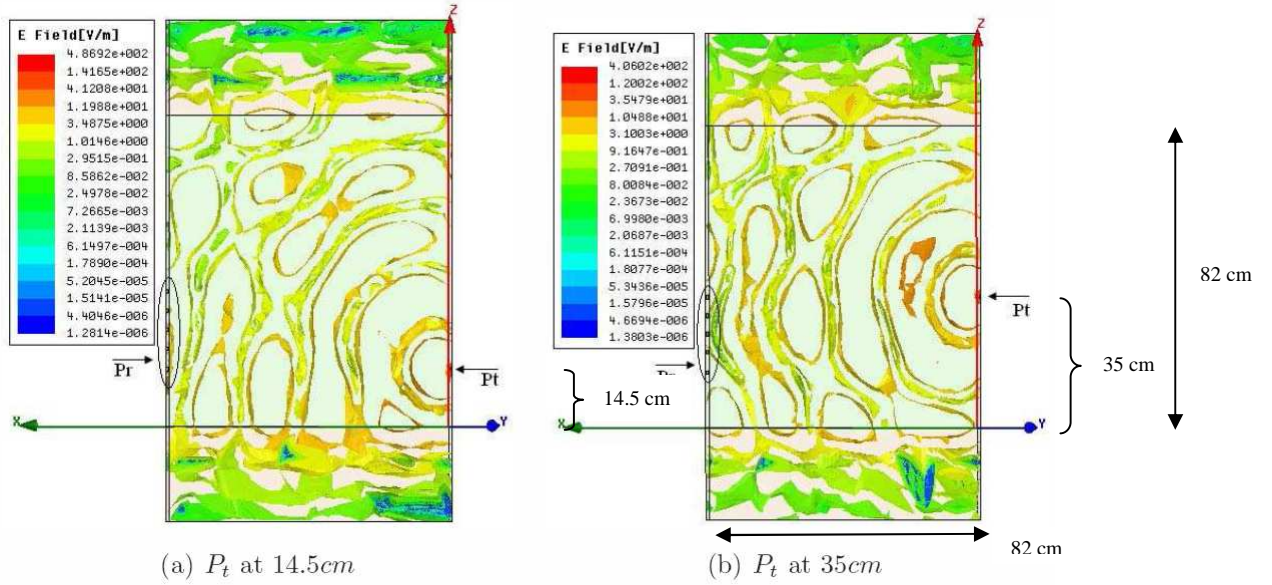


Figure 4.2: E-field propagation, with 5 receiver ports at 515 MHz in dry sand at
a) 14.5 cm, and b) 35 cm, from the bottom.

It was also observed that the number of ports and the distance between all of them, are not enough to analyze all the structure of the EM tank. Also, to use a single frequency of operation is not enough to analyse the EM tank, since the soil electrical properties change and it is necessary to know the behavior of the soil under different excitation frequencies. For this reason, we increase the number of ports to eight as is shown in Figure 4-3. These included four ports in each side separated by a distance of 16.7 cm . The ports 1 (P_1) and 5 (P_5) are localized 15.2 cm from the bottom (Figure 4-3). The selection for the transmitter port is explained in the next section. We also increased the operating frequencies to 285 MHz , 515 MHz and 1.5 GHz .

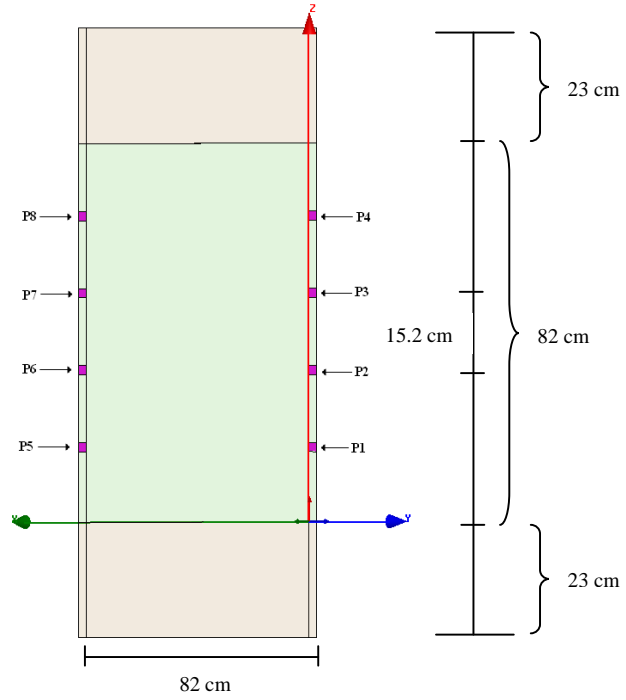


Figure 4.3: Design for the final electromagnetic model at 285 MHz

To analyze the subsurface with the Cross Well Radar(CWR) technology, it is necessary to take into account the operation frequencies, location and distance between ports. In this manner, the final electromagnetic model to study the contaminant detection is obtained.

4.3 Final Electromagnetic Model

For the final electromagnetic model, the electrical parameters of the medium (ϵ , μ and σ) are the ones obtained theoretically for dry and wet sand, and DNAPL. Also, we placed four

ports in each side of the EM tank using a size port of 0.02 *cm* by 0.02 *cm* width and height, respectively.

The characterization of the final electromagnetic model is made by analyzing several simulations. These include different soil conditions for various levels of saturation, as well as different distributions of the electromagnetic field due to sequential change of position for the transmitter port and the receiver ports. The transmission and reflection signals (*S*-parameters) on the ports were analyzed in the presence and absence of DNAPL in the medium. All of these simulations were made at three operation frequencies: 285 *MHz*, 515 *MHz*, and 1.5 *GHz*.

In the HFSS simulator, the *S*-parameters are presented as a *scattering matrix*, which relates the wave emerging from the transmitter port with the wave received in the receptors ports as a function of frequency. Due to this relation, the HFSS simulates a *Network Analyzer*. To characterize many types of these devices and to determine the measurement performance, it is necessary to define the system dynamic range. The Network analyzer dynamic range is essentially the range of power ($P_{max} - P_{min}$) that the system can measure. Specifically [36]:

P_{max} : The highest input power level that the system can measure before unacceptable errors occur in the measurement.

P_{min} : The minimum input power level the system can measure (its sensitivity), set by the receiver of noise floor.

The *receiver of noise floor* is an important network analyzer specification. In general for a network analyzer device, the receiver of noise floor has a range of -92.8 dBm to -102.4 dBm [36]. Based on this range, we chose the $P_{min} = -92.8 \text{ dBm}$ as the noise floor.

4.3.1 Simulations without DNAPL

4.3.1.1 Dry sand

The first simulation was made considering dry sand into the EM tank at the three operation frequencies.

In the Figure 4-4 is shown the E-fields propagation at three analysis frequencies from the P_3 , which is the transmitter port. Observe that the propagation is radial in the x -direction when it is transmitted from the right side ports: If transmitted from ports on the left side, the propagation is radial in the negative x -direction.

The S -parameters are presented in tables and organized as follows: the rows RPort², contain the values of the signal received in each port when this is transmitted from a specific port (EPort³, first column), recall that the position of the excitation point was varied in order

² RPort: Receiver port number

³ EPort: Excitation port number

to analyze all of the space into the EM tank. Therefore, the main diagonal contains the reflection coefficient (S_{ii}) for each port. Tables 4-2, 4-3 and 4-4 show the S -parameters obtained for the three operation frequencies. The blue values indicate the ones that are out of the dynamic range, for this reason will be replaced by $P_m = -124.35dB$ for further analysis of the model results.

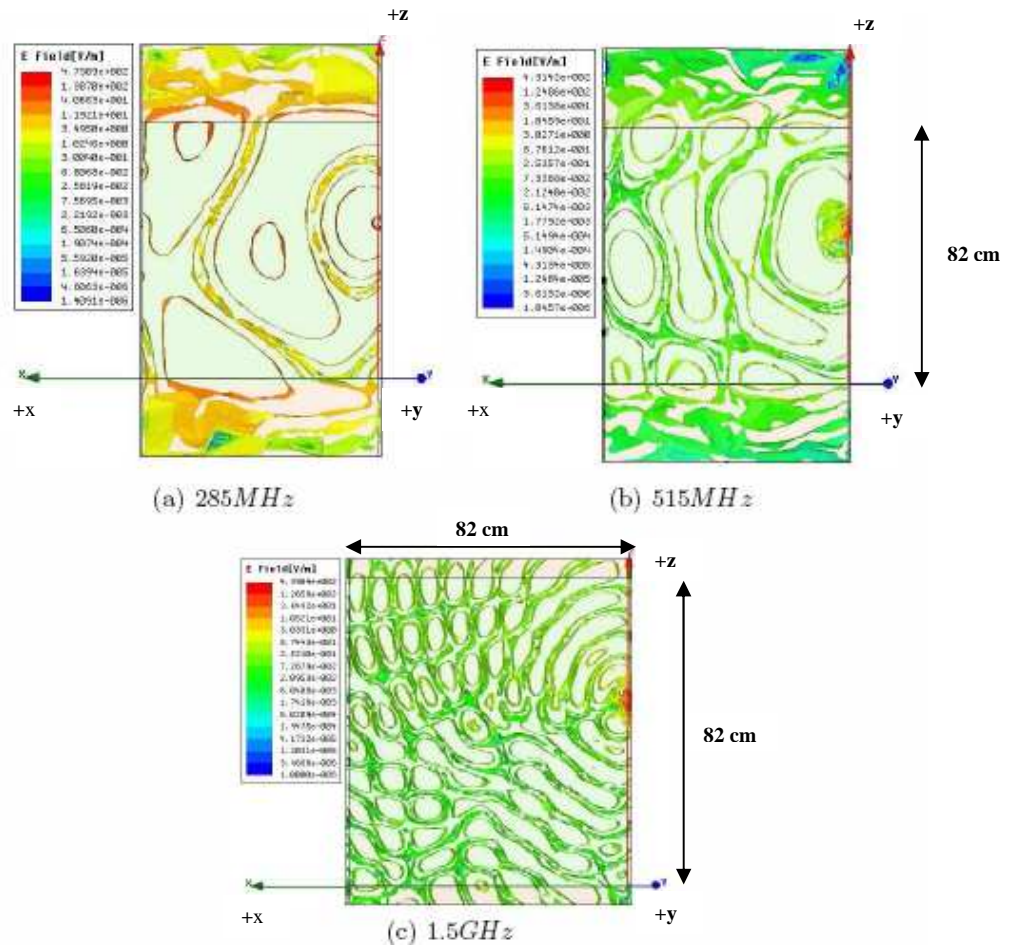


Figure 4.4: E-field propagation without DNAPL with P3 as transmitter port for dry sand, a) 285 MHz, b) 515 MHz and, c) 1.5 GHz

Table 4.2: S-parameters for dry sand at frequency 285 MHz.

RPort EPort	1	2	3	4	5	6	7	8
1	-11	-34.6	-44.3	-94.2	-33.7	-34.9	-38.7	-42.9
2	-109	-12.9	-126	-87.4	-75.1	-80.5	-85.1	-79
3	-44	-30.9	-10.3	-66.6	-87.4	-43.3	-38.9	-71.4
4	-140	-89.4	-76.2	-11.4	-108	-74.3	-71.6	-116
5	-84.1	-33.6	-36.7	-77.9	-10.4	-77.1	-43.6	-54.1
6	-66.1	-39.6	-79.9	-68.6	-34	-10.4	-65.3	-45.3
7	-123	-90.4	-85.5	-119	-90.2	-76.7	-13.1	-80.1
8	-113	-106	-146	-107	-161	-110	-103	-13.7

*Blue cells are values out of dynamic range

Table 4.3: S-parameters for dry sand at frequency 515 MHz

RPort EPort	1	2	3	4	5	6	7	8
1	-12.2	-92.4	-42.1	-45.5	-35.6	-41.3	-40.7	-49.2
2	-35.2	-12	-87.1	-89.2	-40.7	-38.8	-34.8	-39.6
3	-79.2	-73.1	-11.6	-74.5	-77.4	-115	-77.1	-122
4	-44.5	-41.8	-82.8	-11.3	-48.8	-39.3	-39.9	-75.9
5	-75.2	-38.2	-68.9	-50.2	-11	-34.3	-84.2	-74.7
6	-86.4	-39.1	-34.9	-92.1	-97.6	-11.7	-35.7	-78.2
7	-38	-33.8	-38.2	-37.6	-74.9	-34.1	-10.8	-33.4
8	-49.3	-40.2	-40.8	-35.1	-96.3	-41.8	-35.5	-11.7

*Blue cells are values out of dynamic range

Table 4.4: S-parameters for dry sand at frequency 1.5 GHz

RPort EPort	1	2	3	4	5	6	7	8
1	-10.5	-103	-80.6	-119	-111	-65	-93.8	-76.8
2	-76.3	-10.9	-79.7	-91.9	-78.1	-80.5	-128	-132
3	-93.7	-82	-11.9	-114	-83.4	-84.4	-123	-77.3
4	-132	-92	-119	-11.8	-94.9	-80.9	-87.3	-127
5	-75.5	-33.8	-29.4	-43	-11.5	-36.5	-46.2	-42.9
6	-134	-81.2	-86.2	-76.1	-82.3	-11.2	-90.3	-133
7	-61.8	-82.7	-34.9	-34	-45.6	-38.6	-11.1	-65.7
8	-86.7	-110	-67.2	-64.3	-112	-111	-97.3	-10.9

*Blue cells are values out of dynamic range

In the previous tables, the values of the main diagonal are between -10.3 dB and -13.7 dB, indicating the reflected energy from the soil toward the transmitter port. The transmitted energy at the receptor ports found between -29.4 dB and -124.35 dB, (the blue values that are out of the dynamic range $P_m = -124.35dB$ are replaced by this value).

4.3.1.2 Saturated sand

Figure 4-5 shows the E-fields propagation from P_3 as excitation port for the saturated sand, at the three analysis frequencies.

The E-field distributions in saturated sand (Figure 4.5: E-field propagation without DNAPL with P_3 as transmitter port for wet sand and dry sand (Figure 4.4) are different, due to its electrical properties. Observe that the wavelength given by the distance of repetitive cycles in the E-field in saturated sand is smaller than in dry sand because it depends on the dielectric constant (ϵ_r). From equations 3.1 and $v = \frac{c}{\sqrt{\epsilon}}$ 3.2, the wavelength for dry sand and saturated sand at 285 MHz are:

$$\lambda_{DrySand(285MHz)} = 65.9cm \quad 4.4$$

$$\lambda_{SatuSand(285MHz)} = 23.5cm \quad 4.5$$

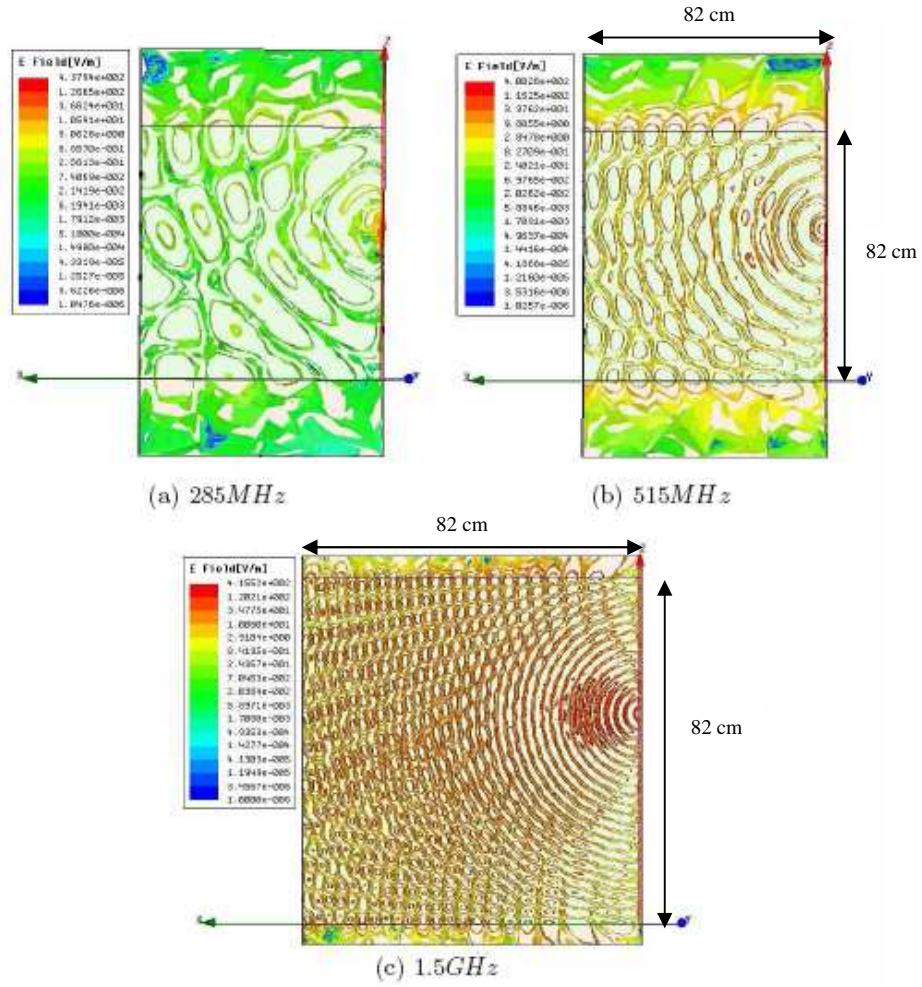


Figure 4.5: E-field propagation without DNAPL with *P3* as transmitter port for wet sand:
a) 285 MHz, b) 515 MHz and c) 1.5 GHz

The results obtained for dry and wet sand are used as a reference, to compare the results obtained simulating different combinations of the soil under the presence of the contaminant and then to characterize the soil. In both cases it is observed that the wave propagation is uniform because the medium is homogeneous.

Table 4.5: S-parameters for saturated sand at frequency 285 MHz

RPort EPort	1	2	3	4	5	6	7	8
1	-13.1	-39.7	-46.7	-86	-74.7	-53.4	-46.4	-42.1
2	-89.4	-13	-84.8	-96.7	-144	-125	-92.9	-98.7
3	-127	-80.1	-11.5	-66.2	-113	-77	-110	-105
4	-106	-87.3	-124	-12.1	-116	-124	-110	-110
5	-102	-53.2	-102	-42.1	-13.3	-40	-49.8	-125
6	-113	-71.2	-72.3	-123	-101	-11	-66.4	-113
7	-47.5	-44.2	-40	-47.8	-99.1	-86.6	-12	-38.8
8	-141	-101	-98.9	-91.5	-161	-95.5	-132	-13

*Blue cells are values out of dynamic range

Table 4.6: S-parameters for saturated sand at frequency 515 MHz

RPort EPort	1	2	3	4	5	6	7	8
1	-11.3	-75.3	-84.6	-93.8	-79.3	-138	-78.1	-83
2	-82.5	-12.3	-85	-98.1	-84.6	-86.8	-132	-130
3	-52	-39.4	-12.6	-41.8	-38.6	-49.7	-42.4	-41.5
4	-99.2	-50.4	-40.1	-11.6	-46.3	-36.1	-79	-37.6
5	-124	-117	-69	-74.2	-11.3	-39.5	-89.5	-69.7
6	-81.9	-85.1	-81.3	-109	-78.6	-11.4	-126	-92.1
7	-71.8	-79.9	-94.3	-41.5	-49	-37.3	-11	-89
8	-129	-79.3	-131	-77.3	-95.4	-86.2	-77.3	-11.4

*Blue cells are values out of dynamic range

Table 4.7: S-parameters for saturated sand at frequency 1.5 GHz

RPort EPort	1	2	3	4	5	6	7	8
1	-5.46	-37.8	-50.8	-80.2	-62.5	-31.7	-47	-62.4
2	-92.7	-5.89	-83.6	-50.8	-31.6	-24.9	-25.1	-81.2
3	-51.9	-42.1	-5.46	-97.8	-43.4	-25.1	-28.2	-26.5
4	-44.6	-47.6	-39.3	-5.67	-73.8	-32.1	-26.1	-24.4
5	-24	-31.8	-43.7	-31.3	-5.32	-79.2	-66.6	-84.3
6	-31.9	-25.2	-25.2	-32	-38.2	-5.7	-96.3	-49.1
7	-43.5	-25.2	-28.3	-73.7	-85.9	-39.6	-5.6	-40.2
8	-31.1	-32.5	-26.5	-72.7	-45.2	-50.9	-40.7	-5.76

*Blue cells are values out of dynamic range

Tables 4-5, 4-6 and 4-7 show the S -parameters obtained for the three operation frequencies. The blue values indicate the ones that are out of the dynamic range. The reflection coefficients (main diagonal) are between -11 dB and -13.3 for 285 MHz, -11 dB and -12.6 dB for 515 MHz and -5.32 dB and -5.89 dB, is found in a range appropriate for the soil conditions.

Since the geometry of the electromagnetic model is symmetrical, it assumes that all of results obtained for the right side ports and the left side ports must be similar. This assumption is verified numerically on the model simulator, comparing the S -parameters obtained for the right side with the mirror of the S -parameters for the left side. Figure 4-6 shows this comparison at 1.5 GHz for saturated sand. The graphical comparison was made between the opposite ports P_1 - P_5 , P_2 - P_6 , P_3 - P_7 and P_4 - P_8 . Note that the ports have a similar behavior. Hence, the analysis to characterize the soil will be made considering only the ports $P_1...P_4$ as transmitter ports.

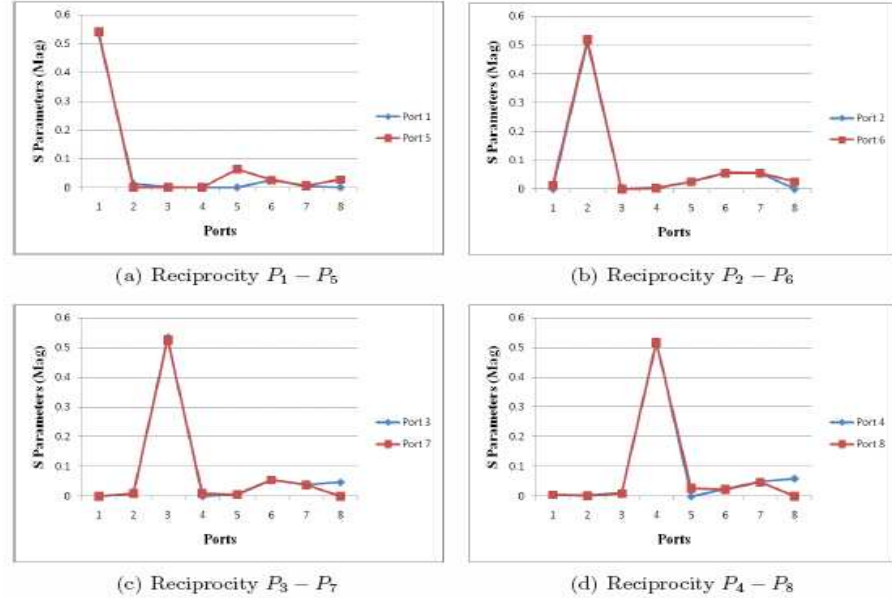


Figure 4.6: Reciprocity analysis of S-parameters for saturated sand at the frequency 1.5 GHz:
a) Reciprocity P_1 - P_5 , b) Reciprocity P_2 - P_6 , c) Reciprocity P_3 - P_7 ,
and d) Reciprocity P_4 - P_8

4.3.1.3 EM response for varying degrees of soil saturation level

To characterize the soil some combinations at different levels of dry and wet sand, were simulated. Initially the EM tank was considered full of dry sand, and then the saturation level was increased from bottom. The analysis was conducted when the tank was 10% saturated and 90% dry (Level L_1), 33.3% saturated (Level L_2), 50% saturated (Level L_3) and, 66.6% saturated (Level L_4).

4.3.1.3.1 First Level (L_1).

The first level (L_1) of wet sand is inserted into the EM tank to 8.2 cm from bottom, as is shown in Figure 4-7. Given that the ports are placed above of the wet sand level (L_1), the

incident wave at the plane between the dry media (medium 1) and wet (medium 2) sand undergo a change due to the different soil electrical properties. In other words, when the incident wave encounters a change medium, a fraction of the wave intensity is reflected into the dry sand and part is transmitted at the wet sand.

When the wave enters the wet sand zone, wave velocity produces contrasts due to changes in dielectrical constant. Therefore the wavelength in medium 2 (saturated sand) is different than in medium 1 (dry sand). Moreover, the E-field propagates in the negative z -direction.

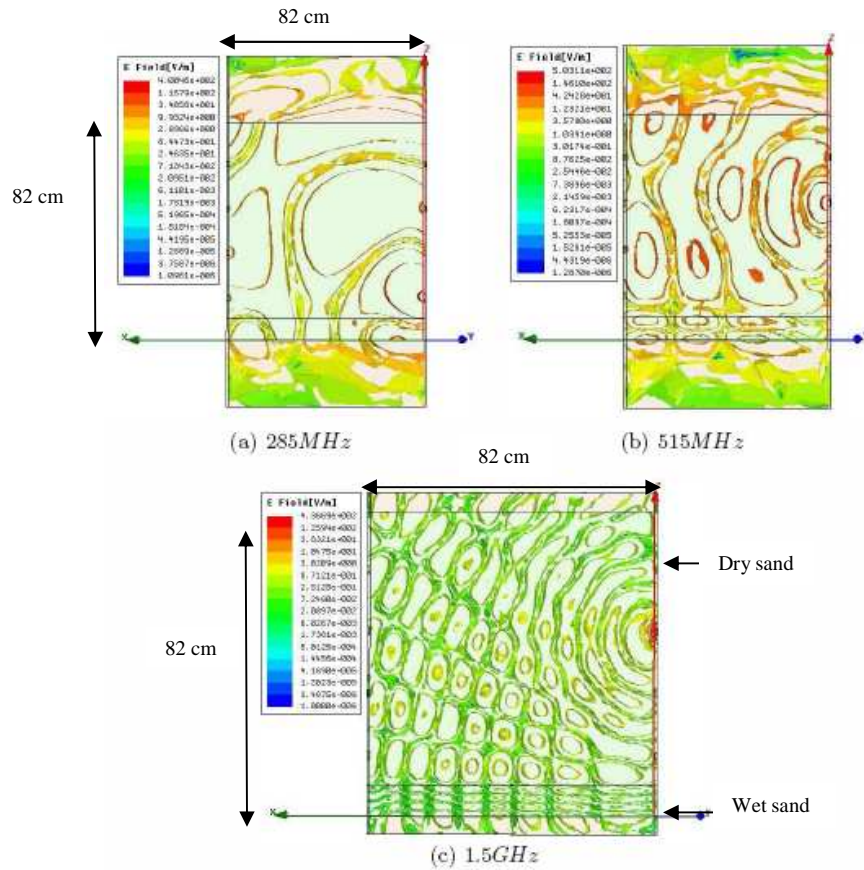


Figure 4.7: E-field distribution from P_3 with 10% saturated level (L_1) inserted: a) 285 MHz, b) 515 MHz and c) 1.5 GHz

The Table 4-8, Table 4-9 and Table 4-10 show the S-parameters obtained for 10% saturated level.

Table 4.8: S-parameters when saturated level L_1 inserted at 285 MHz

RPort EPort	1	2	3	4	5	6	7	8
1	-11.8	-34.2	-39.4	-50.5	-45	-39.1	-42.8	-43.5
2	-73.6	-13.3	-69.5	-140	-76.9	-71.2	-73.1	-73.8
3	-93.1	-130	-13.1	-142	-97	-89.8	-87.9	-89.3
4	-89	-60.8	-69.9	-10.5	-40.3	-73	-70	-67
5	-44.5	-38.8	-98.5	-43.3	-11.5	-33.8	-90.7	-50.6
6	-66.1	-31.1	-74.3	-69.5	-31.5	-10.4	-32.1	-63.4
7	-76.9	-70.5	-69.2	-70.4	-113	-106	-12.6	-68.9
8	-86.6	-37.2	-36.4	-106	-49.8	-62.2	-35	-12.2

*Blue cells are values out of dynamic range

Table 4.9: S-parameters when saturated level L_1 inserted at 515 MHz

RPort EPort	1	2	3	4	5	6	7	8
1	-11	-33.9	-40.3	-45.3	-44.4	-48.4	-39.1	-44.7
2	-36.5	-13.1	-38.3	-43.6	-50.1	-36.8	-34.7	-40.4
3	-42.7	-37.6	-12.5	-84.7	-41.1	-33.9	-42.6	-43.7
4	-98.6	-90.5	-116	-12	-89.9	-87.4	-138	-122
5	-44	-48.8	-80	-75.6	-10.6	-33.4	-74.7	-45.4
6	-90.2	-35.2	-62	-38.4	-34.8	-11.6	-35.9	-41.2
7	-40.4	-33.4	-78.7	-41.9	-41.8	-68.5	-11.9	-35.3
8	-45.3	-92.5	-83.4	-35.4	-47.6	-42.7	-36.3	-12.5

*Blue cells are values out of dynamic range

Table 4.10: S-parameters when saturated level L_1 inserted at 1.5 GHz

RPort EPort	1	2	3	4	5	6	7	8
1	-11.4	-87.3	-108	-97.5	-134	-83.4	-90	-88.8
2	-124	-11.8	-77.3	-87.5	-104	-128	-116	-88.5
3	-77.4	-73.6	-10.9	-122	-66	-108	-70.7	-68.4
4	-43.9	-95.5	-37.2	-12.5	-34.9	-32.7	-98.5	-29.6
5	-35.5	-29.7	-64.1	33.8	-11.4	-33.1	-80.6	-43.4
6	-30.6	-42.4	-32.6	-32.5	-34.2	-12.2	-41.4	-44.5
7	-71.9	-72.8	-70.8	-33.4	-39.7	-40.8	-11.4	-73.4
8	-34.9	-78.3	-34.5	-29.8	-82.9	-45	-80	-12.4

*Blue cells are values out of dynamic range

The analysis of the S-parameters at the three frequencies of the operation when 10% saturated sand is included a, is show in the section 4.3.1.4

4.3.1.3.2 Second Level (L_2).

The level of wet sand is raised to 24.6 cm (33.3%) from the bottom, as shown in Figure 4-8.

Ports P_1 and P_5 are within the L_2 zone (saturated sand). When these ports are transmitters, the wave energy is mostly contained in the saturated region because of total internal reflections in the L_2 zone, although some is transmitted to the L_1 zone (dry sand). For the remaining ports, the behavior of the E-field propagation is same as for level L_1 .

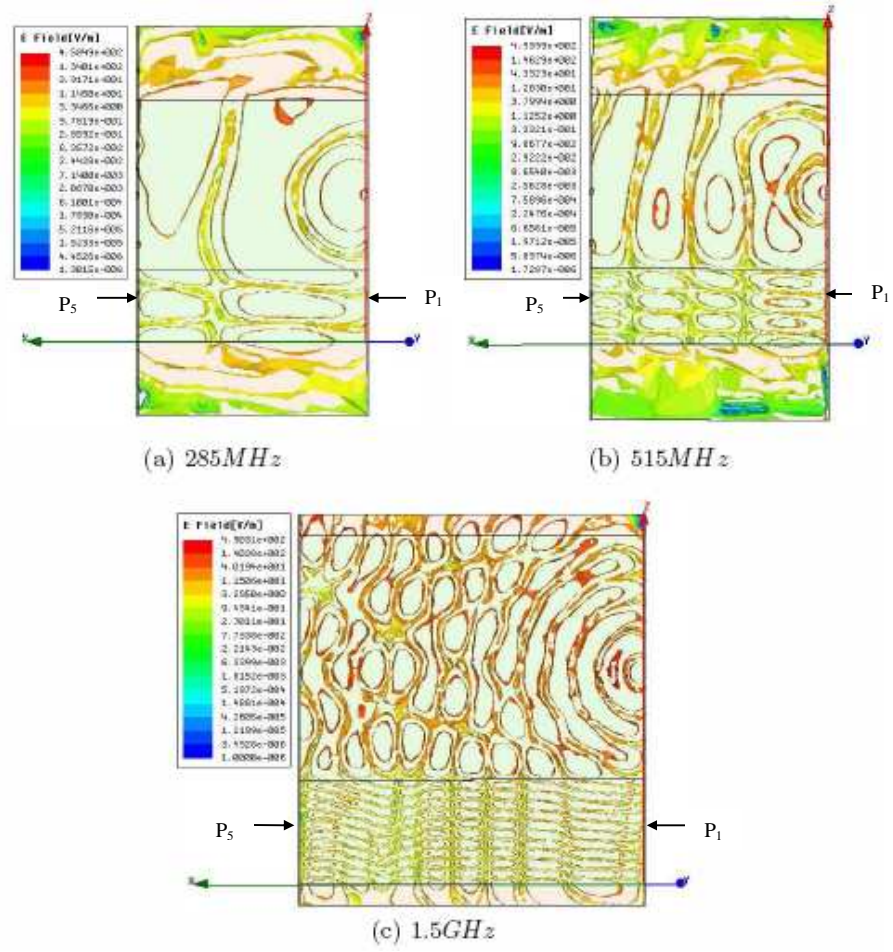


Figure 4.8: E-field distribution from P3 with 33.3% saturated level (L_2) inserted:
a) 285 MHz, b) 515 MHz and c) 1.5 GHz

The Table 4-11, Table 4-12 and Table 4-13 show the S-parameters obtained for 33.3% saturated level.

Table 4.11: S-parameters when saturated level L_2 inserted at 285 MHz

RPort EPort	1	2	3	4	5	6	7	8
1	-11.6	-67.4	-114	-147	-114	-123	-123	-130
2	-39.5	-12.6	-99.8	-127	-47.6	-46	-109	-106
3	-97.9	-33.9	-11.4	-35.2	-94.4	-44.8	-40.1	-83.7
4	-66	-49.6	-77.4	-11.1	-92.1	-40.9	-81.2	-34.2
5	-70.9	-75.9	-117	-113	-11.2	-113	-113	-137
6	-90.9	-44.4	-89.8	-40.3	-77.1	-11.5	-69.9	-86.2
7	-129	-80.4	-76.1	-116	-81.8	-66.2	-12	-75.7
8	-49.3	-40.8	-90.6	-68.6	-106	-49	-34.1	-11.3

*Blue cells are values out of dynamic range

Table 4.12: S-parameters when saturated level L_2 inserted at 515 MHz

RPort EPort	1	2	3	4	5	6	7	8
1	-11.4	-80.9	-91.5	-143	-99.3	-96.1	-96.8	-103
2	-79.1	-11	-33.8	-69.6	-51.8	-44.3	-73.3	-42.6
3	-92.5	-34.2	-11.4	-69.9	-103	-36.3	-34.1	-34.9
4	-155	-92.8	-93.5	-13.5	-111	-93.3	-86.1	-84.5
5	-84.6	-87.3	-134	-144	-11.5	-74.2	-86	-89.5
6	-51.9	-41.7	-83.3	-81.4	-38.4	-10.5	-67.6	-36.6
7	-117	-66	-62.3	-63.5	-78.3	-60.4	-11.7	-64.9
8	-63.9	-75.4	-78.2	-35.1	-90.1	-37	-33.2	-10.7

*Blue cells are values out of dynamic range

Table 4.13: S-parameters when saturated level L_2 inserted at 1.5 GHz

RPort EPort	1	2	3	4	5	6	7	8
1	-9.33	-103	-166	-118	-82.5	-114	-108	-172
2	-38.1	-11.4	-36.8	-49.3	-48.8	-38.8	-62.4	-28.3
3	-50.1	-36.1	-11.2	-70.4	-44.5	-29.7	-77.8	-35.7
4	-118	-49.3	-40.7	-12.3	-45.9	-29.5	-78.8	-28
5	-87.1	-48.2	-45.4	-45.9	-5.91	-87.7	-116	-57.5
6	-47.8	-71.6	-62.2	-68.3	-38.4	-11.1	-82.4	-80
7	-44.6	-62.7	-75.6	-35.5	-50.1	-36.4	-11.2	-86.3
8	-86.9	-117	-123	-136	-99.2	-88.8	-83.2	-11.8

*Blue cells are values out of dynamic range

The analysis of the S-parameters at the three frequencies of the operation when 33.3% saturated sand is included a, is show in the section 4.3.1.4.

4.3.1.3.3 Third Level (L_3).

For this analysis, the level of the saturated medium is increasing until it reaches half of the EM tank (41 *cm*), as shown in Figure 4-9. In this case the ports P_1 , P_2 , P_5 and P_6 are in the wet sand zone. Ports P_3 , P_4 , P_7 and P_8 remain in the dry sand zone. When the transmitter ports are within medium 1, the E-field in medium 2 tends to propagate radially in the negative z -direction. If the transmitter ports are within medium 2, total internal reflection can occur and the behavior of the E-field is similar at the previous cases at the three frequencies.

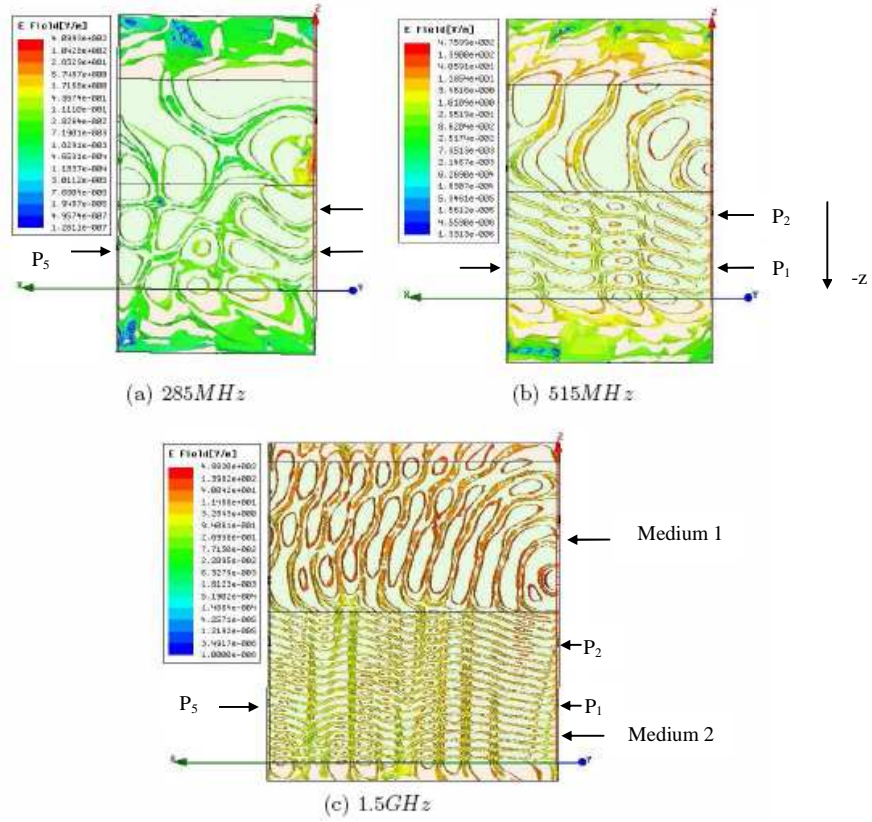


Figure 4.9: E-field distribution from P3 with 50% saturated level (L_3) inserted: a) 285 MHz, b) 515 MHz and c) 1.5 GHz

The Table 4-14, Table 4-15 and Table 4-16 show the S-parameters obtained for 50% saturated level.

Table 4.14: S-parameters when saturated level L_3 inserted at 285 MHz

RPort EPort	1	2	3	4	5	6	7	8
1	-13	-41	-99.4	-106	-36.9	-44.9	-53.9	-53.5
2	-40.3	-12.5	-84.1	-94.1	-44.8	-44.8	-107	-53.5
3	-83.8	-71.2	-11.9	-133	-92.9	-96.3	-132	-101
4	-116	-49.8	-83.4	-11	-51.4	-52.4	-80.8	-81.5
5	-66.1	-44.8	-83.3	-83.9	-11.5	-38	-84	-55.6
6	-88.5	-87	-95.5	-152	-79	-12.6	-133	-98.8
7	-113	-116	-153	-112	-105	-141	-13.4	-101
8	-95.4	-51.5	-75.1	-83.6	-56.1	-77.8	-34.2	-11.1

*Blue cells are values out of dynamic range

Table 4.15: S-parameters when saturated level L_3 inserted at 515 MHz

RPort EPort	1	2	3	4	5	6	7	8
1	-12.7	-41	-92.8	-108	-43.6	-35.5	-52.8	-58.6
2	-39.6	-11.4	-66.6	-46.1	-34.6	-44.7	-52.7	-53.9
3	-103	-38.6	-12	-34.2	-52.6	-53.3	-49.6	-44.4
4	-102	-132	-77	-12.3	-145	-90.7	-85.7	-90.6
5	-42.5	-35.6	-52.1	-58.2	-12.3	-40.6	-50.6	-58.2
6	-75.5	-84.8	-94.2	-95.8	-82.8	-13.1	-78.7	-87.6
7	-97.8	-145	-140	-85.6	-109	-93.2	-11.9	-73.1
8	-55.1	-53.3	-39.5	-33.6	-55.7	-45.3	-61	-10.9

*Blue cells are values out of dynamic range

Table 4.16: S-parameters when saturated level L_3 inserted at 1.5 GHz

RPort EPort	1	2	3	4	5	6	7	8
1	-5.44	-74.2	-54.5	-87	-21.4	-50.9	-47.6	-76.5
2	-86.9	-7.26	-118	-97	-86.5	-65.3	-89.7	-143
3	-53.8	-40.1	-11.4	-34.7	-47.1	-47.4	-35.4	-89.8
4	-55.2	-90.5	-34.1	-11.2	-40.5	-41.3	-26.6	-64.7
5	-21.4	-46.7	-47.4	-41.4	-5.54	-40	-91.1	-99.5
6	-78.2	-76.2	-93.1	-138	-89.6	-7.92	-119	-132
7	-89.2	-130	-85.8	-79	-98.7	-91.6	-11.7	-125
8	-85.9	-41.2	-27	-27.7	-55.4	-110	-68.1	-11.3

*Blue cells are values out of dynamic range

The analysis of the S-parameters at the three frequencies of the operation when 50% saturated sand is included a, is show in the section 4.3.1.4.

4.3.1.3.4 Fourth Level (L_4).

For this analysis, the EM tank is saturated to 57.4 cm which represents about 66.6% of the tank (Figure 4.10). Ports P_1 , P_2 , P_3 , P_5 , P_6 and P_7 are in the saturated sand zone and ports P_4 and P_8 remain into the dry sand zone.

The behavior of the E-field is similar with the level L_3 for the three frequencies analysis.

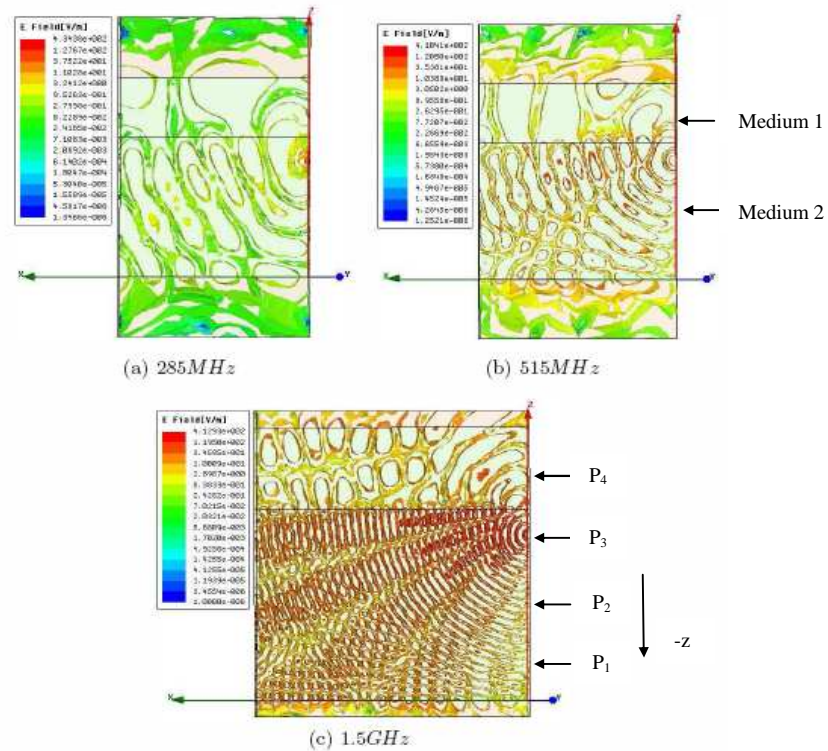


Figure 4.10: E-field distribution from P3 with 66.6% saturated level (L_4) inserted:
a) 285 MHz, b) 515 MHz and c) 1.5 GHz

Tables 4-17, 4-18 and 4-19 show the S-parameters obtained for 66.6% saturated level.

Table 4.17: S-parameters when saturated level L_4 inserted at 285 MHz

RPort EPort	1	2	3	4	5	6	7	8
1	-11.8	-37.9	-91.2	-58	-39	-52.4	-39.1	-91
2	-87.1	-13.4	-83.4	-93.4	-131	-87.3	-130	-143
3	-71.7	-59.9	-11.6	-93.3	-99	-93.6	-70.3	-11
4	-96.4	-46.2	-36.5	-10.8	-86	-91.1	-48.9	-83
5	-111	-87.3	-72.1	-90.2	-11.9	-68.9	-81.6	-88.4
6	-52.5	-42	-96.3	-56.4	-39.6	-12.7	-86.8	-49.4
7	-96.8	-40.5	-75.9	-83.2	-86.1	-82.1	-11.7	-37.1
8	-90.2	-106	-96.3	-150	-93.5	-114	-102	-11.7

*Blue cells are values out of dynamic range

Table 4.18: S-parameters when saturated level L_4 inserted at 515 MHz

RPort EPort	1	2	3	4	5	6	7	8
1	-11.5	-40.2	-49.6	-94.9	-73.8	-44.6	-104	-53.1
2	-76.2	-11.4	-76.3	-82.2	-85	-78.1	-72.8	-87.8
3	-89.2	-75.6	-11.5	-36.7	-90.5	-36.4	-45.6	-48.4
4	-53.3	-43.7	-35.9	-10.6	-55.3	-48.3	-48.2	-41.1
5	-67.9	-45.5	-36	-91.5	-11.4	-39.7	-86.7	-52.8
6	-44.4	-40.4	-75.6	-105	-41.2	-12.4	-39.7	-45
7	-92.6	-37.7	45.2	-50.7	-112	-40	-12.4	-38
8	-95.8	-80.7	-47.1	-40.6	-53.4	-43.6	-78.1	-10.2

Table 4.19: S-parameters when saturated level L_4 inserted at 1.5 GHz

RPort EPort	1	2	3	4	5	6	7	8
1	-5.72	-39	-47.7	-103	-22.9	-38.3	-33.1	-94.6
2	-39.3	-5.43	-48.3	-95.7	-39	-23.9	-31.8	-83.1
3	-47.6	-42.7	-5.38	-40.3	-32.8	-31.2	-22.3	-51.5
4	-111	-105	-96.8	-13	-109	-109	-113	-155
5	-23.1	-39.4	-33.1	-76.8	-5.36	-38.9	-48	-51.1
6	-65.1	-23.8	-31	-50	-39.9	-5.47	-73.4	-50
7	-32.9	-31.3	-22.4	-88.9	-47.3	-70.7	-5.63	-41.2
8	-97.5	-97.2	-135	-90.6	-105	-147	-90.1	-13.6

*Blue cells are values out of dynamic range

The analysis of the S-parameters at the three frequencies of the operation when is included a 66.6% saturated sand, is show in the section 4.3.1.4

4.3.1.4 Analysis of S-parameters for varying degrees of soil saturation level

The S parameters obtained for different soil combinations and for dry sand are compared taking into account the three analysis frequencies and considering P_1 , P_2 , P_3 and P_4 as transmitter ports. Figures 4-11, 4-12 and 4-13, show the relationship between the S-parameters reference results (dry sand) and the four levels of wet sand. The behavior of the electromagnetic model is described for each transmitter port with the different levels of saturated sand as follow:

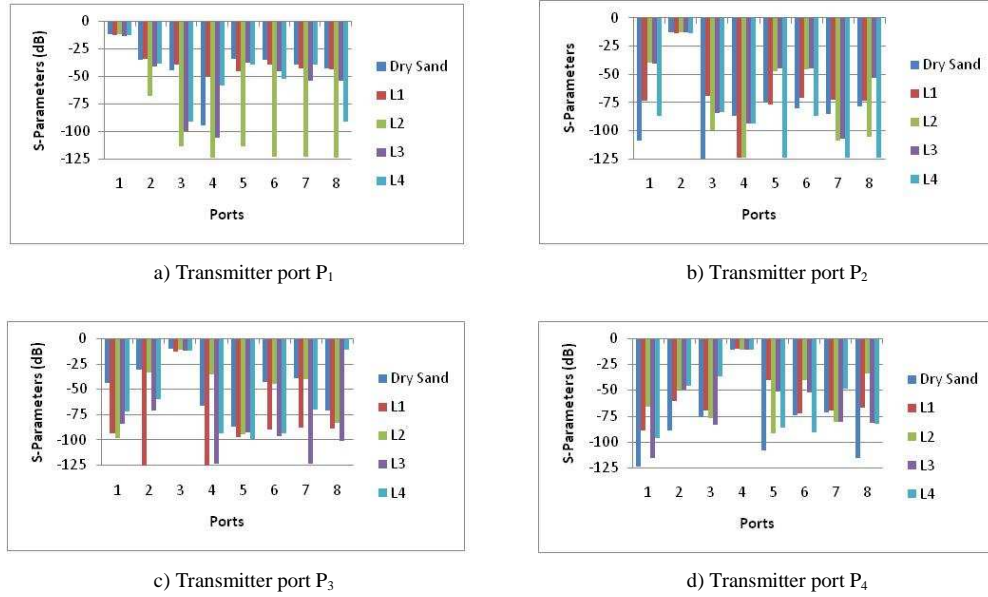
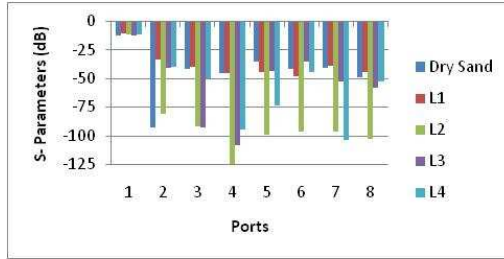


Figure 4.11: Comparison of S-parameters at 285 MHz for the four soils saturated:
a) Transmitter port P_1 , b) Transmitter port P_2 , c) Transmitter port P_3
and d) Transmitter port P_4

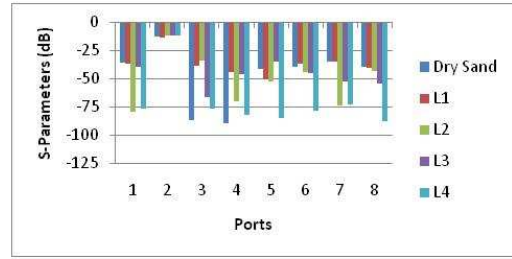
4.3.1.4.1 Dry Sand vs Saturated level L_1

P_1 : Minimum changes of energy are observed at the 3 analysis frequencies. However the receiver ports P_4 and P_2 for 285 MHz and 515 MHz respectively, receive less energy in comparison with the reference results.

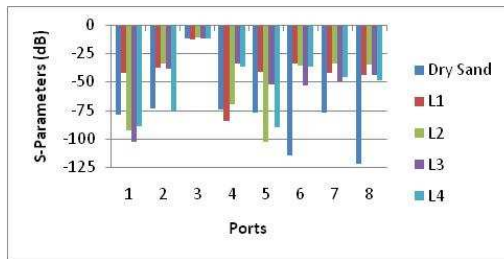
P_2 : At 285 MHz and 515 MHz , the receiver ports located on the same side of the transmitter port show some changes in comparison with dry sand. The receiver ports located opposite at this P_t have a similar behavior between them. At 1.5 GHz , only the results for the receiver ports P_3 , P_4 and P_7 are considered equals with respect to dry sand.



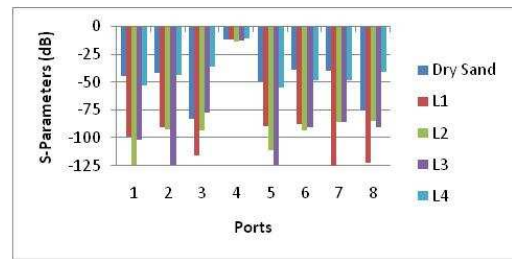
a) Transmitter port P_1



b) Transmitter port P_2



c) Transmitter port P_3



d) Transmitter port P_4

Figure 4.12: Comparison of S-parameters at 515 MHz for the four soils saturated:
a) Transmitter port P_1 , b) Transmitter port P_2 , c) Transmitter port P_3
and d) Transmitter port P_4

P_3 : In general, at 285 MHz and 515 MHz , all of receiver ports undergo changes, except the ports P_4 (285 MHz) and P_5 (515 MHz). At 1.5 GHz , the changes are not observed, except in P_7 .

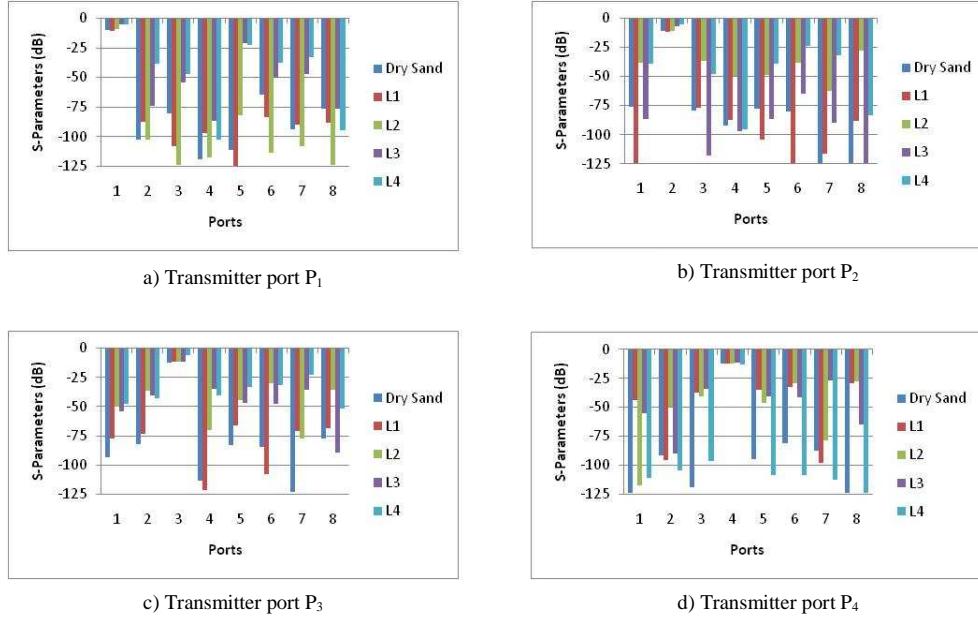


Figure 4.13: Comparison of S-parameters at 1.5 GHz for the four soils saturated:
a) Transmitter port P_1 , b) Transmitter port P_2 , c) Transmitter port P_3
and d) Transmitter port P_4

P_4 : At 285 MHz, the behavior of ports P_3 , P_6 and P_7 are similar, but for the remaining ports the magnitude is bigger than in dry sand. There are no significant changes in behavior at 515 MHz, but the values of the S-parameters tend to decrease. At 1.5 GHz, only the values on ports P_2 and P_7 are similar at the reference results.

4.3.1.4.2 Dry Sand vs Saturated level L_2

P_1 : At 285 MHz and 515 MHz, the S-parameters decrease considerably for all of the receiver ports. At 1.5 GHz, the ports P_3 , P_5 , P_6 and P_8 present changes in these parameters.

*P*₂: For 285 MHz the values change for all of receiver ports. At 515 MHz, only the ports *P*₆ and *P*₈ present values similar to the dry sand. The *S* parameters increase in value for all of receiver ports at 1.5 GHz.

*P*₃: For the receiver port *P*₁ at 285 MHz, the *S*-parameter is decrease. At 515 MHz, the *S* parameters increase for all of ports, except for *P*₅. At 1.5 GHz, is observed that the behavior in all of ports is similar with respect to dry sand, but with its values increased.

*P*₄: At 285 MHz and 515 MHz, the graphics patterns change considerably. At 1.5 GHz, the observation is the same given for transmitter port *P*₃.

4.3.1.4.3 Dry Sand vs Saturated level L₃

*P*₁: The magnitudes for *S*-parameters at 285 MHz decrease with respect to dry sand, keeping a similar behavior of dry sand. At 515 MHz the opposite ports to transmitter port keep their values close to those obtained for dry sand. The other ones change considerably. At 1.5 GHz, port *P*₅ undergoes a change of energy and the other ones keep a behavior similar of dry sand.

*P*₂: Ports *P*₄ at 285 MHz and *P*₁, *P*₄ and *P*₆ at 515 MHz, show changes in its behavior. At 1.5 GHz, only the ports *P*₃ and *P*₇ decrease its magnitude.

*P*₃: In all of frequencies, significant changes were observed as regards to their magnitude and behavior. For 285 MHz the *S*-parameters are decreased while at 515 MHz and 1.5 GHz are increased.

P_4 : Ports P_1 , P_3 and P_7 at 285 MHz, P_3 and P_8 at 515 MHz, and P_2 at 1.5 GHz, keep a behavior similar to dry sand, but increasing its magnitude.

4.3.1.4.4 Dry Sand vs Saturated level L_4

P_1 : The S -parameter at 285 MHz and 515 MHz are reduced and at 1.5 GHz are increased, without present similarity in the behavior.

P_2 : The observation obtained is the same that in P_1 .

P_3 : The observation obtained is the same that in P_1 .

P_4 : For the three frequencies the S -parameters keep a similar behavior as the other ports, but the S -parameters at 285 MHz are increasing and at 515 MHz and 1.5 GHz are decreasing.

The analysis of S -parameters for varying degrees of soil saturation level does not give clear results on the behavior electromagnetic, because the contrast of the soil electrical properties produces multiple reflections on the receptor ports at the three frequencies of operation.

4.3.2 Simulations with DNAPL

The effect of DNAPL such as PCE in the EM behavior in the tank, are evaluated by placing different geometries of EM properties represents DNAPL in the tank. The evaluation was conducted in dry and saturated sand at 285 MHz, 515 MHz and 1.5 GHz. These

geometries are placed between the ports P_3 , P_4 , P_7 and P_8 , and represent the possible spreading of the DNAPL.

4.3.2.1 Dry sand with DNAPL

4.3.2.1.1 DNAPL1

Figure 4-14 presents the E-field propagation into the dry sand with the first contaminant geometry (DNAPL1), having dimensions of 0.06 cm by 0.03 cm of length and height and width of 0.018 cm. This shape represents a small amount of the DNAPL into the soil.

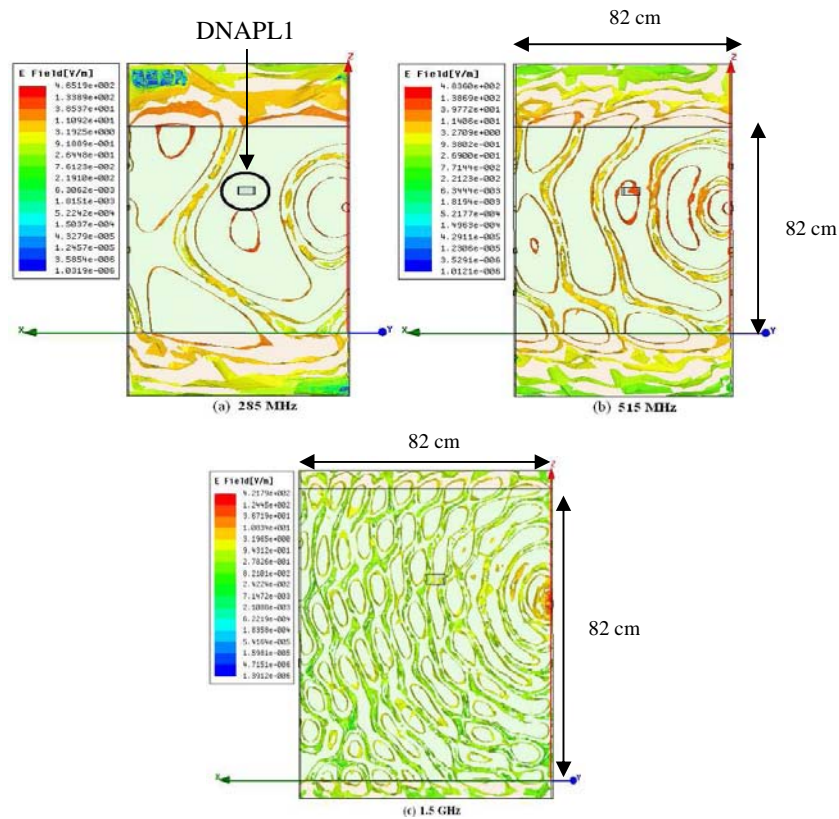


Figure 4.14: E-field distribution in dry sand with DNAPL1 from P_3 : a) 285 MHz, b) 515 MHz and d) 1.5 GHz

In this case, the E-field distribution does not change when the incident wave travels from a medium to other one (dry sand to DNAPL1 and DNAPL1 to dry sand), due to the similarities in the dielectric constants for both media.

Tables 4-20, 4-21 and 4-22 present the *S*-parameters when is included DNAPL1 on dry sand at analysis frequencies.

Table 4.20: S-parameters for dry sand at 285 MHz with DNAPL1

RPort EPort	1	2	3	4	5	6	7	8
1	-13.7	-81.7	-91.8	-163	-121	-83.2	-86.4	-133
2	-102	-11.8	-56.5	-105	-99.6	-98.6	-103	-92.6
3	-45.1	-31.6	-11	-35.2	-39.1	-44.6	-93.1	-82.2
4	-78.7	-104	-59.3	-11.4	-67.1	-121	-88.3	-117
5	-34.4	-35.7	-39.2	-83.3	-11.2	-81	-45.4	-58.3
6	-34.8	-40.9	-44.7	-37.9	-34.8	-11.3	-68.1	-78.9
7	-85.2	-44.1	-40	-74.9	-44.7	-76.7	-10.9	-33.7
8	-84.8	-65.5	-71.9	-33.1	-92.3	-88.7	-91.7	-10.5

*Blue cells are values out of dynamic range

Table 4.21: S-parameters for dry sand at 515 MHz with DNAPL1

RPort EPort	1	2	3	4	5	6	7	8
1	-10.7	-33.6	-39.4	-42.9	-32.2	-69.8	-37.6	-50.6
2	-35.9	-12.3	-95.2	-85	-88.2	-39.5	-35.3	-40.4
3	-42	-36.2	-11.8	-35.7	-40.2	-34.9	-39.9	-40.9
4	-75.4	-72.9	-66.5	-12	-82.8	-71.3	-70.2	-104
5	-35.5	-41.2	-40.3	-48.9	-11.9	-35.6	-42.2	-45.2
6	-40.5	-88.6	-80.8	-39.8	-35.3	-11.5	-35.4	-89.3
7	-38.5	-33.5	-38.6	-88.6	-73	-34	-10.8	-79.7
8	-93.6	-38.3	-37.7	-80.1	-75.7	-40.4	-76.6	-10.8

Table 4.22: S-parameters for dry sand at 1.5 GHz with DNAPL1

RPort EPort	1	2	3	4	5	6	7	8
1	-11.4	-83.8	-88	-47.1	-80	-78.6	-33.6	-40.6
2	-78.4	-11.4	-72.1	-51.2	-31.2	-30.8	-79.2	-32.6
3	-77	-10.3	-10.7	-107	-108	-72.1	-62.6	-61.1
4	-93.2	-95.5	-79	-11.2	-126	-78.4	-116	-122
5	-62.9	-63.2	-97.9	-83.5	-11.5	-71.9	-116	-78.5
6	-84.2	-31.4	-36.7	-34	-37	-12	-77.7	-51.3
7	-109	-104	-66.7	-109	-82.9	-70	-11	-74
8	-91.1	-33	-31	-97.7	-48	-49.5	-36.8	-11.7

*Blue cells are values out of dynamic range

The analysis of the S-parameters at the three frequencies of the operation is show in the section 4.3.1.4 comparing the S-parameters for dry sand without and with DNAPL.

4.3.2.1.2 DNAPL2

A second contaminant geometry (DNAPL2) in introduced into the dry sand. This geometry is composed by two rectangles with dimensions 0.12 *cm* by 0.04 *cm* of length and height and width of 0.018 *cm*. The geometry represents a vertical and horizontal spreading of the contaminant. Figure 4-15 is presented the E-field propagation into the dry sand with the DNAPL2. As the previous case, the E-field distribution does not change at any frequency.

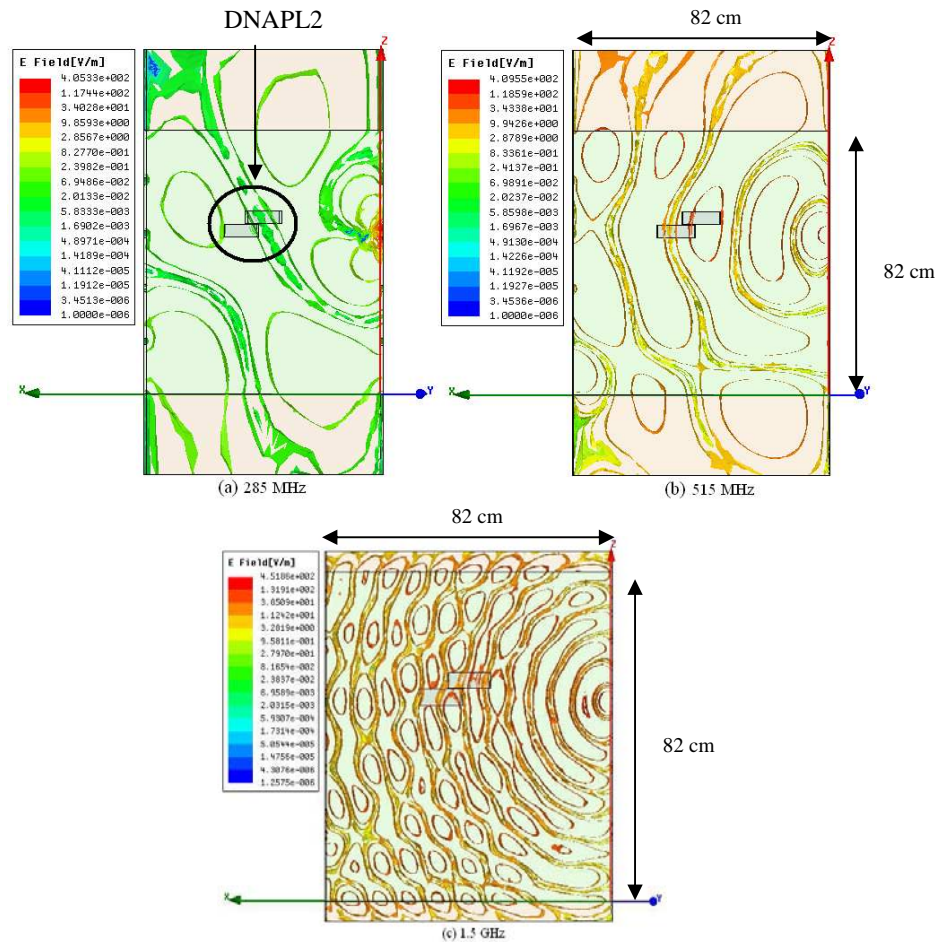


Figure 4.15: E-field distribution in dry sand with DNAPL2 from P₃: a) 285 MHz, b) 515 MHz and d) 1.5 GHz

In Table 4-23, Table 4-24 and Table 4-25, are presented the S -parameters when DNAPL2 is included into the dry sand at the analysis frequencies.

Table 4.23: S-parameters for dry sand at 285 MHz with DNAPL2

RPort EPort	1	2	3	4	5	6	7	8
1	-10.5	-32.7	-94	-68.5	-64.1	-31.3	-36.5	-34.7
2	-78.9	-12	-120	-97.6	-123	-82.2	-85	-122
3	-84.5	-75.6	-11.4	-108	-115	-93.1	-132	-127
4	-132	-95.9	-108	-11.7	-78.8	-125	-110	-117
5	-75.2	-33.7	-38.1	-92.4	-11.8	-90.7	-66.4	-39.3
6	-65.6	-35.3	-37.9	-38	-34.8	-11.2	-33.3	-58.1
7	-70.5	-109	-103	-66	-138	-66	-11.6	-66.8
8	-75.4	-77.4	-116	-114	-78.3	-125	-110	-12

*Blue cells are values out of dynamic range

Table 4.24: S-parameters for dry sand at 515 MHz with DNAPL2

R Port EPort	1	2	3	4	5	6	7	8
1	-12.3	-79	-43.7	-94.1	-33.1	-34.7	-106	-44.5
2	-38.6	-12.6	-37.2	-96.5	-85.2	-42.2	-36.9	-37.5
3	-110	-38.2	-13.1	-92.8	-105	-87.7	-104	-111
4	-43.3	-43.4	-38.3	-12.3	-44.6	-37.4	-34.6	-33.2
5	-31.6	-33.5	-36.2	-43.2	-11.3	-36.5	-41.9	-72.8
6	-33.8	-83.4	-35.3	-36	-37	-11.2	-35.5	-88.7
7	-37.1	-35.9	-42.5	-33.9	43.3	-36.3	-11.9	-85.5
8	-84.8	-80.2	-112	-81.5	-94.1	-144	-77.4	-12.7

*Blue cells are values out of dynamic range

Table 4.25: S-parameters for dry sand at 1.5 GHz with DNAPL2

RPort EPort	1	2	3	4	5	6	7	8
1	-12.1	-78	-89.3	-86.7	-102	-71.1	-71	-87.1
2	-124	-11.6	-146	-91.7	-79.2	-116	-85.3	-80.4
3	-48	-80.1	-12.4	-37.5	-34.5	-36.3	-72.9	-31.9
4	-102	-96.2	-87.8	-13.4	-139	-89.6	-95.6	-90.2
5	-73.8	-72.2	-114	-78.1	-12	-74.8	-84.5	-125
6	-30.6	-30.7	-66.8	-32.9	-36.9	-11.1	-36.3	-50
7	-34	-36.1	-31.9	-31.9	-98.9	-38.1	-12.3	-37.9
8	-41.2	-34.6	-31.5	-31.8	-49.2	-50.9	-86.3	-12.3

*Blue cells are values out of dynamic range

4.3.2.1.3 DNAPL3

A third geometry (DNAPL3) is included into the dry sand, as shown in Figure 4-16. This contains two rectangles and one cylinder, the dimensions for the rectangle are the same as the previous case, and the cylinder is placed vertically with 0.001 cm of radius and 0.05 cm of height.

Change in the E-field distribution when are not observed, due to the little contrast between the dielectric constants of the media.

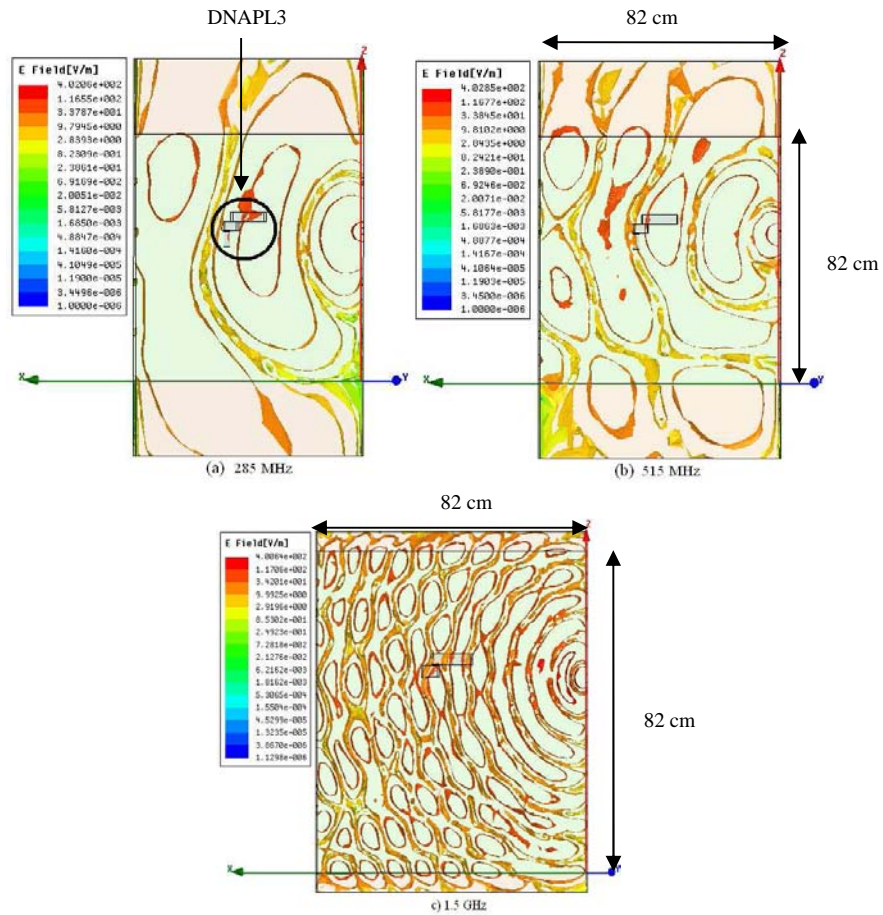


Figure 4.16: E-field distribution in dry sand with DNAPL3 from P₃: a) 285 MHz, b) 515 MHz and d) 1.5 GHz

In Table 4-26, Table 4-27 and Table 4-28 are shown the data obtained when DNAPL3 into the dry sand is included.

Table 4.26: S-parameters for dry sand at 285 MHz with DNAPL3

RPort EPort	1	2	3	4	5	6	7	8
1	-12.1	-35.6	-63.3	-40.3	-33.4	-76.7	-39.2	-89.2
2	-121	-13.1	-136	-90.5	-140	-96.2	-99.4	-88.6
3	-94.9	-33.3	-11.1	-34.3	-38	-88.5	-35.5	-33.2
4	-68.4	-60.3	-75	-10.5	-35.3	-73.9	-65.2	-31.8
5	-30.7	-60.4	-66.8	-34.9	-10.2	-67.3	-84.3	-79.4
6	-33	-35.2	-93.9	-37.5	-33.5	-10.9	-76.8	-58.2
7	-85.2	-38.5	-35.9	-34	-61.6	-33.7	-11.6	-75.1
8	-73.6	-77.8	-33.2	-32.6	-38.8	-61.9	-70.3	-11.2

*Blue cells are values out of dynamic range

Table 4.27: S-parameters for dry sand at 515 MHz with DNAPL3

RPort EPort	1	2	3	4	5	6	7	8
1	-11.7	-65.2	-74.7	-113	-106	-70.7	-112	-111
2	-35.7	-10.9	-34.4	-41.6	-32.7	-40.2	-72.2	-35.1
3	-41.7	-79.2	-11	-36.6	-35.8	-34.3	-75.4	-67.1
4	-44	-34.3	-37.3	-11.9	-32.5	-37.7	-42.7	-42.9
5	-44.2	-43	-38.4	-43.3	-12.4	-37.1	-77.2	-33.3
6	-87.3	-41.9	-36.5	-90.9	-38.2	-12.2	-36.8	-43.1
7	-73.1	-72.4	-78	-70.6	-128	-71.7	-12.7	-128
8	-126	-80.4	-112	-113	-130	-85.8	-82.4	-12.1

*Blue cells are values out of dynamic range

Table 4.28: S-parameters for dry sand at 1.5 GHz with DNAPL3

RPort EPort	1	2	3	4	5	6	7	8
1	-11.5	-79	-118	-90.8	-76.1	-77.6	-74.7	-91.2
2	-63.6	-11.1	-36.5	-81.1	-30.5	-84.8	-69.1	-64.4
3	-88.4	-38.7	-12.5	-38	-85	-36.7	-32	-78
4	-85.8	-50.2	-79.3	-11.7	-86	-84.8	-31	-31.2
5	-32.3	-65.5	-78.6	-40.4	-11.5	-37	-47.7	-89.3
6	-30.9	-31.1	-36.2	-76.8	-36.8	-11.3	-37.5	-86.4
7	-33.8	-36.6	-31.3	-79.8	-49.8	-38.3	-12	-37.2
8	-39.8	-33.1	-30.5	-31.2	-48	-50.6	-36.5	-11.4

The analysis of the S-parameters at the three frequencies of the operation is show in the section 4.3.1.4 comparing the S-parameters for dry sand without and with DNAPL.

4.3.2.1.4 DNAPL4

A fourth geometry is included for the analysis; it contains a rectangle with dimensions 0.2 *cm* by 0.03 *cm* of length by height and width of 0.018 *cm*. This represents a horizontal spreading within the medium. Figure 4-17 shows that this distribution does not result in significant change when the incident wave travels from dry sand to DNAPL and from DNAPL to dry sand, due to little contrast between the electrical properties of the media.

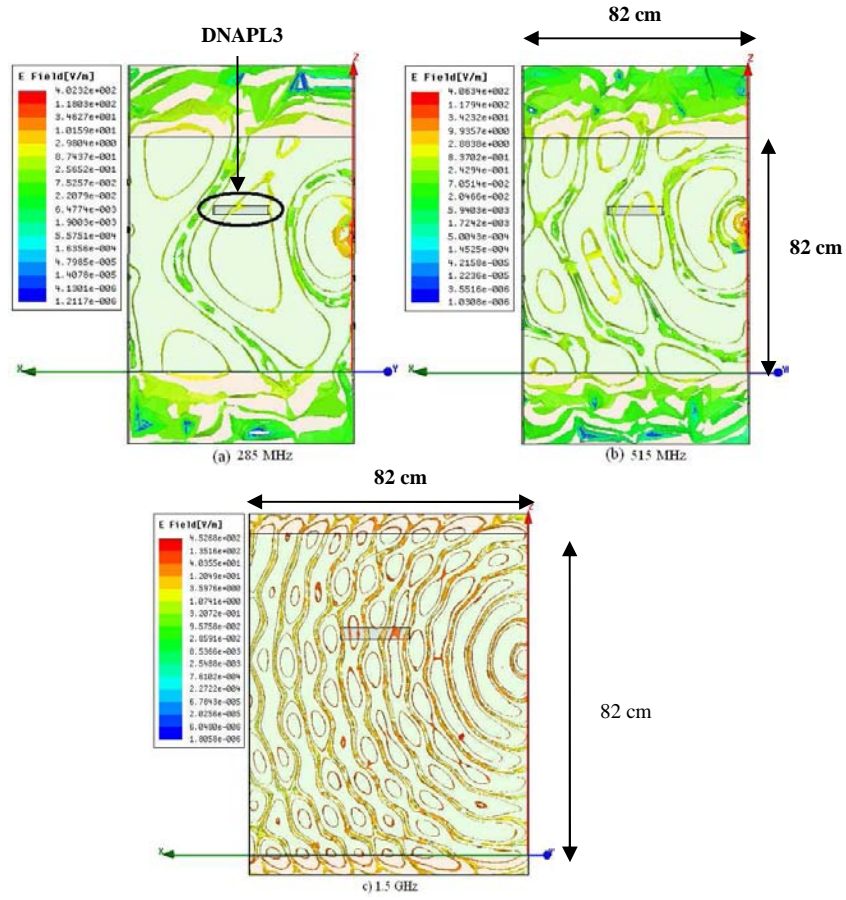


Figure 4.17: E-field distribution in dry sand with DNAPL4 from P₃: a) 285 MHz, b) 515 MHz and d) 1.5 GHz

Tables 4-29, 4-30 and 4-31 show the data obtained when is introduced the DNAPL4 into the dry sand.

Table 4.29: S-parameters for dry sand at 285 MHz with DNAPL4

RPort EPort	1	2	3	4	5	6	7	8
1	-11.2	-35.1	-86.1	-105	-34.5	-35.6	-38.9	-43.1
2	-66.8	-11.7	-102	-75	-65.3	-107	-106	-67
3	-101	-58.4	-11.8	-113	-66.5	-107	-106	-63.5
4	-110	-97.2	-140	-14.3	-95.1	-145	-86	-85.3
5	-101	-66.7	-117	-115	-12	-68.7	-79.8	-85.1
6	-35.6	-91.8	-91.2	-38	-67.8	-11	-31.1	-114
7	-72	-78.4	-116	-99.7	-78.4	-106	-12	-114
8	-113	-116	-61.5	-61.1	-81.5	-75.3	-108	-11.8

*Blue cells are values out of dynamic range

Table 4.30: S-parameters for dry sand at 515 MHz with DNAPL4

RPort EPort	1	2	3	4	5	6	7	8
1	-11.4	-63.2	-97.1	-73.2	-63.6	-69.9	-67.8	-77.5
2	-35.7	-11.9	-94.7	-42.2	-40.8	-38.9	-34.7	-40.3
3	-73.8	-71	-11.7	-62.3	-111	-66.5	-74.2	-102
4	-44.2	-41.5	-34.7	-11.1	-49	-39.3	-39.7	-34.6
5	-73.9	-79.7	-128	-87.4	-13.3	-128	-81.2	-84.3
6	-72.5	-37.7	-33.4	-81.9	-33.6	-10.8	-68.6	-40.4
7	-38.6	-34.1	-75.5	-39	-41	-92.3	-11.3	-34.2
8	-91.8	-112	-122	-68.2	-79.6	-75.5	-130	-12.4

*Blue cells are values out of dynamic range

Table 4.31: S-parameters for dry sand at 285 MHz with DNAPL4

RPort EPort	1	2	3	4	5	6	7	8
1	-12.8	-87.6	-148	-95	-137	-129	-125	-90
2	-70.4	-10.8	-63.1	-76.6	-63.1	-62.1	-111	-62.2
3	-49.4	-38.9	-12.7	-38.1	-35.5	-37.5	-32.1	-32.4
4	-79.3	-110	-67.7	-11.3	-114	-109	-99.3	-65.9
5	-70.5	-69.5	-70.6	-116	-11.2	-74.2	-87.8	-121
6	-30.7	-82.3	-37.3	-65.3	-35.3	-10.9	-36.3	-47.7
7	-70.6	-36.7	-71.6	-30.4	-81.6	-80	-11.1	-80.6
8	-124	-72.6	-104	-71.4	-89.1	-124	-80.8	-11.5

*Blue cells are values out of dynamic range

4.3.2.2 Analysis of *S*-parameters in dry sand without and with DNAPL

In this section shows the analysis of the EM tank when the contaminant is introduced into the dry sand. This analysis was done by comparing the *S*-parameters of the reference results for dry sand, with the *S*-parameters obtained of the contaminant with the contaminated medium (described as consolidated parameters). The consolidated *S*-parameters are the average of the *S*-parameters for the 4 DNAPL geometries. This ensures that the system can detect contaminant regardless the position of them, also there are minor changes because the area of different the 4 DNAPL geometries is small. The comparison for dry sand, with and without contaminant is shown graphically in Figures 4-18, 4-19 and 4-20, for the transmitter ports P_1 , P_2 , P_3 and P_4 at the analysis frequencies.

Figure 4-18, shows few changes of energy at 285 MHz when the contaminant is included within the EM tank. When the signal is transmitted by P_1 and P_2 , there are significant changes of energy on some receiver ports, for P_3 and P_4 due to P_1 and for P_1 and P_3 due to P_2 . These changes do not ensure presence of the DNAPL, because of they could be generated by using different parameters for the simulation. It is observed that when the signal is transmitted by P_3 and P_4 , the *S*-parameters for almost all the receiver ports undergo more significant changes, because the contaminant is placed in front of the transmitter ports.

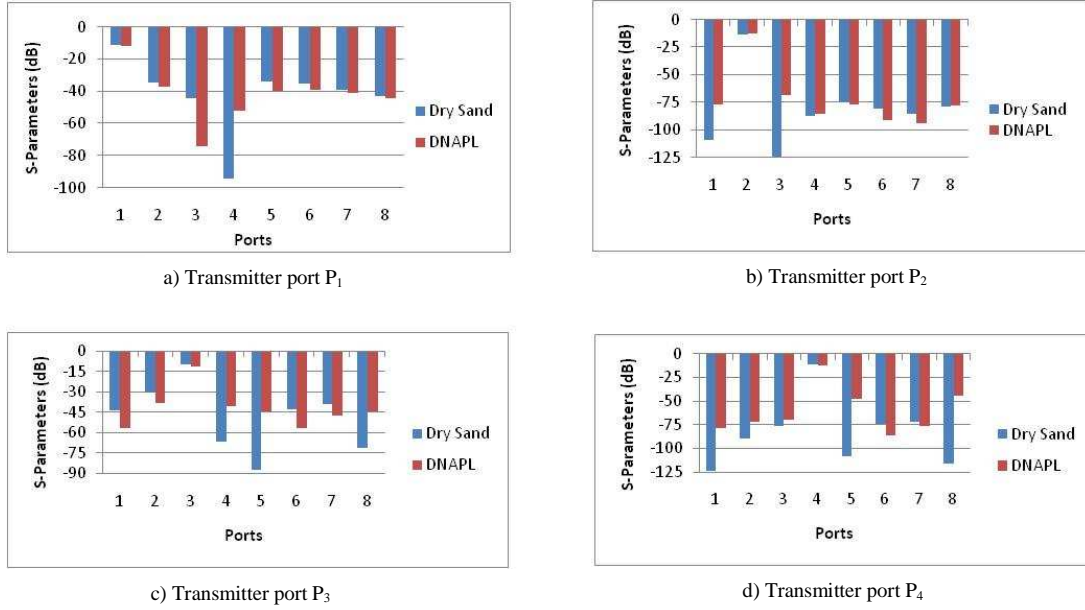


Figure 4.18: Comparison of S-parameters obtain in dry sand with average DNAPL at 285MHz for a) Transmitter P_1 , b) Transmitter P_2 , c) Transmitter P_3 , and d) Transmitter P_4

When the signal is transmitted at 515 MHz (Figure 4.18), there are more changes in the S-parameters for the receiver ports in comparison with those obtained at 285 MHz. When the port Pr_1 is the transmitter, only the energy for the receiver port Pr_2 increases its magnitude. Increments of energy on the Pr_3 and Pr_4 are also for P_{12} . When the signal is transmitted by P_{t3} , all of S-parameters for all of receiver ports are increased. We can say that this change is due to the presence of the DNAPL. Finally, for the P_{t4} are only observed changes for Pr_3 and Pr_8 .

In general, the S-parameters values for all of receiver ports are near of -40 dB due to P_{t3} and P_{t4} , since the 4 DNAPL geometries are opposite.

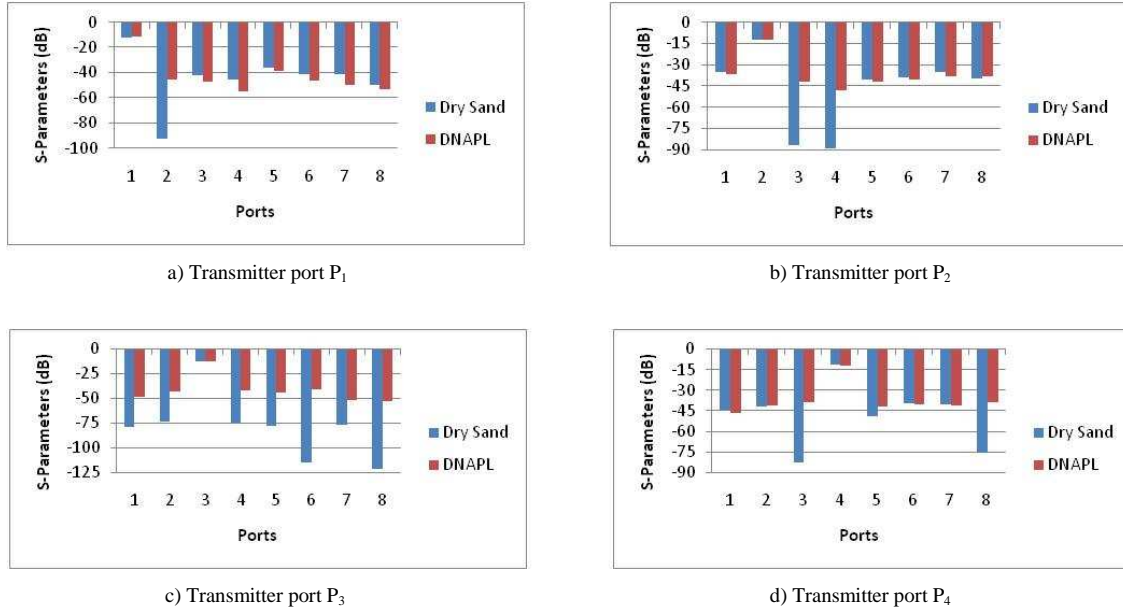


Figure 4.19: Comparison of S-parameters obtain in dry sand with average DNAPL at 515MHz for a) Transmitter P_1 , b) Transmitter P_2 , c) Transmitter P_3 , and d) Transmitter P_4

At 1.5 GHz (Figure 4.20), larger changes in S-parameters were observed for all of receiver ports, compared with the obtained at frequencies 285 MHz and 515 MHz due to the wavelength at 1.5 GHz is smaller.

Small changes of energy are observed for P_{t1} . With P_{t2} and P_{t3} , the magnitude for S-parameters in all of receiver ports is increased. This is due to the close of the DNAPL at these ports. These magnitudes of the S-parameters change are produced by the reflection of the contaminant. Lastly, when the transmitter port is P_{t4} , the ports P_{r5} and P_{r6} do not undergo changes in S-parameters.

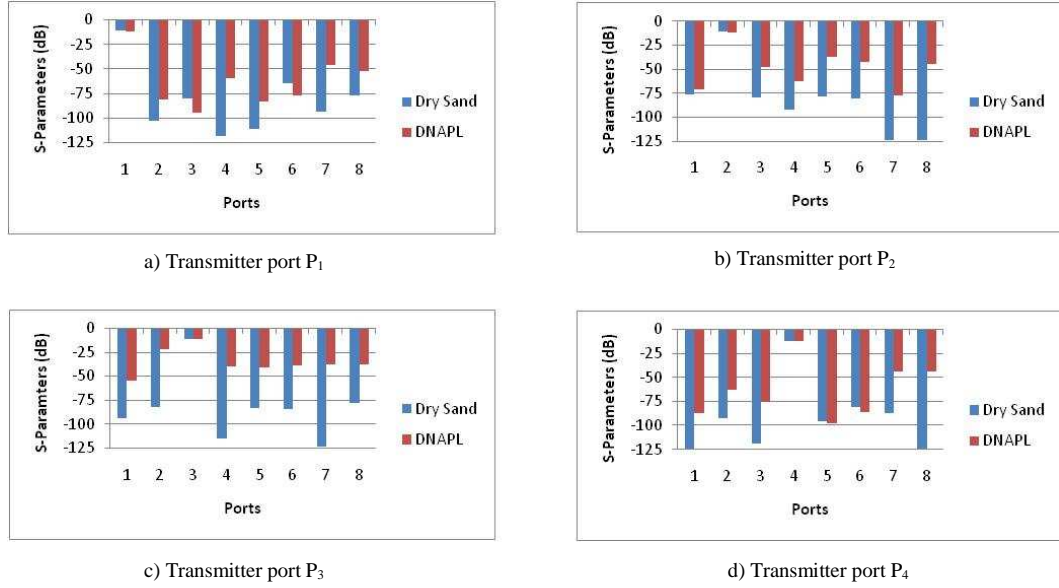


Figure 4.20: Comparison of S-parameters obtain in dry sand with average DNAPL at 1.5 GHz for a) Transmitter P₁, b) Transmitter P₂, c) Transmitter P₃, and d) Transmitter P₄

The detection of the contaminant inside the EM tank in dry sand is possible for specific ports, depending of the depth of the transmitter port at 285 and 515 MHz (Figures 4.18 and 4.19). For 1.5 GHz, the detection of the contaminant is clearer due to the small wavelength (Figure 4.20).

4.3.2.3 Saturated Sand with DNAPL

4.3.2.3.1 DNAPL1

Figure 4-21 shows the E-field distribution of the saturated sand in presence of the first contaminant geometry (DNAPL1). For the three frequencies, when the signal travels from wet sand to DNAPL (from a denser to a less dense medium) an energy concentration is

observed into the DNAPL. This energy concentration does not affect the E-field distribution of the saturated sand when the wave travels from DNAPL to saturated sand. This is possibly due to the small DNAPL size.

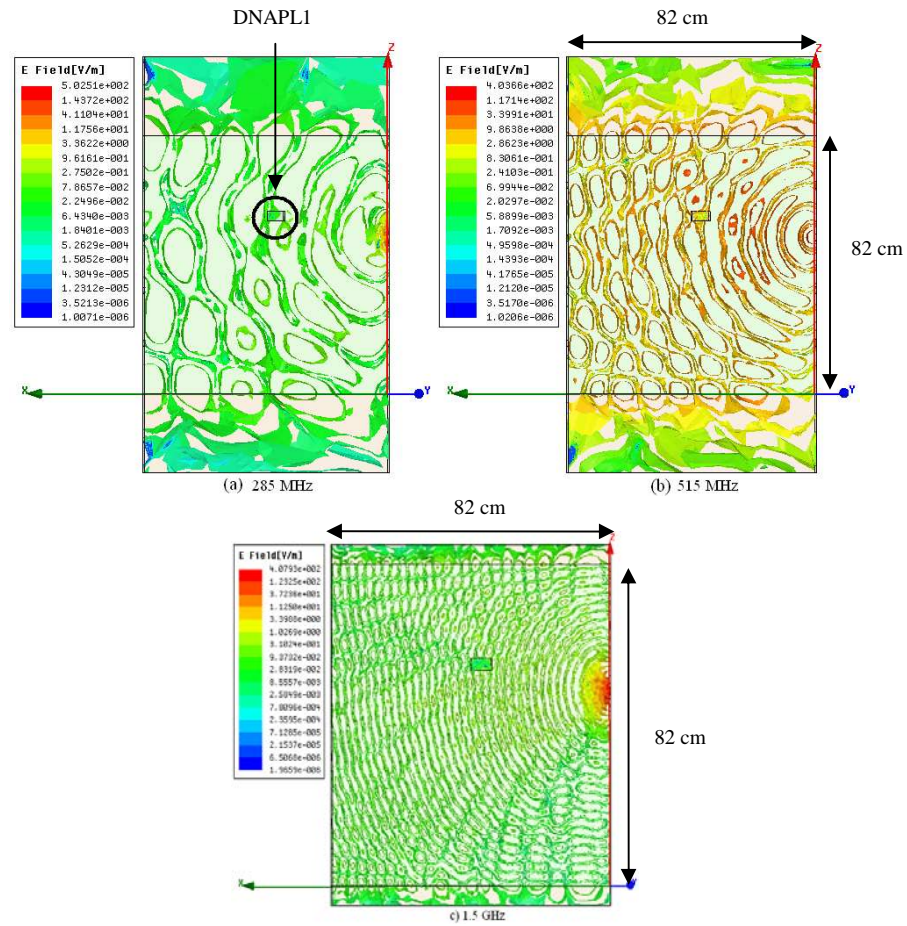


Figure 4.21: E-field distribution in saturated sand with DNAPL1 from P₃: a) 285 MHz, b) 515 MHz and d) 1.5 GHz

Tables 4-32, 4-33 and 4-34 show the data obtained when the DNAPL1 is introduced into the wet sand.

Table 4.32: S-parameters for saturated sand at 285 MHz with DNAPL1

RPort EPort	1	2	3	4	5	6	7	8
1	-11.6	-37.6	-80.8	-98.2	-71	-45.8	-80.9	-76.4
2	-115	-11.9	-121	-83.8	-84.5	-77.8	-116	-86.7
3	-89.2	-77.5	-12	-85.8	-95.7	-90.7	-139	-141
4	-161	-103	-93	-13.6	-151	-101	-102	-92
5	-117	-88.5	-95	-118	-12.9	-133	-103	-107
6	-133	-94.9	-87.3	-99.8	-84.2	-11.7	-111	-125
7	-119	-79.7	-117	-125	-87.2	-73.3	-12.2	-114
8	-87.7	-93.4	-92.8	-86.9	-100	-127	-112	-12.1

*Blue cells are values out of dynamic range

Table 4.33: S-parameters for saturated sand at 515 MHz with DNAPL1

RPort EPort	1	2	3	4	5	6	7	8
1	-11	-73.3	-82.7	-95.1	-70.2	-113	-103	-110
2	-70.2	-10.9	-37.4	-49.6	-41.6	-46.9	-83.2	-36
3	-95.5	-38.9	-11.8	-86.2	-38.1	-46.8	-93.7	-41.9
4	-63	-50.6	-40.3	-11.7	-52.7	-37.4	-41.4	-78.6
5	-92.6	-41.4	-38.3	-101	-12.5	-41.7	-51	-69.1
6	-93.6	-44.6	-87.1	-38.2	-40.6	-12	-77	-49.6
7	-38.4	-43.1	-41.6	-85.2	-49	-38.2	-11.8	-80.2
8	-98.3	-37.2	-77.4	-37.7	-67.1	-93.4	-40.1	-11.6

Table 4.34: S-parameters for saturated sand at 1.5 GHz with DNAPL1

RPort EPort	1	2	3	4	5	6	7	8
1	-7.45	-109	-80.1	-83.2	-64.5	-65	-66.3	-111
2	-38.2	-5.44	-40.1	-45.6	-31.7	-24.2	-26.1	-62.3
3	-96	-97.9	-6.79	-76.8	-87.1	-74.6	-74.6	-76.3
4	-44.5	-49.9	-33	-5.49	-33.4	-40.6	-30.2	-22.6
5	-72.1	-109	-103	-94	-11.2	-79.6	-127	-87.8
6	-32.6	-32.4	-37.3	-35.2	-38.2	-12.8	-38.8	-50.4
7	-94.4	-94.1	-60.4	-98.6	-75.2	-63.2	-11	-68.8
8	-74.9	-70.4	-68.2	-96.4	-87.8	-91	-75.9	-7.6

*Blue cells are values out of dynamic range

The analysis of the S-parameters at the three frequencies of the operation is show in the section 4.3.1.4 comparing the S-parameters for saturated sand without and with DNAPL.

4.3.2.3.2 DNAPL2

In this case, there are some changes in the E-field distribution (Figure 4-22), when the wave incident into the DNAPL and when the wave goes out of the contaminant. This is due to the contrast of the electrical properties of the media.

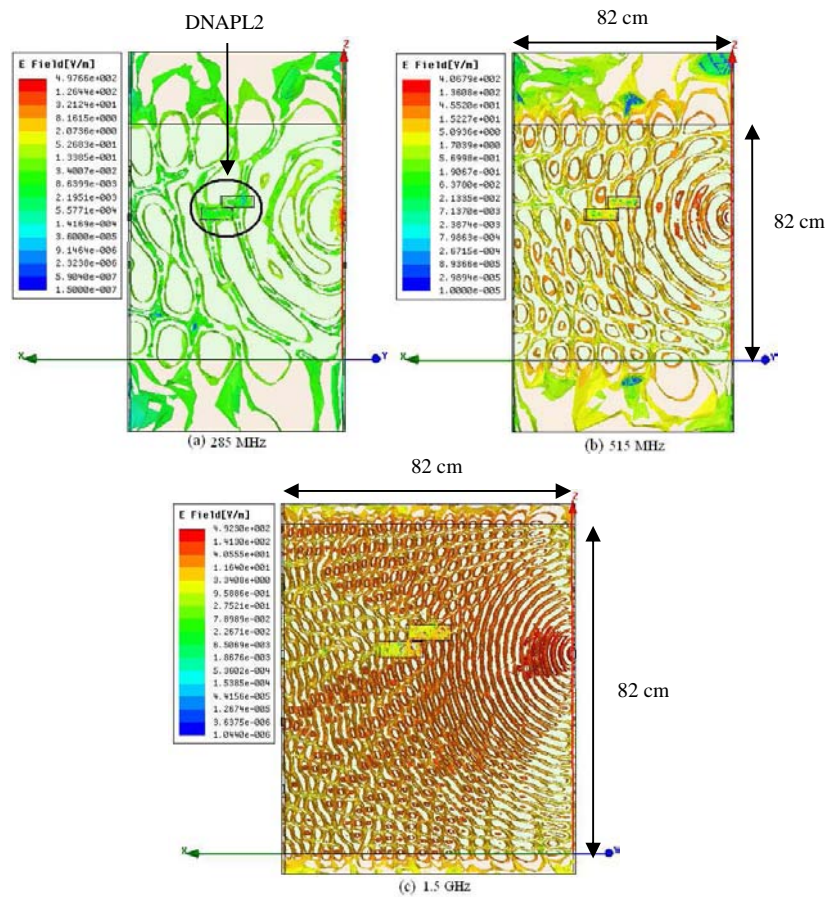


Figure 4.22: E-field distribution in saturated sand with DNAPL2 from P3: a) 285 MHz, b) 515 MHz and d) 1.5 GHz

As the previous case, there is energy concentration into the DNAPL although lower. When the wave travels from DNAPL to saturated sand, loss of energy is observed for the E-field in saturated sand. These changes are more notables at 1.5 GHz.

Tables 4-35, 4-36 and 4-37 show the data obtained when DNAPL2 into the wet sand is introduced.

Table 4.35: S-parameters for saturated sand at 285 MHz with DNAPL2

RPort EPort	1	2	3	4	5	6	7	8
1	-11.3	-70.7	-46	-52.6	-36.6	-37.3	-89.5	-45.6
2	-38.9	-13	-39.7	-50.4	-40.3	-41.4	-42.4	-50.2
3	-125	-79.2	-12	-83	-100	-123	-121	-86.1
4	-143	-97.5	-117	-12.1	-127	-95.1	-84.4	-121
5	-38.7	-39.8	-96.3	-89.5	-12.6	-89	-48.8	-56.6
6	-96	-107	-109	-136	-72.4	-11.5	-101	-121
7	-114	-98.8	-100	-98.5	-161	-95	-14	-93.5
8	-77.6	-112	-69.3	-67.2	-86.3	-104	-99.9	-11.5

*Blue cells are values out of dynamic range

Table 4.36: S-parameters for saturated sand at 515 MHz with DNAPL2

RPort EPort	1	2	3	4	5	6	7	8
1	-11.7	-40	-51.8	-103	-36.3	-48.2	-37.7	-44
2	-40	-11.9	-84.6	-47	-90	-40.9	-41	-90.9
3	-50.9	-36.6	-11	-72	-84.9	-37.8	-42.7	-42.1
4	-150	-101	-91.6	-11.2	-150	-97	-131	-26
5	-79.1	-41.1	-49.5	-44.3	-11.1	-77.3	-52.1	-51.7
6	-106	-41.2	-39.7	-41.9	-39.9	-12.5	-90.3	-47.5
7	-38.5	-41.1	-49.5	-44.3	-54.1	-37.9	-12.4	-91.8
8	-96.2	-41.7	-44	-35.3	-53.9	-47.8	-40.7	-12.8

*Blue cells are values out of dynamic range

Table 4.37: S-parameters for saturated sand at 1.5 GHz with DNAPL2

RPort EPort	1	2	3	4	5	6	7	8
1	-5.31	-35.2	-57.8	-82.4	-21.8	-28.6	-77.7	-35.5
2	-36.6	-5.65	-36.4	-42.7	-37.5	-74.4	-26.8	-32.8
3	-44.6	-36.3	-5.51	-33.2	-32.1	-63.6	-31.2	-73
4	-95.5	-44.7	-83.6	-5.62	-92.4	-42.4	-43.2	-22.1
5	-22	-36.7	-33.4	-37.1	-5.26	-38.4	-78.5	-43.2
6	-30.1	-23.4	-23.6	-43.3	-37.7	-5.65	-89.7	-90.5
7	-36.8	-26.3	-30.5	-41.1	-42.5	-39.1	-5.49	-63.6
8	-92.3	-32.8	-36	-79.2	-44	-44.6	-29.5	-5.49

*Blue cells are values out of dynamic range

The analysis of the S-parameters at the three frequencies of the operation is show in the section 4.3.1.4 comparing the S-parameters for saturated sand without and with DNAPL

4.3.2.3.3 DNAPL3.

The E-field distribution for this experiment is shown in Figure 4-23. In this case, the effects produced when the wave travels from a medium to other one are similar to the previous case. The addition of the cylinder into the DNAPL2 configuration does not present significant changes in the E-field distribution.

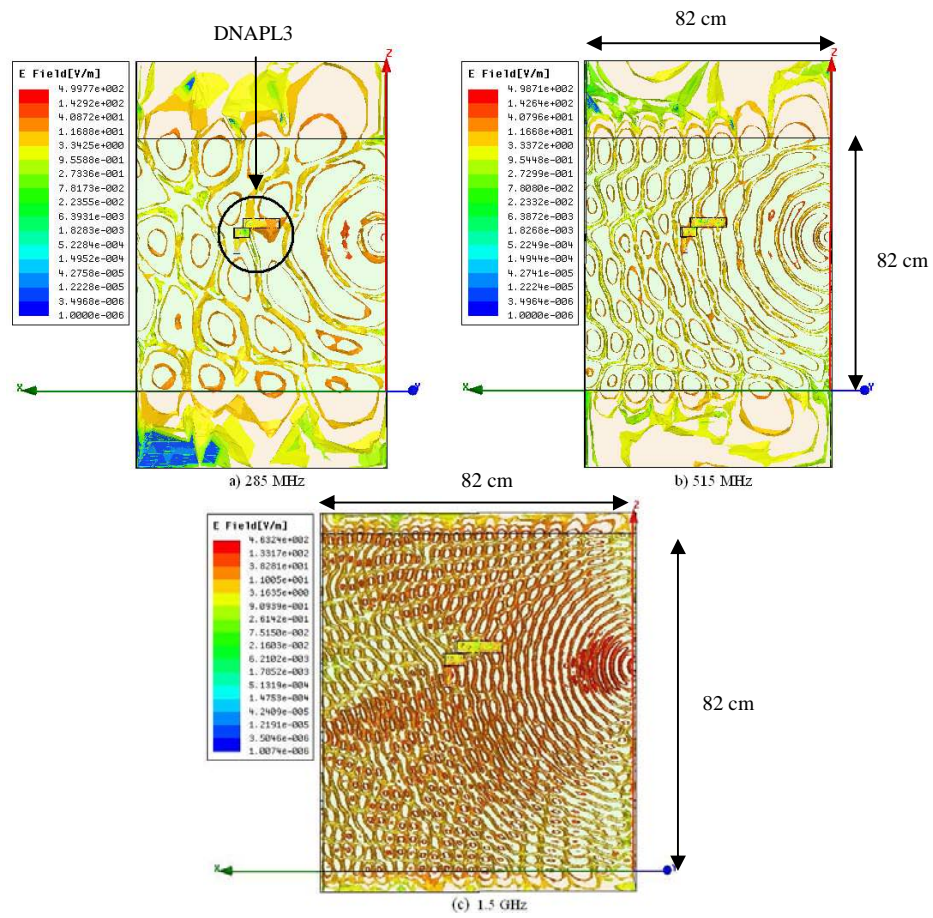


Figure 4.23: E-field distribution in saturated sand with DNAPL3 from P₃: a) 285 MHz, b) 515 MHz and d) 1.5 GHz

Tables 4-38, 4-39 and 4-40 show the data obtained when DNAPL3 into the wet sand is introduced.

Table 4.38: S-parameters for saturated sand at 285 MHz with DNAPL3

RPort EPort	1	2	3	4	5	6	7	8
1	-12	-87	-101	-109	-84	-87	-150	-89.4
2	-130	-12.5	-143	-92.7	-80.4	-133	-132	-88.7
3	-78.5	-37.1	-11.4	-36.4	-83.3	-39	-95.9	-39.3
4	-120	-114	-107	-14.2	-120	-112	-163	-165
5	-38.4	-40.7	-135	-48	-12.9	-39.2	-49.3	-55
6	-116	-73.6	-129	-82.5	-69.4	-11.9	-71.4	-111
7	-130	-133	-123	-85.2	-94.6	-86.7	-12.2	-121
8	-99.9	-101	-154	-90.1	-106	-99.2	-90.2	-14

*Blue cells are values out of dynamic range

Table 4.39: S-parameters for saturated sand at 515 MHz with DNAPL3

RPort EPort	1	2	3	4	5	6	7	8
1	-12.8	-41.8	-50.3	-70.6	-89.6	-47.1	-37.9	-44.3
2	-40.8	-11.8	-38.7	-48.9	-86.2	-43.1	-39.2	-38.6
3	-95.4	-39.2	-12.8	-40.1	-37.5	-39.7	-108	-45.9
4	-104	-44.4	-88.5	-12.2	-37.7	-40.8	-96.7	-57.8
5	-44.1	-92.6	-82.3	-70.1	-12.1	-39.1	-46.1	-80.2
6	-46.3	-42.6	-75.4	-38.8	-39.5	-11.5	-39.6	-49.7
7	-37.5	-89.2	-56.2	-46.3	-96.7	-82.2	-12.3	-88.3
8	-96.5	-92.1	-101	-88.2	-109	-102	-91.9	-12.8

*Blue cells are values out of dynamic range

Table 4.40: S-parameters for saturated sand at 1.5 GHz with DNAPL3

RPort EPort	1	2	3	4	5	6	7	8
1	-5.27	-46.3	-43.9	-101	-23.4	-35.5	-35.7	-44.9
2	-82.2	-5.18	-31.8	-78.4	-32.2	-25.4	-25.2	-34.8
3	-42.4	-32.3	-5.49	-79.3	-35.7	-23.1	-48.2	-34.6
4	-50.3	-44.1	-34.5	-5.26	-35.9	-43.5	-31.2	-24.4
5	-23.5	-31.3	-81.2	-35.5	-5.4	-40.1	-44.8	-39.7
6	-34.1	-68.5	-22.6	-44.6	-85.5	-5.29	-35.1	-33.7
7	-71.8	-61.7	-119	-109	-119	-73.2	-7.03	-72.3
8	-78.6	-101	-98.3	-54.7	-102	-65.5	-63.3	-7.15

*Blue cells are values out of dynamic range

The analysis of the S-parameters at the three frequencies of the operation is show in the section 4.3.1.4 comparing the S-parameters for saturated sand without and with DNAPL

4.3.2.3.4 DNAPL4

For this experiment, the effects in the E-field distribution for saturated sand are the same as the previous case (Figure 4-24), although is observed an E-field distribution clearer into the DNAPL4 due to its geometry.

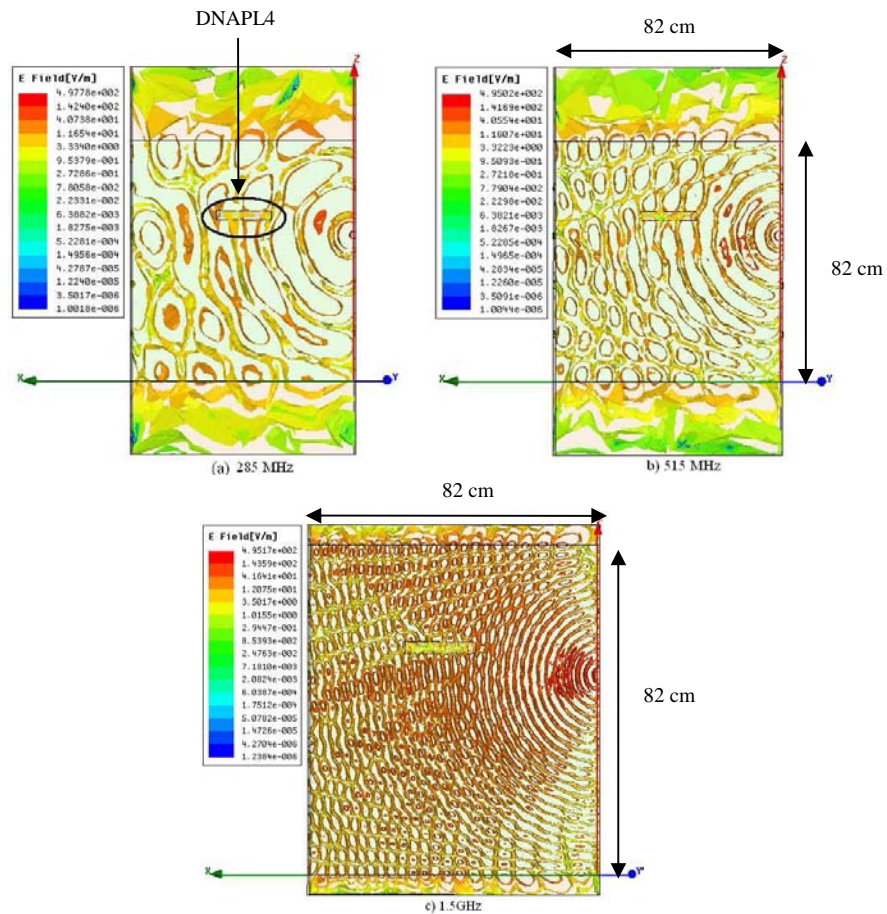


Figure 4.24: E-field distribution in saturated sand with DNAPL4 from P3: a) 285 MHz, b) 515 MHz and d) 1.5 GHz

Tables 4-41, 4-42 and 4-43 show the data obtained when is introduced the DNAPL4 into the wet sand.

Table 4.41: S-parameters for saturated sand at 285 MHz with DNAPL4

R Port EPort	1	2	3	4	5	6	7	8
1	-11.3	-65	-113	-125	-67.4	-126	-111	-112
2	-91.4	-11	-104	-103	-99.2	-66.5	-111	-109
3	-83.3	-36.6	-11.3	-37.6	-103	-83.5	-69.5	-75.4
4	-70.2	-48.6	-38.3	-11.6	-71.4	-48.4	-79.7	-68.3
5	-73.2	-44.7	-48.1	-41.1	-11.6	-37.4	-48	-96.9
6	-48.7	-39.8	-108	-48.8	-73.1	-11.9	-75.6	-87.7
7	-104	-105	-98.4	-102	-133	-79.2	-11.7	-112
8	-80.9	-87.8	-89.1	-79.7	-95.8	-123	-110	-12.2

*Blue cells are values out of dynamic range

Table 4.42: S-parameters for saturated sand at 515 MHz with DNAPL4

RPort EPort	1	2	3	4	5	6	7	8
1	-11.6	-40.1	-51.1	-63.8	-36.2	-39.2	-38.2	-89.6
2	-82.1	-11.8	-38.6	-53.2	-75.4	-51.4	-42.1	-39.8
3	-52.1	-37.6	-11.6	-40.7	-71.6	-40.9	-78.9	-41
4	-91.2	-88	-81.2	-11.3	-84.2	-38.3	-77.6	-36.5
5	-39.2	-39.6	-83.6	-56.6	-12.7	-41.3	-53.5	-66.4
6	-79.3	-88	-123	-81.8	-86.1	-11	-122	-125
7	-72.8	-40.7	-40.5	-40.5	-50.7	-83.5	-11.3	-39.8
8	-102	-99.3	-97.6	-92.2	-109	-104	-92.9	-12.8

*Blue cells are values out of dynamic range

Table 4.43: S-parameters for saturated sand at 1.5 GHz with DNAPL4

RPort EPort	1	2	3	4	5	6	7	8
1	-7.7	-68.7	-77.4	-83.6	-57.3	-65.1	-65.7	-67.9
2	-38.8	-5.59	-40.1	-45.9	-68.4	-22.5	-26.8	-38.8
3	-42.2	-40.6	-5.71	-34.8	-38.3	-29.3	-72.8	-66.1
4	-47.1	-73.9	-33.1	-5.49	-34.9	-33.3	-29.4	-21.5
5	-24.2	-30.9	-37.6	-79.8	-5.4	-38.2	-45.9	-48
6	-82.2	-22.4	-29.3	-34	-38.9	-5.23	-34.8	-56.5
7	-36.6	-25.9	-27.2	-27.5	-91.5	-37.5	-5.39	-43
8	-82.1	-39.9	-32.4	-21.2	-48.5	-58.9	-44.4	-5.54

*Blue cells are values out of dynamic range

4.3.2.4 Analysis of S-parameters in saturated sand

In this section, the analysis of the EM tank when the contaminant is contained in saturated sand is shown. This analysis was done by comparing the S-parameters of the reference results for saturated sand, with the consolidated S-parameters within this medium.

The comparison for saturated sand, with and without contaminant, is shown graphically in Figures 4-25, 4-26 and 4-27, for the transmitter ports P_1 , P_2 , P_3 and P_4 at the analysis frequencies.

Figure 4-25 shows increment of energy (around -50 dB) in all of receiver ports when the signal is transmitted by P_{t2} , P_{t3} and P_{t4} since these are closer to the DNAPL zone.

When the incident wave travels from P_1 , the receptor ports are affected by the presence of contaminant (around -5 dB), principally the Pr_3 and Pr_7 (around -40 dB). This is due to the distance between the P_1 the DNAPL, and to the localization of the DNALP in the EM tank.

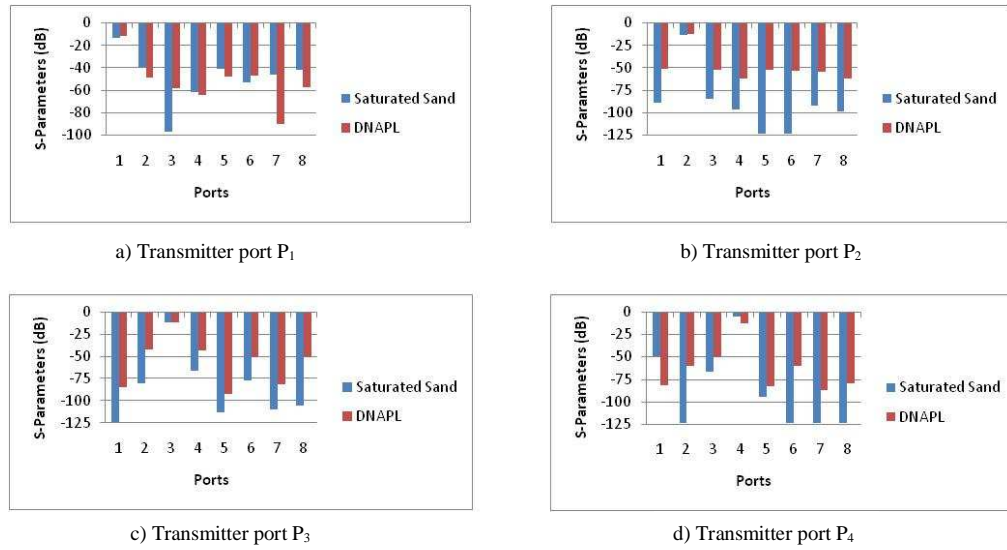


Figure 4.25: Comparison of S-parameters obtain in saturated sand with average DNAPL at 285 MHz for a) Transmitter P_1 , b) Transmitter P_2 , c) Transmitter P_3 , and d) Transmitter P_4

When the signal is transmitted at 515 MHz (Figure 4-26), there are changes in the S-parameters for the receiver ports when the wave is transmitted from all ports.

Mainly, the P_7 port as receptor presents more significant change of the energy when is transmitted from the four ports. These results are expected because the DNAPL is just in front of these ports; therefore the wave is propagating directly.

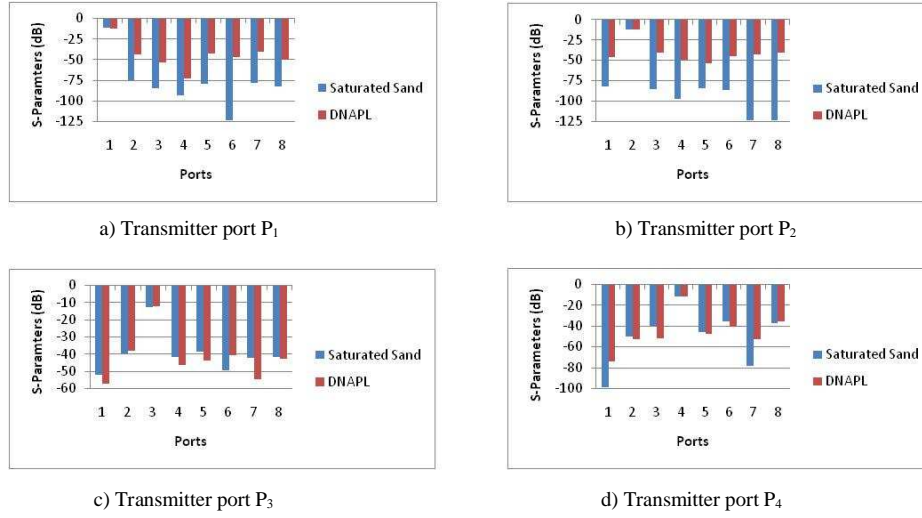


Figure 4.26: Comparison of S-parameters obtain in saturated sand with average DNAPL at 515 MHz for a) Transmitter P_1 , b) Transmitter P_2 , c) Transmitter P_3 , and d) Transmitter P_4

At 1.5 GHz (Figure 4-27), changes of energy in all receptor ports are observed in the presence of the DNAPL. Only in some receiver ports significant changes are observed.

For P_1 as transmitter port, the receptor ports P_5 and P_8 show significant changes (around -30 dB and -20 dB, respectively). For P_2 as transmitter port, the receptor ports P_1 , P_3 and P_8 show significant changes of energy (around -45 dB). When P_3 is the transmitter port, the receptor port P_4 has a change of around -60 dB, and when P_4 is the transmitter port, the receptor port P_5 . These changes of energy are due to the reflections produced by the DNAPL.

From the figures of E-field distribution for saturated sand with the different shape of DNAPL show before (Figure 4.21, Figure 4.22, Figure 4.23, and Figure 4.24), S-parameters are expected to show more significant changes at 1.5 GHz, since there was more contrast due to the dielectric constants of the media. However, the wavelength at this frequency is small,

therefore the changes in magnitude of the S-parameter very significant in comparison with the S-parameters at the frequencies 285 and 515 MHz.

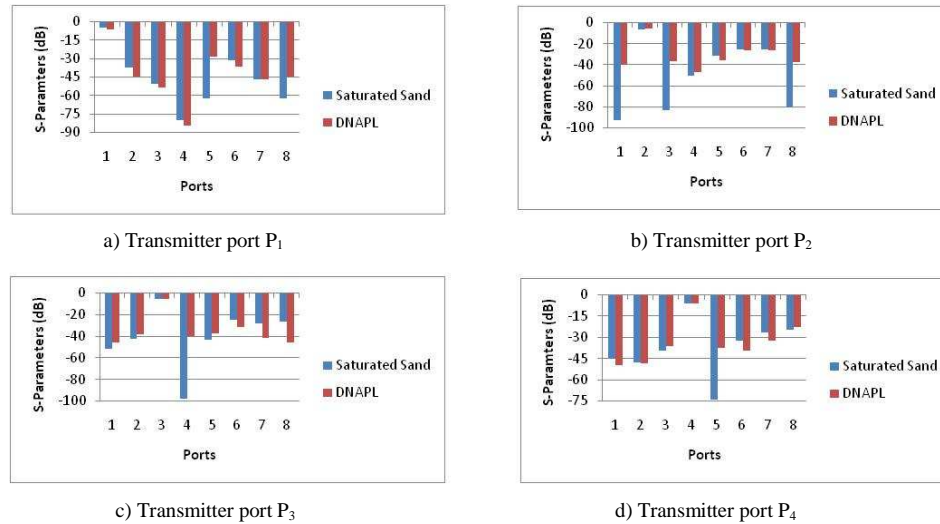


Figure 4.27: Comparison of S-parameters obtain in saturated sand with average DNAPL at 1.5 GHz for a) Transmitter P₁, b) Transmitter P₂, c) Transmitter P₃, and d) Transmitter P₄

In order, changes of energy in the transmitter ports when the wave is reflected from the medium were no observed. These changes were observed comparing the S-parameters of dry sand without and with DNAPL and the S-parameters of saturated sand without and with DNAPL.

Also, the detection of the contaminant with different electrical properties of the media and positions of the transmitter port was achieved at the frequencies of operation.

4.4 Electromagnetic Model Using XFDTD

To corroborate the results obtained in the HFSS simulator, when different contaminant geometries are included in the dry and saturated sand, an electromagnetic model in the XFDTD simulator was implemented. In these simulations, the EM tank was simulated with dry and saturated sand in order to obtain the reference results. Two different shapes for the DNAPL (DNAPL1 and DNAPL2) into these media were also simulated. The analysis made for these simulations was done in the same manner as the one realized for HFSS simulator.

4.4.1 *Dry Sand*

This section presents the *S*-parameters for simulations of dry sand without and with contaminant, at the three analysis frequencies and its analysis. The E-field propagation in it simulator, is considered similar to the E-field propagation shows in HFSS. Tables 4-44, 4-45 and 4-46, show the *S*-parameters obtained for dry sand without DNAPL using XFDTD simulator at the frequencies of operation.

The convergence in the XFDTD simulator is determined dissipating the electromagnetic energy to zero. Due to numerical noise in the calculation, the values are diminished by at least 30 dB or $1/1000^{\text{th}}$ from the peak values [31].

Table 4.44: S-parameters of dry sand at 285 MHz with XFDTD

RPort EPort	1	2	3	4	5	6	7	8
1	-3.25	-18.82	-25.43	-20.82	-10.62	-11.88	-17.59	-18.51
2	-18.82	-2.83	-11.46	-25.04	-11.89	-29.25	-21.73	-18.46
3	-25.43	-11.46	-2.86	-19.09	-17.6	-21.73	-26.37	-12.3
4	-20.82	-25.03	-19.08	-3.06	-18.51	-18.44	-12.29	-10.63
5	-10.62	-11.88	-17.59	-18.51	-3.25	-18.82	-25.43	-20.82
6	-11.89	-29.25	-21.73	-18.46	-18.82	-2.83	-11.46	-25.04
7	-17.6	-21.73	-26.37	-12.3	-25.43	-11.46	-2.86	-19.08
8	-18.51	-18.44	-12.29	-10.63	-20.82	-25.03	-19.08	-3.07

Table 4.45: S-parameters of dry sand at 515 MHz with XFDTD

RPort EPort	1	2	3	4	5	6	7	8
1	-3.52	-11.89	-18.41	-18.59	-15.07	-18.43	-19.68	-15.91
2	-11.9	-3.92	-22.42	-17.92	-18.42	-16.51	-13.65	-19.9
3	-18.4	-22.42	-3.89	-11.92	-19.67	-13.65	-15.88	-18.89
4	-18.59	-17.92	-11.93	-3.74	-15.91	-19.9	-18.9	-15.06
5	-15.07	-18.43	-19.67	-15.91	-3.52	-11.89	-18.41	-18.59
6	-18.42	-16.51	-13.65	-19.9	-11.9	-3.92	-22.42	-17.92
7	-19.67	-13.65	-15.88	-18.89	-18.4	-22.42	-3.89	-11.92
8	-15.91	-19.9	-18.9	-15.07	-18.59	-17.92	-11.93	-3.74

Table 4.46: S-parameters of dry sand at 1.5 GHz with XFDTD

RPort EPort	1	2	3	4	5	6	7	8
1	-3.71	-29.91	-20.53	-20.86	-21.78	-22.97	-15.29	-29
2	-29.56	-3.86	-21.3	-21.33	-23.08	-19.5	-29.33	-16.12
3	-20.52	-21.3	-3.92	-29.4	-15.29	-29.33	-20.65	-23.96
4	-20.87	-21.37	-29.88	-3.4	-29.9	-16.13	-23.9	-26.29
5	-21.78	-22.97	-15.29	-29	-3.7	-29.58	-20.53	-20.86
6	-23.08	-19.5	-31.33	-16.12	-29.56	-3.86	-21.3	21.33
7	-15.28	-29.33	-20.65	-23.97	-20.52	-21.3	-3.92	-29.4
8	-29.01	-16.13	-23.9	-26.3	-20.87	-21.37	-29.88	-3.4

The analyses of the S-parameters in dry sand without contaminant at the frequencies of operation are made comparison the consolidated S-parameters in dry sand with of the two DNAPL geometries (sections 4.4.1.1 and 4.4.1.2).

4.4.1.1 Dry Sand with DNAPL1

Tables 4.47, 4.48 and 4.49 present the S-parameters when DNAPL1 is included on dry sand at analysis frequencies. This geometry has dimensions of 0.06 *cm* by 0.03 *cm* of length and height and width of 0.018 *cm*, respectively.

Table 4.47: S-parameters of dry sand with DNAPL1 at 285 *MHz*

RPort EPort	1	2	3	4	5	6	7	8
1	-3.25	-18.8	-25.4	-20.81	-10.63	-11.88	-17.57	-18.49
2	-18.81	-2.83	-11.45	-25.04	-11.88	-29.22	-21.73	-18.46
3	-25.39	-11.45	-2.86	-19.07	-17.59	-21.74	-26.37	-12.29
4	-20.82	-25.04	-19.05	-3.07	-18.5	-18.42	-12.28	-10.62
5	-10.63	-11.88	-17.57	-18.5	-3.25	-18.8	-25.39	-20.8
6	-11.89	-29.22	-21.74	-18.45	-18.82	-2.83	-11.45	-25.03
7	-17.59	-21.73	-26.37	-12.29	-25.37	-11.45	-2.86	-19.05
8	-18.5	-18.44	-12.29	-10.62	-20.8	-25.04	-19.03	-3.07

Table 4.48: S-parameters in dry sand with DNAPL1 at 515 MHz

RPort EPort	1	2	3	4	5	6	7	8
1	-3.51	-11.88	-18.4	-18.62	-15.08	-18.37	-19.62	-15.95
2	-11.87	-3.9	-22.41	-17.94	-18.38	-16.5	-13.63	-19.84
3	-18.42	-22.41	-3.86	-11.92	-19.64	-13.65	-15.84	-18.91
4	-18.62	-17.92	-11.92	-3.73	-15.91	-19.91	-18.8	-15.07
5	-15.08	-18.35	-19.66	-15.91	-3.514	-11.9	-18.41	-18.62
6	-18.4	-16.48	-13.64	-19.88	-11.89	-3.9	-22.38	-17.93
7	-19.6	-13.63	-15.84	-18.83	-18.43	-22.28	-3.87	-11.9
8	-15.95	-19.87	-18.87	-15.07	-18.62	-17.9	-11.9	-3.72

Table 4.49 : S-parameters in dry sand with DNAPL1 at 1.5 GHz

RPort EPort	1	2	3	4	5	6	7	8
1	-3.7	-34.29	-20.51	-20.84	-21.9	-23.22	-15.31	-29.17
2	-34.25	-3.86	-21.14	-21.3	-23.34	-19.39	-31.53	-16.11
3	-20.5	-21.14	-3.9	-42.98	-15.32	-30.97	-20.56	-23.88
4	-20.85	-21.34	-43.41	-3.4	-29.3	-16.19	-23.83	-26.15
5	-21.9	-23.23	-15.32	-29.29	-3.72	-32.84	-20.45	-20.94
6	-23.3	-19.39	-30.96	-16.17	-32.84	-3.9	-21.17	-21.3
7	-15.31	-31.52	-20.56	-23.9	-20.44	-21.16	-3.92	-42.5
8	-29.18	-16.12	23.82	-26.15	-20.95	-21.33	-42.85	-3.4

4.4.1.2 Dry Sand with DNAPL2

A second contaminant geometry (DNAPL2) is introduced into the dry sand. This geometry is composed by two rectangles with dimensions 0.12 cm by 0.04 cm of length and height and width of 0.018 cm, respectively. Table 4.50, 4.51 and 4.52 present the S-parameters when DNAPL2 is included on dry sand at 285 MHz, 515 MHz and 1.5 GHz.

Table 4.50: S-parameters in dry sand with DNAPL2 at 285MHz

RPort EPort	1	2	3	4	5	6	7	8
1	-3.25	-18.8	-25.41	-20.82	-10.64	-11.88	-17.57	-18.5
2	-18.81	-2.83	-11.45	-25.04	-11.89	-29.22	-21.73	-18.46
3	-25.39	-11.45	-2.86	-19.07	-17.59	-21.74	-26.37	-12.3
4	20.82	-25.04	-19.06	-3.07	-18.5	-18.43	-12.28	-10.62
5	-10.64	-11.88	-17.57	-18.5	-3.25	-18.81	-25.39	-20.81
6	-11.89	-29.22	-21.74	-18.45	-18.82	-2.83	-11.45	-25.03
7	-17.59	-21.73	-26.37	-12.29	-25.38	-11.45	-2.87	-19.05
8	-18.5	-18.44	-12.29	-10.62	-20.81	-25.04	-19.03	-3.07

Table 4.51: S-parameters in dry sand with DNAPL2 at 515MHz

RPort EPort	1	2	3	4	5	6	7	8
1	-3.51	-11.89	-18.4	-18.62	-15.08	-18.37	-19.63	-15.95
2	-11.88	-3.9	-22.41	-17.94	-18.38	-16.49	-13.64	-19.84
3	-18.42	-22.41	-3.86	-11.92	-19.64	-13.65	-15.84	-18.91
4	-18.62	-17.92	-11.92	-3.73	-15.91	-19.91	-18.8	-15.08
5	-15.08	-18.35	-19.66	-15.91	-3.51	-11.9	-18.41	-18.62
6	-18.4	-16.49	-13.65	-19.88	-11.89	-39.02	-22.38	-17.93
7	-19.61	-13.64	-15.84	-18.83	-18.43	-22.38	-3.88	-11.9
8	-15.95	-19.87	-18.87	-15.08	-18.62	-17.91	-11.91	-3.73

Table 4.52: S-parameters in dry sand with DNAPL2 at 1.5 GHz

RPort EPort	1	2	3	4	5	6	7	8
1	-3.7	-34.29	-20.51	-20.85	-21.91	-23.23	-15.31	-29.17
2	-34.26	-3.86	-21.15	-21.31	-23.35	-19.39	-31.59	-16.11
3	-20.51	-21.15	-3.91	-42.98	-15.32	-30.97	-20.57	-23.88
4	-20.86	-21.35	-43.42	-3.41	-29.3	-16.19	-23.84	-26.16
5	-21.9	-23.23	-15.32	-29.29	-3.72	-32.85	-20.45	-20.95
6	-23.34	-19.39	-3.1	-16.18	-32.84	-3.9	-21.17	-21.3
7	-15.31	-31.53	-20.57	-23.9	-20.44	-21.17	-3.93	-42.48
8	-29.18	-16.12	-23.82	-26.16	-20.95	-21.34	-42.86	-3.41

These DNAPL geometries are placed between the ports P_3 , P_4 , and P_7 , P_8 , and represent the possible spreading of the DNAPL. In the Tables previous, the reflected energy (reflection coefficient) from the medium toward the transmitter port in the main diagonal is showed. The transmitted energy (transmission coefficient) to the receptor ports is presented in the row and column of the tables.

4.4.1.3 Analysis of S-parameters in dry sand

Figures 4.28, 4.29 and 4.30 showed the comparison between the S-parameters in dry sand and the consolidated S-parameters of the two DNAPL geometries in dry sand.

The comparisons of S-parameters at 285 MHz (Figure 4.28) do not present significant changes of energy, due to few contrasts of the soil electrical properties of dry sand and the contaminant. However, when P_4 is transmitter port, energy changes (around -7 dB) in P_1 receptor port is observed, since the DNAPL is near the P_4 port.

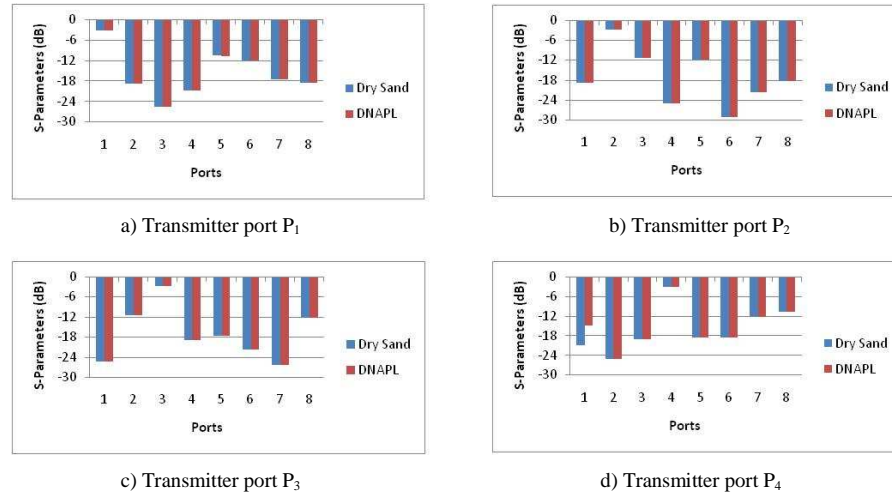


Figure 4.28: Comparison of S-parameters in dry sand with average DNAPL at 285MHz for a) Transmitter P₁, b) Transmitter P₂, c) Transmitter P₃, and d) Transmitter P₄

At 515 MHz the detection of the contaminant does not observed. These results are waiting, due to few contrasts that there are between soil electrical properties (Figure 4.14 and Figure 4.15).

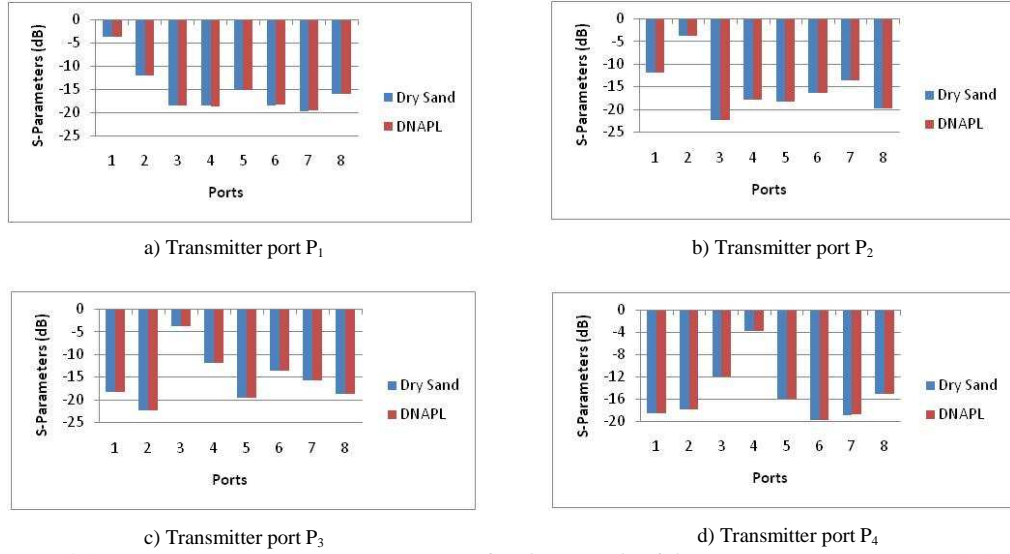


Figure 4.29: Comparison of S -parameter in dry sand with average DNAPL at 515MHz for a) Transmitter P_1 , b) Transmitter P_2 , c) Transmitter P_3 , and d) Transmitter P_4

Figure 4-30 shows the comparison of S -parameters for the dry sand with and without DNAPLs at the three operation frequencies. Energy changes between -2 dB and -3 dB is observed for specific ports. Energy changes in the receptor ports coincide with energy changes in the receptor ports in HFSS simulator in the same conditions.

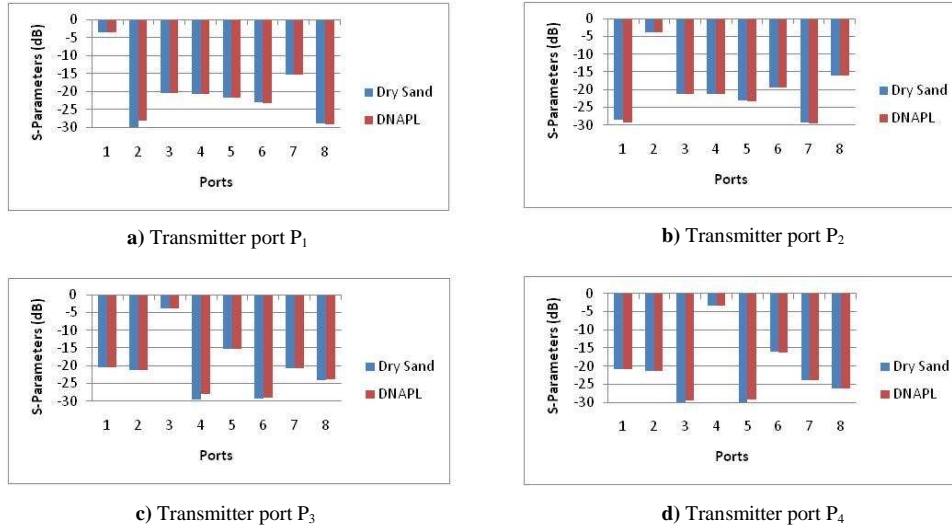


Figure 4.30: Comparison of S-parameters in dry sand with average DNAPL at 1.5 GHz for a) Transmitter P₁, b) Transmitter P₂, c) Transmitter P₃, and d) Transmitter P₄

In Figure 4.28, Figure 4.29 and Figure 4.30 energy changes in the receptor ports do not observed when is included DNAPL in the EM tank at 285 and 515 MHz, due to few contrasts between the soil electrical properties. Therefore the detection in XFDTD in these conditions is not possible. For 1.5 GHz energy changes in the receptor ports is observed. These ports coincide with some ports in HFSS when the transmitter ports are P₁, P₂, P₃ and P₄. The detection at 1.5 GHz is possible in dry sand.

4.4.2 Saturated Sand

In this section are presented the S-parameters for saturated sand without and with contaminant, at the analysis frequencies and its analysis. Tables 4-53, 4-54 and 4-55, present the S-parameters for saturated sand at using XFDTD simulator.

Table 4.53: S-parameters in saturated sand at 285 MHz with XFDTD

RPort EPort	1	2	3	4	5	6	7	8
1	-3.25	-18.81	-25.43	-20.82	-10.62	-11.88	-17.59	-18.51
2	-18.82	-2.83	-11.46	-25.04	-11.89	-29.25	-21.73	-18.46
3	-25.43	-11.46	-2.86	-19.09	-17.6	-21.73	-26.37	-12.3
4	-20.82	-25.03	-19.08	-3.07	-18.51	-18.45	-12.29	-10.63
5	-10.62	-11.88	-17.59	-18.51	-3.25	-18.81	-25.43	-20.82
6	-11.89	-29.25	-21.73	-18.46	-18.82	-2.83	-11.46	-25.04
7	-17.6	-21.73	-26.37	-12.3	-25.43	-11.46	-2.86	-19.08
8	-18.51	-18.44	-12.29	-10.63	-20.82	-25.03	-19.08	-3.06

Table 4.54: S-parameters in saturated sand at 515 MHz with XFDTD

RPort EPort	1	2	3	4	5	6	7	8
1	-3.52	-11.89	-18.41	-18.59	-15.07	-18.43	-19.67	-15.91
2	-11.9	-3.92	-22.42	-17.92	-18.43	-16.51	-13.65	-19.9
3	-18.4	-22.42	-3.89	-11.92	-19.67	-13.65	-15.88	-18.89
4	-18.59	-17.93	-11.93	-3.74	-15.91	-19.9	-18.9	-15.06
5	-15.07	-18.43	-19.68	-15.91	-3.52	-11.9	-18.41	-18.59
6	-18.42	-16.51	-13.65	-19.9	-11.9	-3.92	-22.42	-17.92
7	-19.67	-13.65	-15.88	-18.89	-18.4	-22.42	-3.89	-11.92
8	-15.91	-19.9	-18.89	-15.06	-18.59	-17.92	-11.93	-3.74

Table 4.55: S-parameters in saturated sand at 1.5 GHz with XFDTD

RPort EPort	1	2	3	4	5	6	7	8
1	-3.7	-33.59	-20.53	-20.86	-21.78	-22.97	-15.29	-29
2	-33.56	-3.86	-21.3	-21.33	-23.08	-19.51	-31.33	-16.12
3	-20.52	-21.3	-3.92	-43.4	-15.29	-31.33	-20.65	-23.97
4	-20.87	-21.37	-43.89	-3.4	-29.01	-16.13	-23.9	-26.29
5	-21.78	-22.97	-15.28	-29	-3.7	-33.29	-20.53	-20.86
6	-23.08	-19.5	-31.33	-16.12	-33.56	-3.86	-21.3	-21.33
7	-15.3	-31.33	-20.65	-23.96	-20.52	-21.3	-3.91	-43.4
8	-29.9	-16.13	-23.9	-26.29	-20.87	-21.37	-43.88	-3.4

4.4.2.1 Saturated sand with DNAPL1

Tables 4.56, 4.57 and 4.58 present the S -parameters when DNAPL1 is included on saturated sand at analysis frequencies. The DNAPL geometry was described in the section 4.3.2.1.1.

Table 4.56: S -parameters in saturated sand with DNAPL1 at 285 MHz

RPort EPort	1	2	3	4	5	6	7	8
1	-3.25	-25.4	-18.8	-20.81	-10.63	-11.88	-17.57	-18.5
2	-18.81	-2.83	-11.45	-25.04	-11.88	-29.22	-21.73	-18.46
3	-25.39	-11.45	-2.86	-19.07	-17.59	-21.74	-26.37	-12.3
4	-20.82	-25.05	-19.06	-3.07	-18.5	-18.42	-12.28	-10.62
5	-10.64	-11.88	-17.57	-18.5	-3.25	-18.81	-25.39	-20.8
6	-11.89	-29.22	-21.74	-18.45	-18.82	-2.83	-11.45	-25.03
7	-17.6	-21.73	-26.37	-12.29	-25.38	-11.45	-2.87	-19.05
8	-18.5	-18.44	-12.29	-10.62	-20.81	-5.04	-19.04	-3.07

Table 4.57: S -parameters in saturated sand with DNAPL1 at 515 MHz

RPort EPort	1	2	3	4	5	6	7	8
1	-3.51	-11.89	-18.4	-18.62	-15.08	-18.37	-19.63	-15.95
2	-11.88	-39.06	-22.41	-17.94	-18.39	-16.49	-13.64	-19.84
3	-18.42	-22.41	-3.86	-11.92	-19.64	-13.65	-15.84	-18.91
4	-18.62	-17.92	-11.92	-3.73	-15.91	-19.91	-18.8	-15.08
5	-15.08	-18.35	-19.66	-15.91	-3.51	-11.9	-18.41	-18.62
6	-18.4	-16.49	-13.65	-19.88	-11.89	-3.9	-22.38	-17.93
7	-19.61	-13.64	-15.84	-18.84	-18.43	-22.38	-3.88	-11.9
8	-15.95	-19.87	-18.87	-15.08	-18.62	-17.91	-11.91	-3.73

Table 4.58: S-parameters in saturated sand with DNAPL1 at 1.5 GHz

RPort EPort	1	2	3	4	5	6	7	8
1	-3.7	-34.29	-20.52	-20.85	-21.91	-23.23	-15.32	-29.18
2	-34.26	-3.86	-21.15	-21.31	-23.35	-19.39	-31.53	-16.11
3	-40.21	-34.64	-5.27	-44.37	-40.7	-31.04	-28.72	-37.96
4	-39.4	-49.22	-44.74	-5.41	-32.52	-34.13	-36.13	-27.03
5	-29.29	-36.15	-40.7	-32.69	-5.3	-39.96	-44.17	-50.29
6	-31.23	-32.25	-31.05	-34.58	-39.95	-5.18	-36.3	-40.72
7	-36.67	-27.41	-28.72	-36.4	-44.17	-36.3	-5.15	-42.9
8	-34.51	-37.51	-37.97	-26.78	-50.3	-40.72	-42.91	-5.38

4.4.2.2 Saturated sand with DNAPL2

Tables 4.59, 4.60 and 4.61, present the *S*-parameters when DNAPL2 is included on saturated sand at analysis frequencies. The DNAPL geometry was described in the section 4.3.2.1.1.

Table 4.59: S-parameters in saturated sand with DNAPL2 at 285 MHz

RPort EPort	1	2	3	4	5	6	7	8
1	-4.93	-25.84	-30.58	-42.42	-20.24	-23.78	-26.39	-22.75
2	-25.85	-4.17	-20.21	-29.68	-24.84	-19.81	-24.95	-30.43
3	-30.59	-20.21	-4.45	-25.02	-28.07	-24.33	-21.18	-32.75
4	-42.47	-29.64	-25.04	-4.51	-21.63	-29.19	-29.71	-21.52
5	-20.24	-24.83	-28.07	-21.59	-4.86	-26.26	-30.29	-37.4
6	23.78	-19.81	-24.33	-29.22	-26.27	-4.18	-20.38	-30.99
7	-26.39	-24.95	-21.18	-29.74	-30.29	-20.38	-4.42	-25.78.
8	-22.75	-30.43	-32.75	-21.52	-37.4	-30.99	-25.78	-4.49

Table 4.60: S-parameters in saturated sand with DNAPL2 at 515 MHz

RPort EPort	1	2	3	4	5	6	7	8
1	-1.7	-36.92	-43.49	-57.37	-35.68	-43.62	-32.86	-41.2
2	-11.88	-3.9	-22.41	-17.94	-18.38	-16.49	-13.64	-19.84
3	-18.42	-22.41	-3.86	-11.92	-19.64	-13.65	-15.84	-18.91
4	-18.62	-17.92	-11.92	-3.73	-15.91	-19.91	-18.8	-15.08
5	-15.08	-18.35	-19.66	-15.91	-3.51	-11.9	-18.41	-18.62
6	-18.41	-16.49	-13.65	-19.88	-11.89	-3.9	-22.38	-17.93
7	-19.61	-13.64	-15.84	-18.84	-18.43	-22.38	-3.88	-11.9
8	-15.95	-19.87	-18.87	-15.08	-18.62	-17.9	-11.91	-3.73

Table 4.61: S-parameters in saturated sand with DNAPL2 at 1.5 GHz

RPort EPort	1	2	3	4	5	6	7	8
1	-5.16	-29.86	-29	-29.08	-28.39	-29.06	-29.19	-29.6
2	-29.7	-5.27	-29.35	-29.24	-29.92	-29.8	-27.35	-29.12
3	-41	-29.36	-29.68	-29.41	-29.51	-26.12	-28.03	-29.99
4	-29.09	-29.37	-29.41	-5.39	-29.52	-35.48	-34.48	-25.96
5	-28.4	-29.04	-29.51	-29.51	-5.24	-29.58	-37.5	-29.94
6	-28.96	-29.8	-26.08	-29.78	-29.51	5.22	-29.4	-36.38
7	-29.97	-27.35	-28.12	-29.28	-29.39	-29.4	-5.23	-27.52
8	-29.61	-29.05	-29.99	-25.95	-29.94	-29.48	-29	-5.62

4.4.2.3 Analysis of S-parameters

Figure 4.28 showed the comparison of the S-parameters in saturated sand without contaminant and the consolidated S-parameters of the two DNAPL geometries.

Figure 4.31 shows increment of energy between -3 dB and -5 dB in all of receiver ports when the signal is transmitted by the four transmitter ports due to contrast of the two media. For HFSS also in all receiver ports increment of energy are observed with the same soil electrical properties.

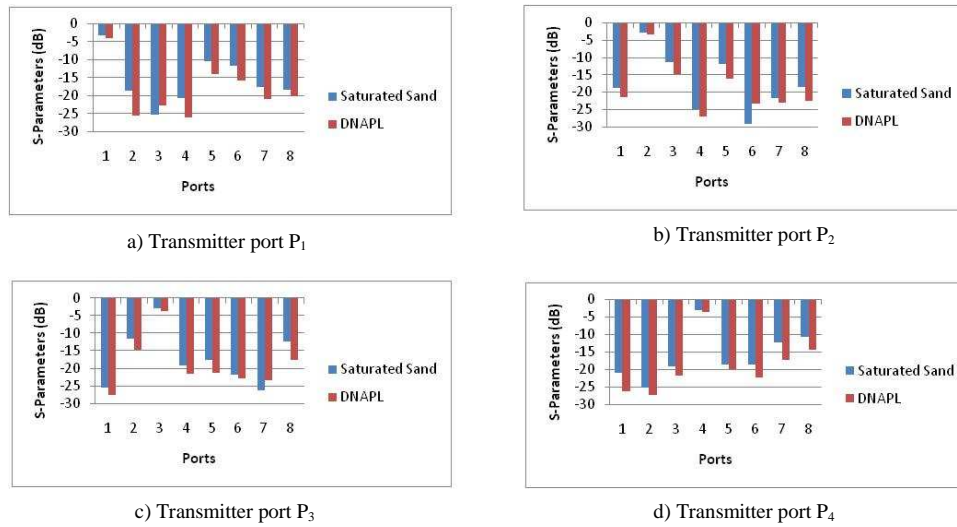


Figure 4.31: Comparison of S-parameters in saturated sand with average DNAPL at 285 MHz, for a) Transmitter P_1 , b) Transmitter P_2 , c) Transmitter P_3 , and d) Transmitter P_4

At 515 MHz (Figure 4.32), only the receiver ports P_1 significant changes of energy are observed. These results by comparison with the obtained for HFSS simulator, are not similar. These comparisons are expected due to the contrasts of the soil electrical properties at 515 MHz.

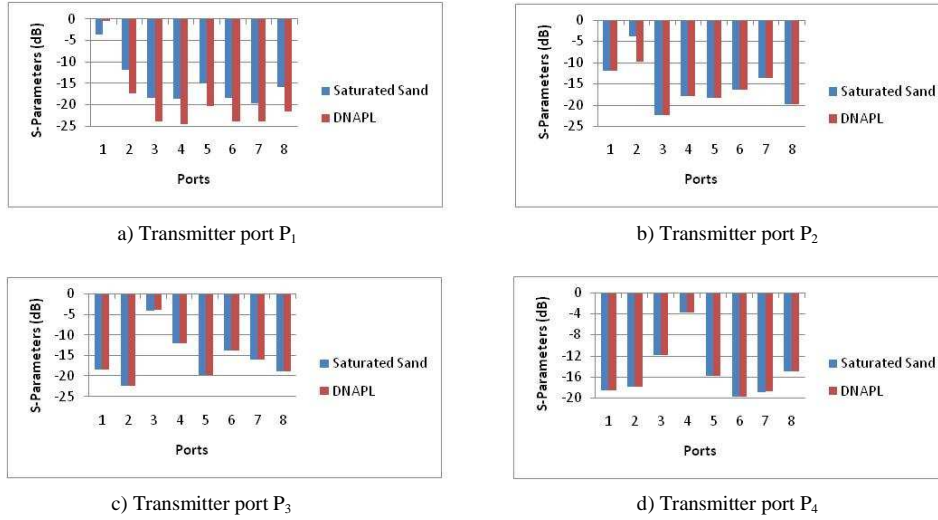


Figure 4.32: Comparison of S-parameters in saturated sand with average DNAPL at 515MHz for a) Transmitter P_1 , b) Transmitter P_2 , c) Transmitter P_3 , and d) Transmitter P_4

When the signal is transmitted at 1.5 GHz (Figure 4.33), the transmission from the four ports, produce energy changes in all the receiver ports. These changes are expected, since in HFSS simulator these changes are observed. The energy changes are due to the reflections produced by the contrasts with DNAPL.

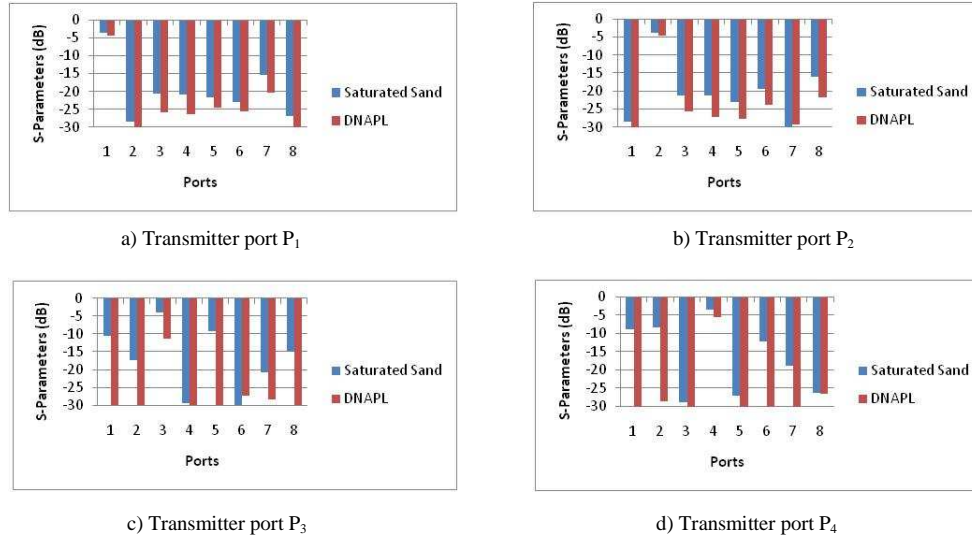


Figure 4.33: Comparison of S-parameters in saturated sand with average DNAPL at 1.5 GHz for a) Transmitter P_1 , b) Transmitter P_2 , c) Transmitter P_3 , and d) Transmitter P_4

The previous analyses, the detections in dry and saturated sand without and with contaminants at the three frequencies of operations is possible using P_1 , P_2 , P_3 and P_4 as transmitter ports, since the behavior of the S-parameters is similar in the two simulators in the same conditions.

5 SUMMARY, CONCLUSIONS AND RECOMMENDATIONS

5.1 Summary and Conclusions

An electromagnetic analysis was presented to determine if it is possible to detect contaminants in the laboratory scale 2D Soil-Bed setup. To do this, we first developed the electromagnetic model of the structure, and then several simulations were obtained in order to study the effect of the DNAPL in dry and saturated sand, and combinations of them. Also, we computed new operation frequencies and changed the transmitter port positions, to do a better study of the S-parameters and E-field distribution into the EM tank.

Due to the EM tank symmetry, we only considered transmission energy from one side of the tank.

To determine the electromagnetic field distributions under different subsurface conditions, different degrees of soil saturation level in dry sand were simulated. The simulations did not show a clear benchmark that can describe the medium constitution taking into account the S-parameters. Particular behaviors of the generated E-field distributions were, however, observed for different conditions.

To detect possible soil contamination, different DNAPL geometries were introduced into the dry and saturated sand, determining the E-field distribution and the S-parameters.

The analysis of the *S*-parameters was done by comparing the reference *S*-parameters for dry and saturated sand, with the consolidated *S*-parameters for four DNAPL geometries within these medium. With this comparison, the detection was possible in dry and saturated sand. This detection depends on the frequency of operation, since these must be a multiple of the structure, and position and amount of ports used to have a better spatial resolution.

In the analysis of the E-field distribution, it was observed brightness changes in the wave propagation when was included the contaminant in saturated sand at the three frequencies of operation. These changes were due to the difference between the electrical properties of them. These differences imply that there is soil contaminant only in saturated sand, since in dry sand the few contrast do not produced brightness changes in the wave propagation when was included contaminant.

Analyses were mostly made in the HFSS simulator and were composed for the experiments made with DNAPL using the XFDTD simulator. In the case of dry sand with DNAPL using XFDTD, the results were not conclusive since the *S*-parameters did not present significant changes with respect at reference results for dry sand. The small difference between these parameters could be caused by the definition of the dynamic range for this simulator (surrounding of -30 dB) in contrast to the obtained for HFSS (surrounding

of -124.35 dB). However, these results were expected due to few contrasts of the media electrical properties. For saturated sand, the results at 285 MHz and 515 MHz were similar with the obtained by HFSS.

Therefore, it was concluded that the detection of contaminants using the Cross-Well Radar method is possible for different soil conditions using HFSS and XFDTD simulators, taking in the account the frequencies of operation, position and amount of ports used.

5.2 Recommendations

In order to obtain more precise resultant, it is necessary to keep in mind the follow factors:

- To use the phase information of S-parameters in the analysis, to determine if detection of the contaminant can be improved.
- To analyze the system through simulations in the time domain to obtain answers in a wide range frequency and with this to determine other frequencies for the detection of the contaminant.

REFERENCES

- [1] Mohammad Farid. *DNAPL Detection using cross well radar*. PhD thesis, Northeastern University, Boston Massachusetts, 2004.
- [2] María Fernanda Serrano Guzman. *Detection and monitoring of DNPLs in the subsurface under transient conditions using cross well radar*. PhD thesis, University of Puerto Rico, Mayaguez campus, 2008.
- [3] Environmental Protection Agency (EPA). "Geophysical techniques to locate DNAPLs: Profiles of federally funded projects". Report 542-R-98-020, Environmental Protection Agency, 1998.
- [4] María F. Serrano-Guzmán, Ingrid Padilla, and Rafael Rodríguez. "Two-dimensional detection of underground contamination and buried objects using cross-well radar". *Radar Sensor Technology X, Proc. SPIE*, 6210(1), 2006.
- [5] M. Farid, A. N. Alshawabkeh, and C. Rappaport. "Modeling borehole dipole antenna patterns for cross well radar DNAL imaging". *Electronic Proceedings of the 12th Pan-American Conference on Soil Mechanics and Foundation Engineering*, Cambridge, MA. 2003.
- [6] ITRC. "Dense Non-Aqueous Phase Liquids (DNAPLs): Review of emerging characterization and remediation technologies". *Interstate Technology and Regulatory Council*, 2000, accessed on September 2006.
- [7] M. B. Silevitch. "An engineering research center for subsurface sensing and imaging systems". *NSF proposal number 9986821*, pages A-1, C-33, August 1999.

- [8] National Research Council. *Seeing into the Earth: Noninvasive characterization of the shallow subsurface for environmental and engineering applications*. National Academy Press, Washington D.C., 2000.
- [9] C. Rappaport. "Computational methods to model wave phenomena: General overview, finite differences, and visualization". *CenSSIS Seminar*, November 2002.
- [10] David M. Pozar. *Microwave Engineering*. Jhon Wiley & Sons, Inc., third edition, 2005.
- [11] Sandra Cruz Pol. *Electromagnetic Wave Review*. ECE UPRM, Mayaguez PR.
- [12] C.A. Balanis. *Advanced Engineering Electromagnetics*. Wiley, 1989.
- [13] Franco M. Francisca and Victor A. Rinaldi. Complex dielectric permittivity of soil organic mixtures (20 MHz-1.3 GHz). *Journal of Environmental Engineering*, 129(4):347-357, April 2003.
- [14] W.G. Fano and V. Trainotti. Dielectric Properties of Soils. *IEEE Annual Report Conference on Electrical Insulation and Dielectric Phenomen*, 2001.
- [15] S. Haffa, D. Hollmann, and W. Wiesbeck. The finite difference method for S-parameter calculation of arbitrary three-dimensional structures. *Microwave Theory and Techniques, IEEE Transactions on*, 40(8):1602-1610, Aug 1992.
- [16] R. H. Jansen. The spectral-domain approach for microwave integrated circuits. *IEEE Trans. Microwave Theory Tech*, Oct. 1985.
- [17] L. P. Dunleavy and P. B. Katehi. The spectral-domain approach for microwave integrated circuits. *IEEE Trans. Microwave Theory Tech*, Dec. 1988.

- [18] T. Angkaew, M. Matsuhara, and N. Kumagai. Finite-element analysis of waveguide modes: A novel approach that eliminates spurious modes. *Microwave Theory and Techniques, IEEE Transactions on*, 35(2):117-123, Feb 1987.
- [19] K. Yee. Numerical solution of initial boundary value problems involving Maxwell's equations in isotropic media. *Antennas and Propagation, IEEE Transactions on*, 14(3):302-307, May 1966.
- [20] M. Sadiko. *Numerical Techniques in Electromagnetics*. CRC Press, FL, 1992.
- [21] William H. Weedon and Carey M. Rappaport. "A general method for FDTD modeling of wave propagation in arbitrary frequency-dispersive media". *IEEE Transactions on antennas and propagation.*, 45(3), March 1997.
- [22] K. Kunz and R.J. Luebbers. *The Finite Difference Time Domain Method for Electromagnetics*. CRC Press, FL, 1993.
- [23] A. Salvia. Método de las diferencias finitas en el dominio del tiempo (FDTD), accessed on 2007.
- [24] M. Farid, A. N. Alshawabkeh, and C. Rappaport. Modeling borehole dipole antenna patterns for cross well radar DNAL imaging. *Electronic Proceedings of the 12th Pan-American Conference on Soil Mechanics and Foundation Engineering*, Cambridge, MA 2003.

- [25] C. M. Rappaport, Shuang Wu, and Scott C. Winton. FDTD wave propagation in dispersive soil using a single pole conductivity model. *IEEE Transactions on Magnetics*, 35(3), May 1999.
- [26] Klaus Beilenhoff, Wolfgang Heinrich, and Hans L. Hartnagel. Improved finite-difference formulation in frequency domain for three-dimensional scattering problems. *IEEE Transactions on microwave theory and techniques*, 40(3):540-546, March 1992.
- [27] M.N.O. Sadiku and A.F. Peterson. A comparison of numerical methods for computing electromagnetic fields. *Southeastcon '90. Proceedings., IEEE*, pages 42-47 vol.1, Apr 1990.
- [28] M.N.O. Sadiku. A simple introduction to finite element analysis of electromagnetic problems. *Education, IEEE Transactions on*, 32(2):85-93, May 1989.
- [29] A. Noreika and P. Tarvydas. Electromagnetic field modeling using edge finite elements. *Electronics Conference, 2008. BEC 2008. 11th International Biennial Baltic*, pages 99-102, Oct. 2008.
- [30] V. Radonic, V. Crnojevic-Bengin, and L. Zivanov. Comparison of commercially available full-wave em simulation tools for microwave passive devices. *Computer as a Tool, 2005. EUROCON 2005. The International Conference on*, 2:1699-1702, 2005.
- [31] Remcom. *XFDTD Reference Manual 6.5*. Remcom Inc., 2007.
- [32] H. Zhan, M. Farid, et al. Scale Model Experimental Validation and Calibration of the Half-Space Green's Function Born Approximation Model Applied to Cross-Well Radar

- Sensing. *IEEE Transactions on geosciences and remote sensing*, 45(5):2423-2428, August 2007.
- [33] H. Zhan, A. Morgenthaler, et al. Half-Space Born Approximation Modeling and Inversion for Cross-Well Radar Sensing of Contaminants in Soil. *IEEE International geosciences and remote sensing symposium*, 2550-2553, July 2007.
- [34] R. Chawn Harlow and Eleanor J. Burke et al. Measuring spectral dielectric properties using gated time domain transmission measurements. *Vadose Zone Journal*, 2:424-432, 2003.
- [35] Ansoft. *HFSS User's guide - High Frequency Structure Simulator v10*. Ansoft Corporation, 2005
- [36] Agilent Technologies. *Agilent Understanding and Improving Network Analyzer Dynamic Range*. Agilent Technologies, 2000.